DOCTORAL DISSERTATION

Shearing of granular materials

János Török

Thesis advisors: Prof. János Kertész
Dr. Stéphane Roux

Department of Theoretical Physics
Budapest University of Technology
Budapest, Hungary

Physique des Fluides et des Transferts
Université de Paris-Sud
Orsay, France

2000

Preface

Granular materials are so common in our everyday life that no one really realizes that he is in daily contact with it. It is enough to think about our kitchen where most of the primary materials are in the form of powder like salt, sugar, wheat, spices, etc. Vacations may also give us a possibility to get in contact with other granular materials as snow and sand. But the main user of these type of materials is the industry where we find powders everywhere: Chemical products, coal, soil, stone, agricultural products, seeds, etc.

As one may suspect the detailed study of these materials has a long history in the engineering literature. A lot of effort has been done to give a useful description of the unusual behaviour realized by granular materials. The results of these studies are already used in commercial codes and as well in technical realizations of production. However, in the last decade physicists have also started to interest in this field. The renaissance of the subject has been due to on one hand the development of the description of disordered media and on other hand modern computers allow a particle based simulations of these systems on a large enough scale to be compared to experiments.

Throughout our research we have focused on one particular problem in granular materials: the shearing. Many of the interesting features seen in granular materials can also be observed in the shearing process, like logarithmic density increase, shear strain localization in shear bands, memory effects and glassy like behaviour, screening or arching, pattern formation and unusual system size dependence, which are reproduced by the parameter free mesoscopic model that we investigate numerically and analytically.

In the first chapter we give a short review of some interesting aspects of granular media related to our work. In Chapter 2 and 3 the numerical and analytical results of the mesoscopic model are presented. Chapter 4 deals with the Self-Quenching Walk. The Appendices A-D contain some technical details which would unnecessarily interrupt the tracking of the material. The Thesis terminates with a short Summary, a Bibliography and a List of publications.

The present work was done under the guidance of my two supervisors, János Kertész and Stéphane Roux in cooperation with a post. doc. student of the latter,

Supriya Krishnamurthy. I would like to express my gratitude towards all of them, to my supervisors for the very fine and edifying guidance and to Supriya Krishnamurthy for the valuable and helpful discussions.

During these four years of cooperation I had the opportunity to be part of two scientific groups, of the Theoretical Physics Department of the Budapest University of Technology and Economics and of the Laboratoire PMMH of the École Supérieure de Physisque et de Chimie Industrielles de la Ville de Paris. I would like to thank for all the members of those groups for the various help they supplied for me. Let me name here among them Prof. Hans J. Herrmann who warmly accepted me in his institute after the departure of Stéphane Roux, and some of the Ph.D. and post. doc. students: László Borda, Erwan Hascoët, Antal Károlyi, László Kullmann, Vittorio Loreto, Gadi Oron, Márton Sasvári and Gerd Sauermann.

I would like to thank the help of András Czirók as a friend and also as a colleague.

The cooperation in frame of this Ph.D. could be realized by the scholarships of the French Government and the Soros Foundation.

Finally, I would like to thank my Parents and my Brother for their continuous support and patience.

Contents

Chapter 1

Introduction

The aim of this introduction is to present briefly those aspects of granular media which will be used during the detailed analysis of our results. Starting with the definition of granular materials as well as the packing and preparation problems we show how sensitive granular materials are to fluctuations. This thesis focuses on the shear process and in the second part of this overview we try to identify its characteristic features.

1.1 Definition of the granular material

According to the most widespread definition, granular materials are assemblies of interacting particles large enough that the thermal fluctuation of the individual grains can be neglected [JNB96]. One crucial question is the number of particles in the sample. No one will consider the experiment of the collision of two balls as a typical granular material. In general, an acceptable lower limit of the particles is given in the order of $100 \sim 1000$. However, in some cases assemblies of some 10 particles can show some interesting features of granular materials and thus can be a good candidates for studying specific phenomena [SzyLab99, FTVV99, RadRou95, OroHer98]. One can also think of systems with large number of particles that are not typical examples of granular materials, because of too strong (concrete) or too weak (stars in a galaxy) interaction. In practice if we mention granular materials we think of grains with a size of the order of $1\mu\text{m} \sim 1\text{mm}$.

There are a number of immediate consequences of the above definition. First, as the particles are too large for thermal fluctuations, they have their own temperature that is not correlated with their velocity. Kinetic energy into a closed granular assembly is not conserved as it can be dissipated through friction and inelastic collisions. Thus if we do not pump energy in a granular system it will relax to an equilibrium state where no particles move [GolZan93, JNB96].

The relatively large size of the particles enable them to carry friction forces and

thus build up structures with non-vanishing stresses like sand piles or arches. These structures remain unchanged unless disturbed by forces ten orders of magnitude larger than thermal fluctuation e.g. the potential energy of a grain of sand raised by its diameter is 10^{12} times larger than k_BT at room temperature [JNB96]. However, there are apparent differences between solids and granular materials. Granular materials may support much less stress than solids at the same time the relative motion among particles in granular materials does not destroy the sample, only reorganizes its structure which is not the case for the solids.

If one applies large enough forces, granular materials flow [Wood90, TorRou00]. In some cases it is a fluid-like flow but sometimes it has completely different microscopic and macroscopic mechanics. Generally, only a small region of the material is moving while the rest remains inactive. This can be the surface if one has a flow on an inclined plane [SavLun88, BouGen96], or the narrow domain of the shear band during shear [AhaSpa99]. At the case of free flow in a pipe long memory of the construction can be observed with velocity profiles different from that of the fluids [ThomGre91].

Usually, it is a crucial question what is the interstitial fluid among the particles since it may change completely its properties [PDB95, SSH96, TAP+99, MLEH99], like the well known example that sand-castles can not be made of dry sand [HalLev98, HAA+97]. In the scope of this thesis we consider only *dry* granular materials, when the grains are in air or in vacuum and we will also omit the study of fast dynamics of granular materials so for our purposes the interstitial fluid does not play any role.

In the next sections we show what other unexpected behaviour can emerge from the interesting structure of the granular materials.

1.2 Static properties

1.2.1 Density

In experiments with usual solid and fluid materials we often use terms as: "Let us fill the container with this fluid" or "let us take a sample with such dimension". These expressions are not so innocent in the case of granular materials. Many properties of the sample depend on the precise way of the preparation [VHC+99, deGennes98].

In general, the notion density in the case of granular materials often means packing fraction η, the space occupied by the particles. The real density of the material (that of a single grain) does not play any role in the great majority of the phenomena observable in granular materials. However, as the material is composed of small grains naturally there is some space among the grains as their shape does not allow for a complete filling of the container. This empty space among the particles is responsible for many unexpected properties.

In nature only disordered packings exist. Even in the case of very high η, e.g. in

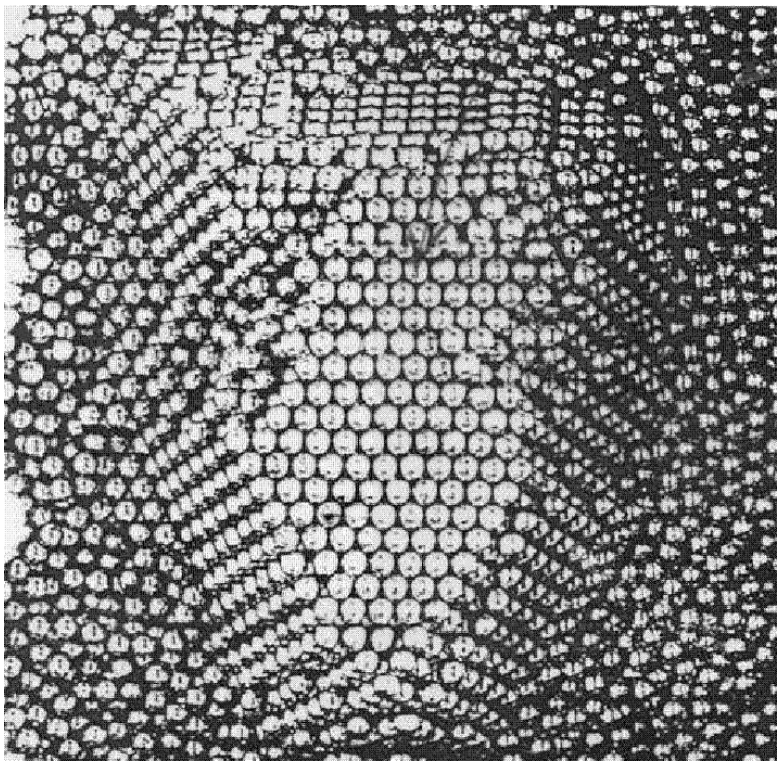

Figure 1.1: A packing example using steel beads from Ref. [Bernal65]. The closest hexagonal packing with $\eta \simeq 0.74$ on the top of a random close packing with $\eta \simeq 0.64$.

sandstones the positions of the grains are fortuitous but the high pressure changed the shape of the particles to reduce the volume of the interstitial fluid(gas). Crystal like arrangement of particles can only be made under very special conditions with highly monodisperse materials [WooJac57, AldWai57, LinCha82, PMW97]. Usually this needs a gentle thermal like motion of particles in very small or no gravity. In the following we will only consider random packings.

Properties of random packings may vary in a wide range. If we consider only uniform spheres stable samples can be made in the packing fraction range of 0.555 (random loose packing) to 0.645 (random close packing) [Scott60, OnoLin90] (Fig. 1.1). If different shapes are also allowed we may get sample for nearly all values of η (e.g. sandstones or aggregates of snowflakes).

The most striking feature of the packing density of the granular materials that it has the most important impact on its stability [HJV96, DouDae98, ConHerr96]. In the next paragraph we sketch some reasons behind it, however, the correct functional form of the density dependence of the maximum of the static friction force is not trivial [HJV96].

The grains in a granular assembly touch each other in relatively small areas that

can be considered in most cases a punctual contacts. The position of a grain under gravity is stable if it has at least four contacts that are not in a plane. (Three contacts are only enough if two of them are below the grain but this prevents the particle from holding others.) In fact this is the loosest possible configuration one can generate if the contact network percolates through the whole sample [OnoLin90, GarTho85]. The lowest packing fraction that can be reached is around $\eta \simeq 0.555$.

If we consider monodisperse grains the maximum of the number of contacts a particle may have is 12 in hexagonal packing which is the theoretical upper limit for the packing fraction thus $\eta \simeq 0.74 < 1$. In random close packing the above coordination number of 12 can not be reached, the average is in general around 7 [Berryman83, JodTor85]. If we consider now the maximum of static shear force that one can be applied to a sample it is easy to understand that fewer contacts are easier to break up thus denser granular samples are easier to shear.

In natural or industrial packings (medical pills, concrete, hillside, etc.) loose packed, thus more fragile, parts may initiate unwanted processes, like breaking or avalanches. In spite of this importance loose packings have very narrow literature. As they change under very small forces their reproducible preparation for experiments is an extremely difficult task and in general can only be made on a small scale [OnoLin90].

Close packed samples have much broader literature [CumCra87] and have also more application as in general in industry one may want to create products which resist against usual interactions [JodTor85, OroHer00]. Scientific experiments usually start from close packed samples as they can be made easier in a reproducible manner [VHB99].

1.2.2 History

It is very surprising that not only the density of the sample plays an important role in its properties but also the complete history of its preparation. A spectacular experiment has been done recently to demonstrate this effect [VHC+99]. Sand piles were made in two different ways: First by the usual procedure of pouring the sand from a punctual source at the center of the pile was used. In the second experiment they sifted the sand through a sieve to produce a uniform rain-like current of the sand. In both cases the cone was on a cylindrical plate to get rid of the excess sand through avalanches. Local normal forces under the pile were measured in both cases. A distinct difference between the two preparation methods was found: In the second case the maximum of the pressure was in the center, under the highest point while in the first case a local minimum was observed at the same place and the maximum was found at about 1/3 of the pile size off the heap as shown on Fig. 1.2.

There are two basic reasons for the "good memory" of granular material. First, a granular sample is usually built up progressively. In such cases newly added par-

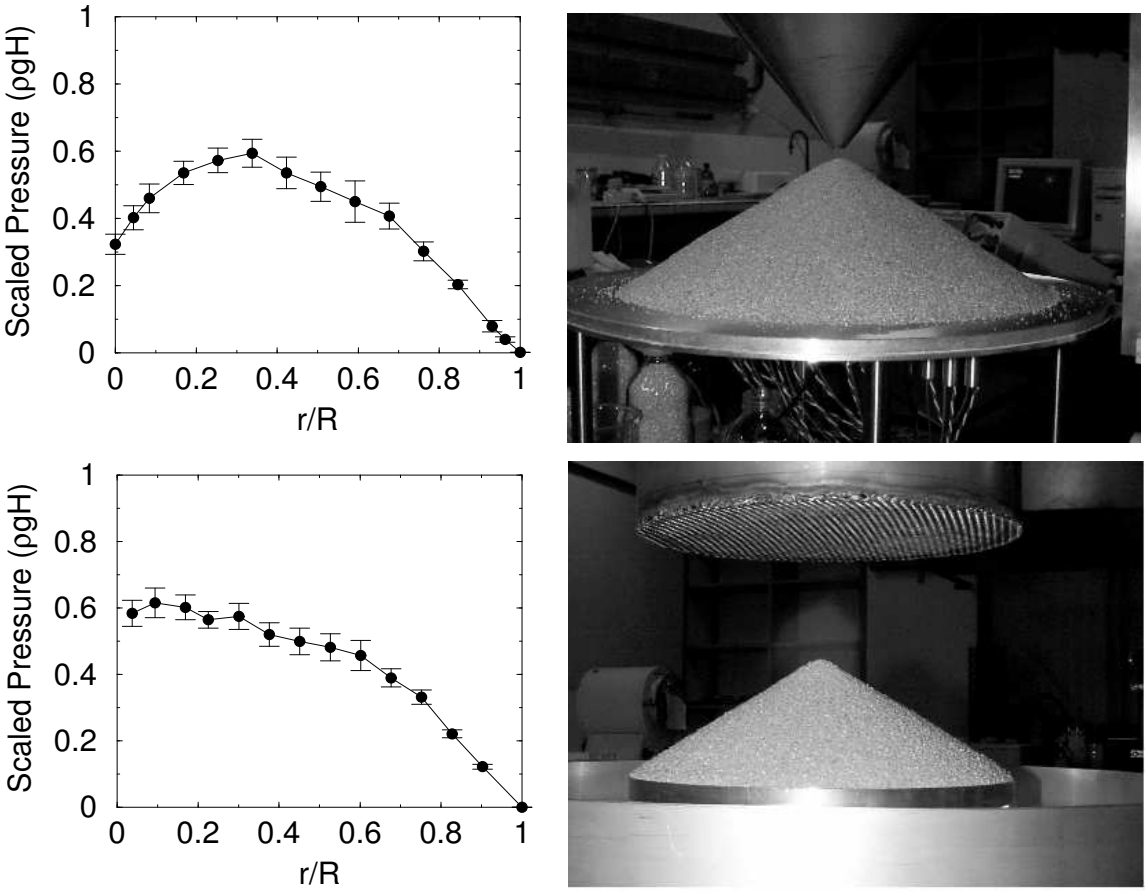

Figure 1.2: Normal stress profiles beneath conical piles of granular materials of height H from Ref. [VHC+99]. The piles are made by different construction techniques illustrated by the accompanying photographs. The distance from the center of the profiles is normalized by the radius R and stresses are normalized by $\varrho g H$.

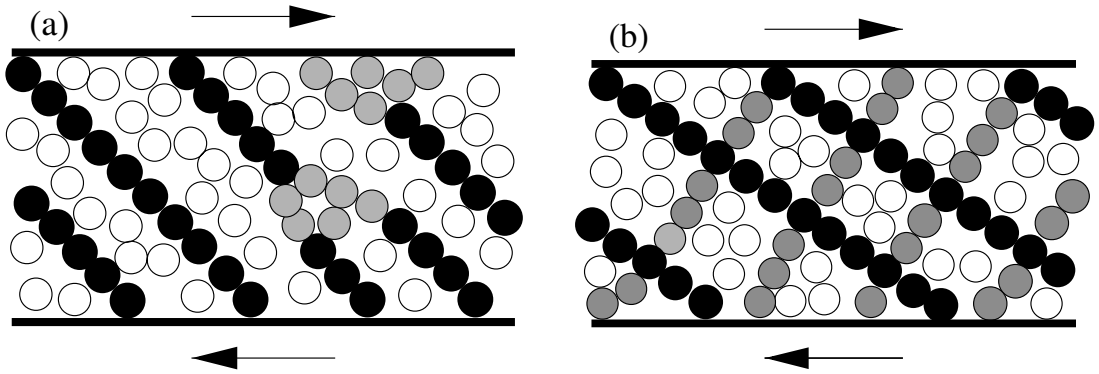

Figure 1.3: Visualization of the strengthening process of granular materials under shear from Ref. [CWBC98]. The figure shows an idealized network of particle chains that can withstand large shear forces.

ticles interact only with a small external shell of particles while the inner structure remains intact [Savage84, MelBal95, FMB97, BCPE94, BCPE95, DAD99]. Moreover, Wittmer *et al.* [WCC97] claim that during the construction of a sandpile the eigendirections of the stress tensor is frozen in once a particle is buried, resulting a perfect memory of the surface directions and dynamical state. Furthermore, dynamical processes in granular materials rarely produce a homogeneous material even on large scale [Williams76, CSB76, DurMaz99]. It is known that flow [SavLun88, BouGen96], shear [SSH96] and shaking [ROF64, KJN93, RSPS87] induces particle separation based on size [Williams76, CSB76], on friction coefficient [FTVV99] and on shape [MBCW98, Makse97]. As all granular materials are results of some mechanical process, the inhomogeneities characteristic for such processes will be present in the resulting sample.

Other dynamical processes may change the position of the particles and build up spatial correlations among them enable the sample to react differently for influences in various directions. A typical example of this is the shear induced hardening [CWBC98, LGNG00]. After some strain in a given direction chains of particles are built up "against" the shear (Fig. 1.3) thus further strains can be made upon the granular sample only with very large stresses, however as these particle chains may support load only from one direction shear strains in the opposite direction can be realized easily.

There are a number of tries to take into account the texture and the orientation of the contacts of the granular sample in calculations like the fabric tensor [RouRad98, Schollmann99] or the Voronoï analysis [LMOT99, ROTG99] but their proper use and understanding still needs a lot of work.

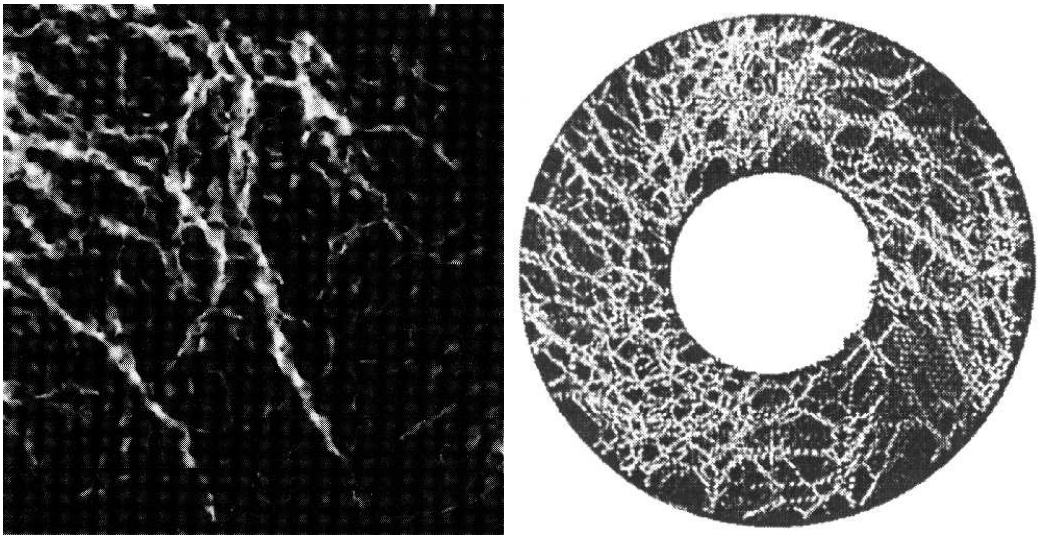

a) b)

Figure 1.4: Experimental visualizations of force chains using photoelastic materials.
a) (from Ref. [LNS+95]) is a three dimensional experiment where the photoelastic material was index-matched with the surrounding fluid and a force is exerted on a piston that covers the top surface of the container.
b) (from Ref. [VHB+98]) shows the resulting force chains of a two-dimensional Couette shear experiment where the inner ring was turning clockwise.

1.2.3 Force chains

In granular materials forces can only be transmitted via the contacts of the small grains. The disordered displacement of the contact points give rise to very inhomogeneous contact force network [TBG+86, LNS+95, VHB+98, VHB99] (Fig. 1.4). Besides the contact disorder there is also a positive feedback in the realization of a force network. If forces are larger in a certain direction they have tendency to strengthen contacts and thus "deviate" forces coming from above. The result is a long force chain in the material [CLM+96]. This can lead to interesting features like formation of arches.

Experiments

The measure of inter-particle forces is a difficult task for experimentalists. The earliest method consists of using photoelastic materials. Especially, in two dimensions it gives an accurate way of displaying stresses on particles [VHB99, HBV99, VHB+98, TBG+86] that can be seen on Fig. 1.4 b). One may also try this method in three dimensions using index matched fluid [see [LNS+95] Fig. 1.4 a)] but quantitative measurements are extremely difficult to carry out.

Another technique consists of measuring only the external forces that the grains

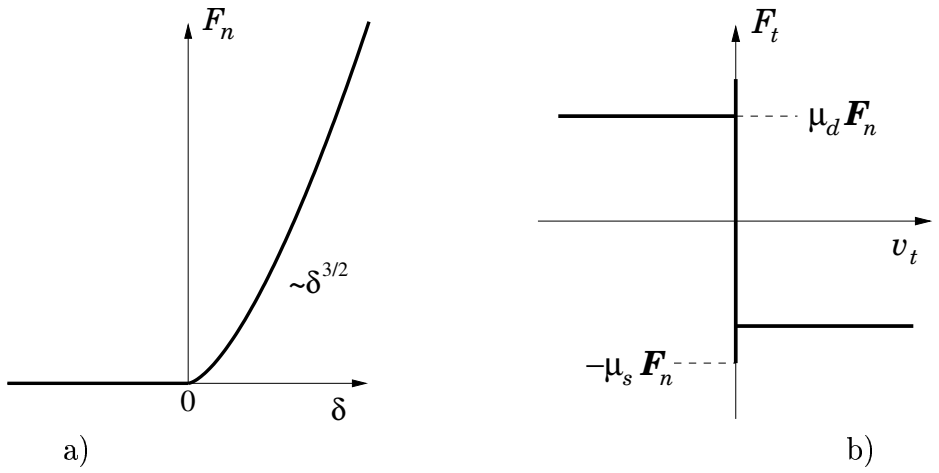

Figure 1.5: a) The Hertz normal contact force [Hertz82, Johnson85] as the function of displacement of the grain respect to the touching position (δ). It is difficult to handle in calculations the non-linearity around $\delta = 0$.
b) The graph representing the Coulomb's law of friction forces. The static friction force can be larger than the dynamic.

exert on the container [VHC+99, LMF99, MJN98]. This was either done by placing a carbon paper and a paper between the particles and the wall of the container and measuring the size of the traces [MJN98] or by direct force sensors at certain positions [VHC+99] and also by a small balance with moving the sample around with the help of a thin paper [LMF99]. The difficulties of such measurements lies in their accuracy. They need in general very large forces and thus they are not suitable for free packings on the other hand it was shown that small displacement of particles can induce large changes in the force chains [Liu94, LiuNag93] thus the small displacement of the captors should be verified by well chosen control experiment [VHC+99] and thus considered with care.

It is not obvious that force distributions on the boundaries of a granular sample are the same as inside. So forces should be also measured among the inner particles of the sample. There was one interesting experiment that challenged this problem. Tsoungui *et al.* [TVC98a, TVC98b] used a fine powder to colour the particles in the packing while the contact areas remain unpainted. The size of the unpainted region can be calibrated to normal forces.

The result of these experiments show that the distribution of the forces larger than the average decreases as an exponential function and the maximum lies also around this point. Small forces are difficult to measure and up to now there is no conclusive agreement in the literature on their distribution.

Analytic force calculation in regular assemblies

If we consider small regular assemblies of mono-disperse spheres it is possible to calculate analytically the force network [Hong93, Huntley93, OroHer98]. The difficulty of these calculations lies in the high non-linearity of the contact forces [see Fig. 1.5 a)]. In general uncharged, dry grains can exert only repulsive forces that disappears as soon as the two grains do not touch each other.

In order to calculate the forces we have to determine *a priori* the contact network. If the supposed force network is not the correct one, we get negative forces between particles. The earlier works [Hong93, Huntley93] used arrangements with no horizontal contacts while in the work of Oron *et al.* [OroHer98] an iterative method was used to achieve the correct force network.

Dynamical methods

All dynamical methods used to determine force networks in granular packings uses some kind of relaxation process. Starting from a loose configuration and than the sample is allowed to relax due to external (gravitational or pressure like) forces. Different methods are the following: molecular dynamics [Luding97, TVCR98], contact dynamics [RJMR96, RBR96] or an exact numerical calculation in a frictionless model [OuaRou97, Ouaguenouni97, Roux00].

There are a number of difficulties that one should encounter if tries to perform such a calculation. Apart from the above mentioned non-linearity of the normal force its value also needs some attention. As the inhomogeneities of the normal forces are very large we observe forces in a range of multiple order of magnitude [Luding97]. The correct simulation of such a system needs extremely slow relaxation that strongly limits the size of the samples.

If friction forces are considered in the relaxation process that is also highly nonlinear: Fig. 1.5 b). Apart from this non-linearity stresses may be transmitted via chains of touching particles and thus particles relatively far from each-other may interact. The contact dynamics is a nice method to take this into account [RadRou95].

Typical results from refs. [RJMR96, Roux00] are shown on Fig. 1.6. These models give a good quantitative and qualitative accordance with experimental results showing exponentially decaying distribution of large forces, however their extension to three dimensions is still an open problem due to heavy calculation needs. Let us mention that in the case of compressible particles the well known finite element method can also be used, which gives essentially the same results [MJS00].

Lattice models

Lattice models have been developed to circumvent the above mentioned difficulties. The material is considered on a mesoscopic scale with no direct site-particle identifica-

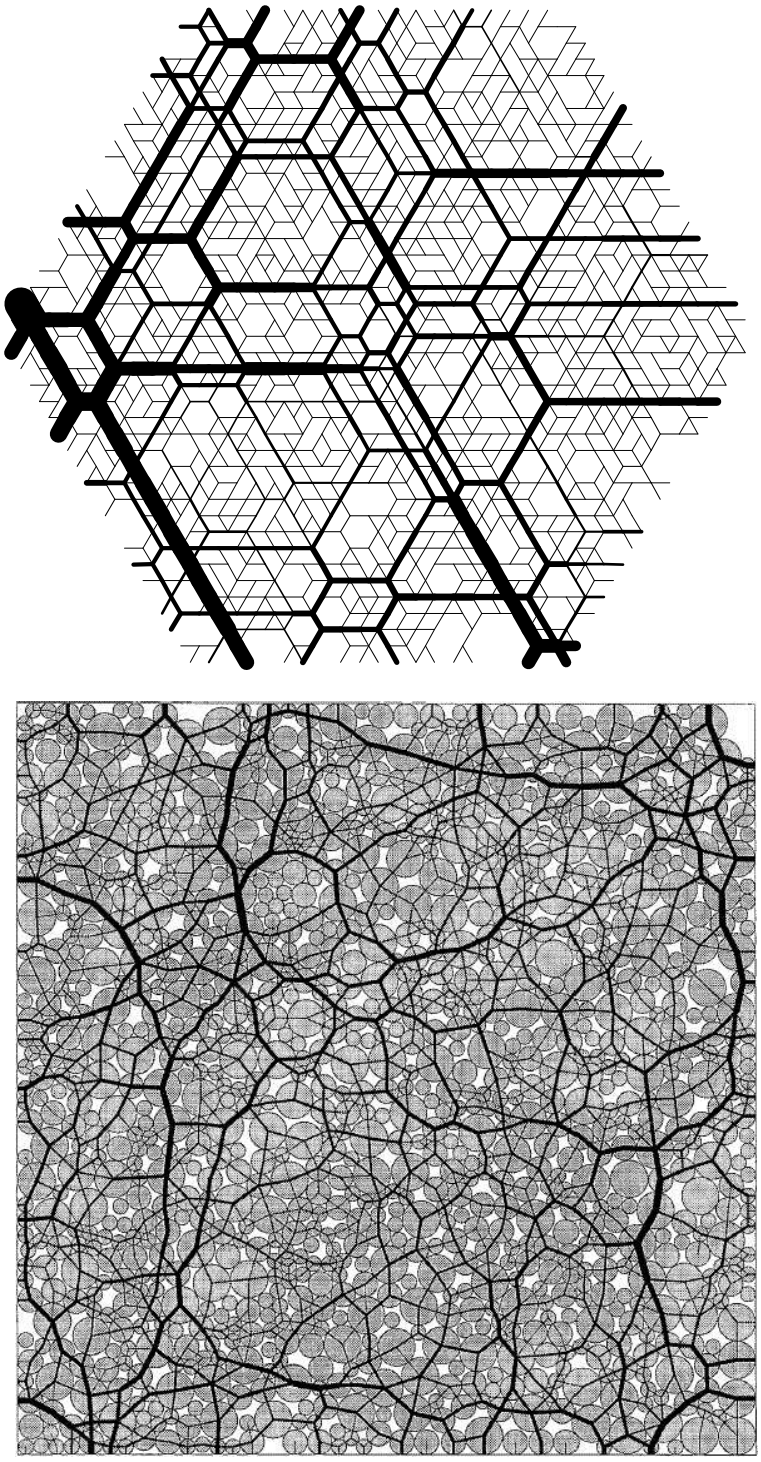

Figure 1.6: The above figure is taken from Ref. [Roux00] shows the force network of a hexagonally packed frictionless granular assembly with small polydispersity. The lower figure shows a typical result obtained by a contact dynamics method from Ref. [RJMR96]. In both cases the thickness of the lines indicates the value of the force.

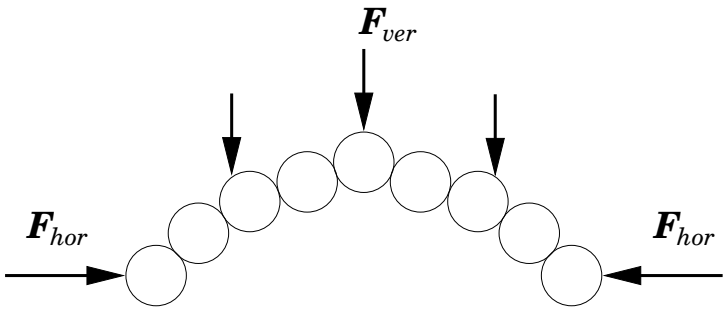

Figure 1.7: Illustration of an arch. The above load is finally supported by the two extreme particle and horizontal forces.

tion and rules of force transition are defined among the sites. Both scalar (q-model) [CLM+96, ClaBou97, CBCW98] and vectorial [HHR97] versions of this idea were introduced.

All forces that are exerting on a site (including gravitational forces) are redistributed among its neighbours in a random way. In the scalar version only the vertical components are taken into account while in the vectorial version the remaining horizontal component of the force is assigned to the horizontal neighbouring site.

In spite of the simplicity of these models they successfully account experimental results especially the dip in the normal force under the heap of a sandpile. The scalar model can be solved analytically and gives a parabolic equations for stress transmission.

Arching

The phenomena called arching is a direct consequence of the force chains. The strong normal forces enable the chain of particles to sustain relatively high tangential forces (Fig. 1.7) and thus bridge over distances much larger than the particles size [DKV98, Louge96]. This behaviour is responsible that in silos the pressure on the bottom does not increase above a certain height of materials [ClaBou97, VCB+00, VanCle99].

An other interesting property of the arches that they can protect the underlying structures from mechanical effects. The relatively high normal forces in the arching chain enable them to support high tangential friction forces thus protect easily deformable regions [TKKR00a]. This is the so called screening effect.

Arches play important role in the dynamical processes. They may keep together small domains of particles which move together [DML96].

1.3 Dynamical properties: Shearing

There are a number of interesting dynamical processes studied in the literature like: Flows (chute, shear, in tubes, ...), shaking (vertically, horizontal), fluidization, shear (triaxial experiments, compaction, ...), avalanches, etc. (see e.g. [HHL98, JNB96, JaeNag92]). However, in this brief introduction we focus only on shearing processes which is the main subject of the thesis.

1.3.1 Continuum solid mechanics

Shear is the most studied among all dynamical processes. If we apply forces to static granular samples the most common response is a shear that may only be a local process. The mechanical properties of a material are usually tested by rheological experiments. Parameters determined from rheological and triaxial devices consists the basis of the classical solid mechanics description [Wood90, WooBud80].

Using continuum solid mechanics, modeling the rheology of granular media has reached a high degree of sophistication in terms of constitutive equations. Whatever the complexity of load paths being studied, an accurate account of experimental stress strain relationship can now be achieved provided enough parameters or internal variables are included in the description of the behavior laws [Wood90]. However, such approaches are descriptive and leave unanswered questions pertaining to the scale of grains.

1.3.2 Dilatancy versus compaction

The dilatancy concept of sheared granular materials was introduced in the last century by Reynolds [Reynolds85]. This implies that compacted sand must expand in order for it to undergo any shear. In a close packed sample there is not enough free space among particles for their relative movement thus it has to be created via dilution. This dilution is not done in a uniform way but it is localized in a narrow domain, in the shear band [PABT92] [Fig. 1.8 a)].

In contrast if we consider a loose packed sample the sample contains enough space for particles to move. Moreover, as the denser configuration of granular packing is more resistant the whole sample will densify with increasing shear strain [TKKR00a, LMP00, NicPou00] [Fig. 1.8 b)].

The shearing process in granular materials is thus a competition between two phenomena: The dynamical movement of the particles allows for a reorganization of the packing to a more resistant, denser state. Meanwhile, the relative motion of the particles due to geometrical constraints needs free space for moving that involves dilatancy. The resolution of this duality lies in the different behaviour for dense and loose samples.

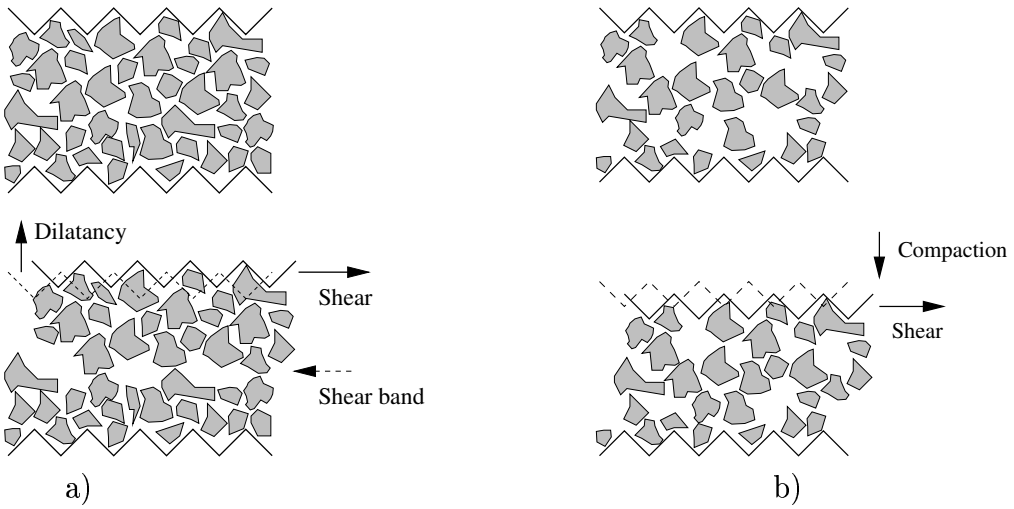

Figure 1.8: a) During shearing of compacted granular materials the relative motion of the particles can only be realized if the sample is diluted in a region (shear band) to have enough space for the randomly placed particles to move respect to each-other.
b) Shearing of a loose sample will have tendency to bring the sample in a more compacted state which is resistant against shear. This is done in a more homogeneous way thus no shear band is observed.

In dense samples after a threshold of shear forces the stress is released via internal motion of particles which induces dilatancy in a narrow domain in the shear band. This region becomes thus less dense and resistant than the rest of the sample (in ref. [OnoLin90] Onoda *et al.* shows experimentally that the loose packing limit of granular materials can be found inside the shear band) thus easier to shear. In other words the position of the shear band is lasting in dense granular materials.

In loose samples the motion of particles in a narrow domain induces compactification thus the material gets more resistant, activity thus repelled to other regions and finally the whole sample gets denser to a critical state [LamWhi68, PLR00]. As the activity takes place in the whole volume no distinct shear band can be found [SMB97, ZolChe92, AhaSpa99]. However, this process is more complex and its detailed study it can be found in the next chapter.

Let us note here that the above train of thought is valid only if the volume of the sample changes according to the inner changes and the particles are rigid. If the size of the container is fixed another scenario can be observed [VHB99, HBV99]. In this case in the low density limit the system is able to organize itself in such a way that the greater part of the particles are closer to the not moving wall [SKW00] while only a small portion of particles are moved. However, if the system is dense a stable shear band cannot form. Instead one can find locally rearranging particles producing thus a more homogeneous behaviour but for this elastic particles are needed [HBV99].

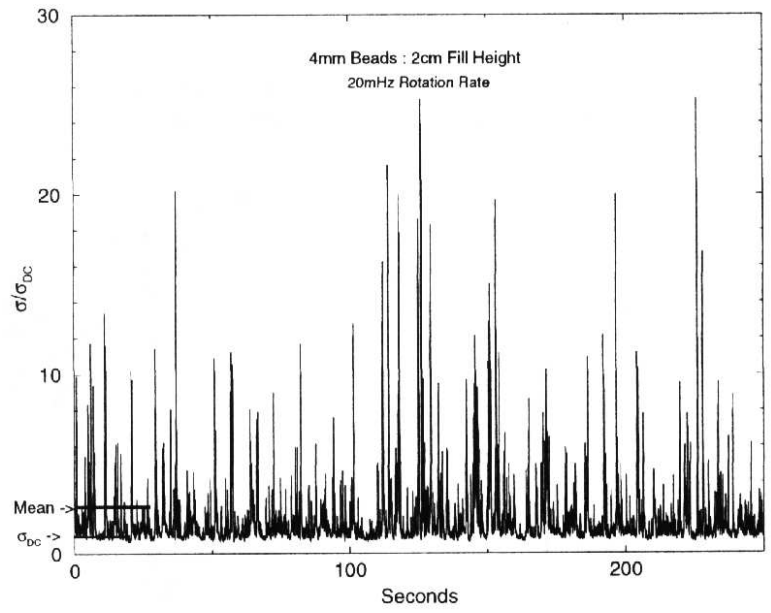

Figure 1.9: Normal stress measured under a continuously sheared granular bed from Ref. [MHB96]. Note that fluctuations orders of magnitude larger than the average can be observed.

1.3.3 Fluctuations

As discussed in the previous section shear in granular materials means particle packing reorganization. Even in the most simple tests, such as steady simple shear imposed over large strains, the local displacement fields appears very unsteady, with short quiescent periods where the displacement field is spatially smooth separated by sudden change where the configuration of grains reaches a local instability, and undergoes of rapid reorganization through significant displacements at the grain level. This temporal variability manifests itself in giant stress fluctuations observed experimentally when particles and walls are stiff, and when the high frequency part of the stress signal is not filtered out [MHB96].

Local fluctuations may have macroscopic manifestation like the position of the shear band. When a granular sample reaches its macroscopic yield limit, for a homogeneous loading, plastic strain localizes on a shear band. For a homogeneous medium this point is a bifurcation point with a high level of degeneracy. In two dimensions, shear bands are straight lines, but although their orientation is fixed, their location is not. Disorder, of any amplitude, will break this degeneracy and lead to a unique geometry of this first shear band [TorRou00].

Static manifestation of the macroscopic appearance of the fluctuation can be observed e.g. on the pressure on the bottom in a silo considering the same amount of powder [BroRic66] which may vary by 20%. This weight furthermore changes very

abruptly when temperature changed by only a few degrees Celsius, which induces only very small ($\sim 10^{-5}$ grain diameter) changes of the grain size [CBCW98, ClaBou97, Liu94, LiuNag93].

1.3.4 Slow dynamics

Relaxation processes in granular material are in general extremely slow (See Fig. 1.10). However, the issue of slow dynamics, rare events and anomalous diffusion is object to ongoing research in statistical physics [BouGeo90, DMF99, LalDou98, RajMor98, SchSok98, KNT99]. One example of slow dynamics is the compaction of granular materials due to shaking. Experimental [KFL+95, NKB+98], numerical [NCH97, CLHN97, LMP00] and theoretical [NKB+98, BPA99] analyses show that compaction due to vertical vibration is logarithmically slow. The reasoning presented in Ref. [NKB+98] illustrates in a nice way how the effect of free volume can lead to the observed logarithmic behaviour.

If each grain has a volume V_g and we start with a number n of grains per unit volume, then the volume fraction is given by $\varrho = nV_g$. In general there exists a maximum possible volume fraction, $\varrho_{\max}$, corresponding to the configuration of grains that occupies the most amount of volume. Then, at some volume fraction ϱ, the average free volume available to each grain for rearrangements is $V_f = V_g(1/\varrho - 1/\varrho_{\max})$.

During compaction, individual hard-core grains move, and when a void large enough to contain a grain is created, it is quickly filled by a new particle. When the volume fraction is large, voids the size of a particle are rare and a large number of voids must rearrange to accommodate an additional particle. We can estimate the rate of compaction by assuming that N grains must rearrange in such a way that they contribute their entire free volume to create a grain-sized void, $NV_f = V_g$. We find that this number increases as $N = \varrho\varrho_{\max}/(\varrho_{\max} - \varrho)$ during the compaction process. For independent, random grain motion during a tap, the probability for N grains to rearrange and open up a grain-size void is then e^{-N}. Consequently,

$$\frac{d\varrho}{dt} \propto (1-\varrho)e^{-N} = (1-\varrho)e^{-\varrho\varrho_{\max}/(\varrho_{\max}-\varrho)} \tag{1.1}$$

The rate at which the density increases is proportional to the void volume and the probability for such a rearrangement. The latter exponential factor reduces the rate and dominates for large ϱ. In the limit $\varrho \to \varrho_{\max}$ we have $N \simeq (\varrho_{\max})^2/(\varrho_{\max} - \varrho)$ and the solution of this equation is given asymptotically by

$$\varrho(t) = \varrho_{\max} - \frac{A}{B + \ln(t)} \tag{1.2}$$

where A and B are constants. This formula was verified for vertical shaking both numerically and experimentally as shown on Fig. 1.10 a).

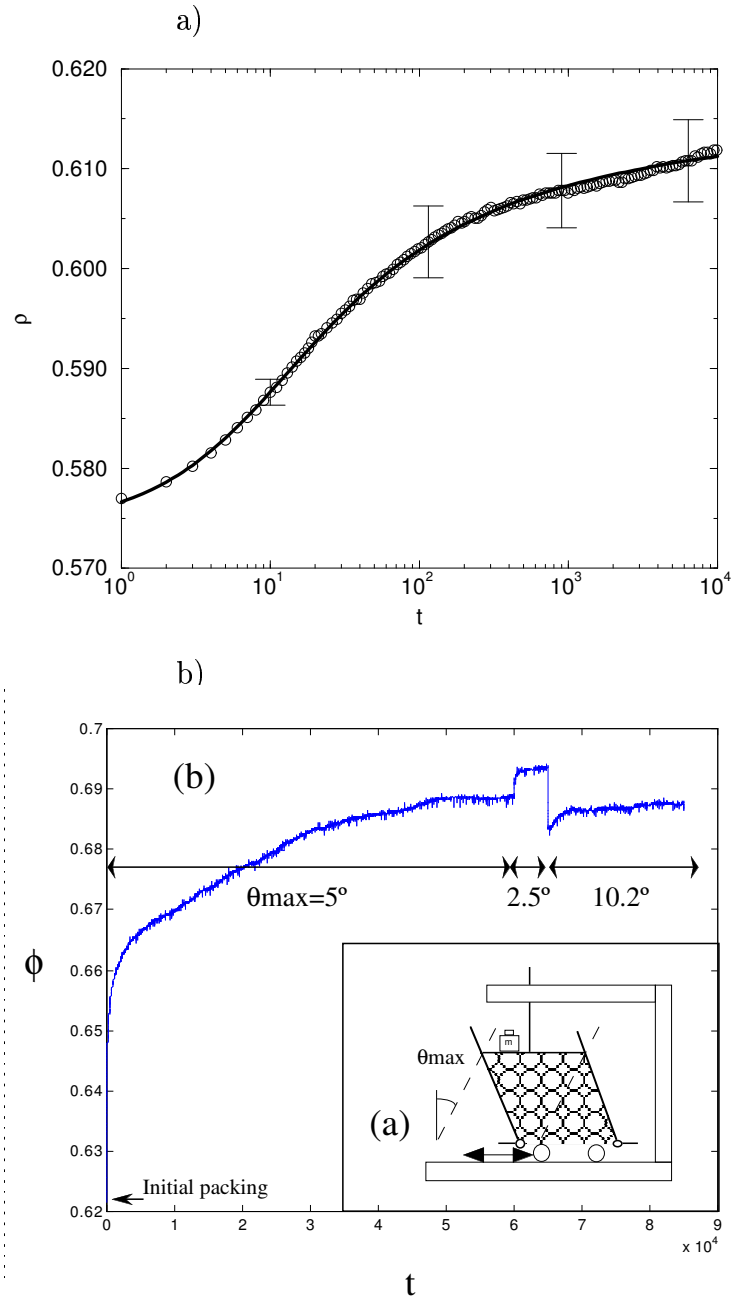

Figure 1.10: Time evolution of packing fraction in a) shaking, b) shearing.
a) Experimental results taken from Ref. [BKN98]. The maximal acceleration in the experiment was $\Gamma = a_{\max}/g = 2.3$ and the data was measured near the bottom of the container. The solid line is a fit of Eq. 1.2.
b) Experimental result of periodic shear from Ref. [LMP00]. The sketch of the apparatus is shown in the inset. The step in the curve is due to a change of the shearing amplitude forth and back. The response to this change of excitation is typical for ageing in glassy materials.

The above presented train of thought of geometrical frustration of the grains in a granular packing also holds for the shearing process of loose granular materials. Moreover, in the vertical shaking all particles have the excitation energy to rearrange while in shearing only particles belonging to the shear band have the possibility for relative motion respect to their neighbours. Shear band was shown to be a narrow domain of some $10 \sim 20$ particles [AHT00] so the shear band has to visit all parts of the sample to give the possibility for a global density increase [TKKR00a, TKKR00b]. However, with the ascendent density the nature of the shear band gets more and more localized slowing down the relaxation process [TKKR00c, LMP00]. We expect thus that compaction due to shear will be even slower than that due to shaking.

Let us mention here a recent model of S. Luding *et al.* [LMP00] where based a glassy like random energy landscape model a very good description of the slow relaxation process can be obtained can be obtained reproducing also the ageing properties observed experimentally [LMP00, NicPou00].

1.4 Brief review of relevant statistical physical models

1.4.1 Directed polymers

Within the province of condensed matter physics, there exists a variety of interesting physical situations where we are concerned with the statistical fluctuations exhibited by an essentially linear elastic object such as longitudinally stretched polymer or DNA in a gel matrix, vortex lines in ceramic super-conductors and dislocation lines in disordered solids [H-HZ95].

The directed polymer model consists of the dynamics of a line stretched longitudinally (t direction) in such a way that the longitudinal distance between the two ends is constant but transversal fluctuations are allowed including the displacement of the ends. In a continuum formulation the directed polymer in a $n+1$ dimensional random medium is conveniently described by a vector field $\boldsymbol{x}(t)$. Its mechanical properties with fixed ends are described by the restricted partition function:

$$Z(\boldsymbol{x},t) = \int_{(0,0)}^{(\boldsymbol{x},t)} \mathcal{D}\boldsymbol{x} \exp\left(- \int_0^t ds \left[\frac{1}{4\Gamma} \left(\frac{d\boldsymbol{x}(s)}{ds} \right)^2 - \mathcal{V}(\boldsymbol{x},s) \right] \right), \tag{1.3}$$

where Γ is the diffusion constant or inverse line tension and $\mathcal{V}(\boldsymbol{x},t)$ a position dependent function meant to mimic the role of the local pinning impurities of the medium and will be referred as potential. The most tractable and thus most widely chosen disorder is assumed to be uncorrelated with zero mean and variance:

$$\langle \mathcal{V}(\boldsymbol{x},t)\mathcal{V}(\boldsymbol{x}',t') \rangle = V^2 \delta(\boldsymbol{x}-\boldsymbol{x}')\delta(t-t') \tag{1.4}$$

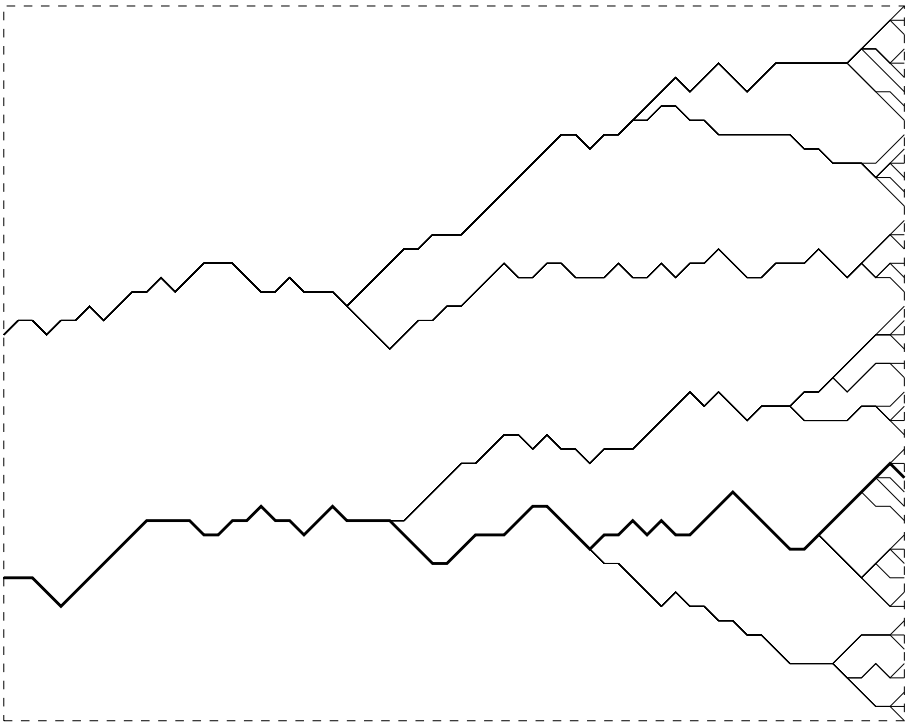

Figure 1.11: Locally optimal paths in a $64x50$ tilted square lattice reaching the right hand side of the sample. The global optimum is marked with a thick line.

The lattice version of the model is defined similarly but with sums instead of integrals.

$$Z(\boldsymbol{x}, t) = \sum_{\mathcal{P}\in\Omega} \exp\left(-\frac{1}{T}\sum_{i\in\mathcal{P}} \varepsilon_i\right), \tag{1.5}$$

where Ω denotes the ensemble of all directed path with fixed ends [the origin $(0,0)$ and $(\boldsymbol{x}, t)$] on the lattice a random potential ε_i is assigned to each bond (site). The missing kinetic term is taken into account by the rules of the dynamics that for each step in the forward direction only one bond step is allowed in the transverse directions.

The physical quantity of immediate interest is the wandering exponent ζ which is defined via the relation $|\boldsymbol{x}| \sim t^{\zeta}$. This describes the roughening of the directed polymer in random media resulting from a competition between the line tension which discourages deviations from linearity, and the pinning potential which causes the directed polymer to wander in an ever-increasing fashion from the central axis, in search of optimal energy configurations.

It was shown by Huse and Henley [HusHen85] and Kardar [Kardar85] that for the $1+1$ dimensional directed polymer problem the above exponent is $\zeta = 2/3$.

Let us note that the first results concerning this problem were at the $T = 0$ limit. Unlike to other well known quenched disordered systems like spin glasses in this

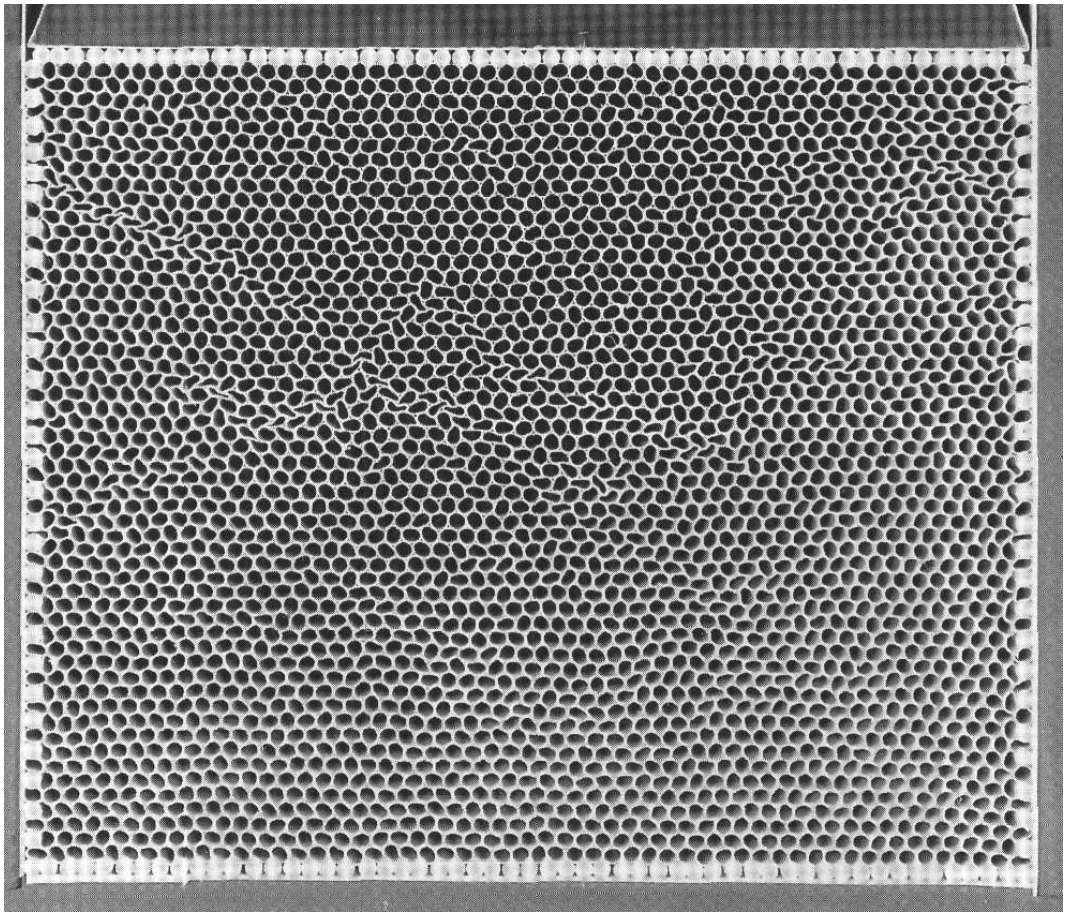

Figure 1.12: A snapshot of the experiment of Ref. [PABT92] where hexagonally packed drinking straws were uniaxially compressed. The figure illustrates the rough, localized band of deformation (crushed straws) wandering across the sample.

model the global minima can be found by the transfer matrix method (see [DVP78] and Appendix A).

The zero temperature limit of this model is also of interest. It was shown in many brittle fracture experiments that the ground state of the directed polymer can be relevant in describing these phenomena, like paper tear [Kertesz92, KHW92], blown fuse network [HHR91] or deformation localization [MHHR92, PABT92]. In these experiments some kind of "load" has to be born by a number of coupled elements with locally fluctuating threshold values. Up to the point when the first threshold is reached the load is more or less homogeneously distributed among the elements. Once the load upon the weakest element is larger than the maximal value it has to be redistributed among the neighbouring sites. The load can be increased until the elements reaching their threshold value percolate across the system. It is natural to suppose that the realized fracture path across the sample is the minimal path that is

in other words the ground state of a directed polymer in a random potential where the potential is the local threshold values.

In this present work the above idea was used to describe the shear band in a sheared granular material.

1.4.2 Active random walks

The motion of random walkers in a random environment is one of the basic problems in the physics of disordered systems [ABSO81, HavAvr87, BouGeo90, BCGD90, Sinai82, DMF99]. It is known that the effect of the environment on the walker results in anomalous diffusion in some cases and logarithmically slow diffusion in others [ABSO81, Sinai82]. Apart from their intrinsic interest, these simple models also find applications in several physical processes, such as the diffusion of electrons in a disordered medium [BBSA79] or glassy activated dynamics [DMF99]. In particular, the Sinai model [Sinai82] has been extensively studied from this point of view. It is known that for this model, the walker becomes logarithmically slow, moving as $R(t) \sim \log^2(t)$ where $R(t)$ is the average distance at time t of a walker from the launching point. Apart from this, two-time aging dynamics studied in this model also provide close analogies to glassy phenomenology [DMF99].

In another framework, a "trapping" model ([MonBou96] and references therein) was introduced to provide a simple example of the glass transition. A single walker explores a random landscape of energy traps with e.g. an exponential distribution, from which it can escape through activated hops. At low temperatures, it was shown that the system cannot reach a steady state due to the unfavorable competition between the depth of the visited traps and the time needed to escape from them. The corresponding slow dynamics, and disappearance of an equilibrium state was interpreted as a glass transition. In this mean-field model, introducing an interaction between the walker and the random energy landscape was shown to not change the results [MonBou96]. However, the fact that the trapping time distribution is a power-law provides a natural (statistical) history dependence. (The dynamics is controlled by the deepest energy well visited so far).

Active walker models where the walker and the environment mutually affect each other have been studied earlier in different contexts. One such model — the Eulerian Walkers Model (EWM) — has been studied [PDDK96] within the framework of self-organized criticality (SOC) [BTK87]. The "landscape" here is defined by an arrow at each site. The walker follows the direction of the arrow at its site after which the direction of the arrow is changed according to some fixed rules. Besides many correspondences between the EWM and the Abelian Sandpile Model of SOC [Dhar90], it was also shown that the motion of the walker was sub-diffusive in two dimensions, *i.e.* $R(t) \sim t^{1/3}$. In one dimension, $R \sim t^{1/2}$ due to a very simple organization of the landscape under the rules. For $d > 2$ it was argued that the walker is diffusive.

Active walker models were frequently used mainly in biophysical and sociological concepts describing collective motions and pattern formation like bacterial colonies [BST+94] or human or ant trial systems [HSK+97]. In the case of bacterial colonies the potential field was the concentration diffusing chemical material emitted by bacteria. While in the trial systems the walker modified the path in such a way that the previously used paths were potential wells easier accessible for other walkers. In both cases the authors focused on collective phenomena and objects created by the walkers. In Chapter 4 however, we will focus on the potential landscape created by a sole walker and on its mean square distance from the origin.

We also mention here the model of "True" Self-Avoiding Walk (TSAW) that was introduced in a different context [APP83] but belongs to the class of the active walks. The definition of the TSAW model is the following: The walk takes place on a d-dimensional hypercubic lattice. At any step the traveler may move to any of the $2d$ nearest neighbours of the lattice site he is at. The probability of stepping to site i depends on the number of times n_i this site has already been visited and is given by

$$p_i = \exp(-gn_i) \left[\sum_{i=1}^{2d} \exp(-gn_i) \right]^{-1}, \tag{1.6}$$

where the sum runs over all $2d$ nearest neighbours of the current position of the walker, and g is a positive parameter which measures the intensity with which the walk avoids itself. Let us comment that the sum over i of p_i is equal to 1, meaning that the traveler never stays at the points.

The model was introduced to study the Self-Avoiding Walk problem at the $g \to \infty$ limit but was found also interesting as it is defined. Moreover, this model can be solved exactly as was done by Bálint Tóth [Toth94, Toth95] and the value of g does not change the scaling properties of the system.

Chapter 2

A model of shearing

2.1 Definition of a statistical model for shear

We will address here the question of the behavior of granular media subjected to a simple shear for large strains. We restrict ourself to the simplest granular media one may consider, namely rigid (undeformable) grains with Coulomb friction. This refers experimentally to dry sand subjected to a low confining pressure. We are concerned here with large strains, and thus in order to avoid the problem of boundary conditions which would limit the maximum strain, we consider an annular shear cell. To simplify the problem further, we consider only the case where the problem is invariant along the shear direction. As shown in Figure 2.1, the displacement will be a single function of the coordinate of a radial cross-section (x, y), and constant along the orthoradial direction z. Moreover, we are interested only in the quasistatic regime, i.e., time as such is irrelevant, and only the total strain matters. Thus, in the sequel, the "time" which will be referred to is only seen here as a practical means to parameterize the total strain being imposed on the medium.

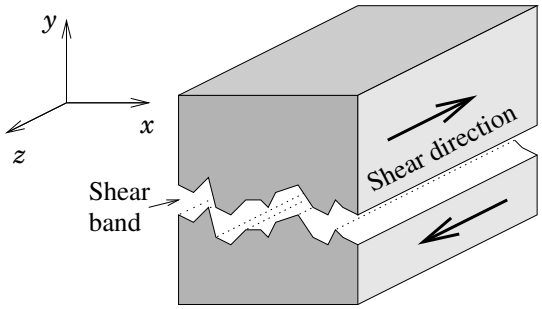

Figure 2.1: Schematic picture of the shear process. The shear band is parallel to the shear direction z due to the periodic boundary conditions in this direction. We sum up along this direction to get a two dimensional sample in the xy plane.

One of the important observations of soil mechanics concerning such media is the concept of critical state [LMP00, NicPou00]. Depending on the preparation of a sample, the behavior under shear may differ considerably. For loose sand, (low density), the deviatoric stress to apply increases with the total shear strain and simultaneously, a densification is observed [LMP00, NicPou00]. However, as the shear train increases, the density and shear stress seem to reach a plateau independent of the initial density. This state is called the "critical state". On the contrary, if the initial density is large, a single shear band forms, while the rest of the medium remains frozen. The apparition of the shear band is preceded by volume expansion of the medium, but as the band is formed, all further properties remain quasi constant. A detailed experimental investigation has recently revealed that inside the shear band, the density tends to approach the "critical" density estimated on similar materials prepared in a loose state. This concept of the critical state has received considerable experimental evidence over the years, and is implemented in a number of continuum constitutive laws. Let us finally add that a large part of experiments deal with rather moderate total strain well below unity.

A simple picture which is consistent with the critical state concept is that both the friction and the dilution angle increase with the density, and that the critical state is the density for which the dilution angle is zero (no change in volume under shear). Retaining the density as the only internal variable is an approximation. Other characteristics of the texture of the medium such as the fabric tensor (giving informations about the orientation of contact normals), certainly play a significant role. For the purpose of simplicity, we will in the following only retain one single scalar internal variable governing the friction angle. It could be either simply the density or a combination of density and texture. Nevertheless, in all cases we will refer to this internal variable as "density", irrespective of its precise meaning. From what we mentioned, we already see that the critical state concept seems incompatible with the observation of instantaneous shear bands occurring in loose granular media as shown by numerical simulations [SMB97]. Indeed, for loose packings, we mentioned that in experiments the strain appeared to be homogeneous, and not localized. The only way to conciliate both observation is to note that the shear bands occurring during small time intervals would visit the entire sample so that under "time" averaging, a homogeneous strain field would result. But this turn implies that a certain variability is incorporated in the local description. Starting with a homogeneous continuum description will only produce either a homogeneous strain field or a localized shear band which will last for a long time. Therefore we will implement in our model for shear some randomness susceptible to evolve under a very quick time scale. As long as a single internal variable, the density, is used it is the field which will display these local random fluctuations. Thus at every instant of time, the state of the medium will be characterized by a density $\varrho(x, y)$ in a two dimensional description,

which represents an average of the density along the orthoradial direction z. From this density, we deduce a corresponding local friction coefficient $\mu(x, y)$. The latter is assumed to be a single function of the density, which is monotonously increasing [HJV96]. For simplicity, we will assume a linear relationship in the following although this is unessential.

The strain is imposed on to the shear cell through prescribed displacements on the bottom and top planes. As particles are considered rigid, (no elastic deformation), the shear cell can only move if the shear force exceeds a threshold value proportional to the normal pressure. This limit stress is given by the "weakest internal surface". Indeed, in our anti-plane geometry, the shear strain will localize on the surface (i.e. path in the (x, y) plane) which will fail first. The latter is assumed to be given by the following problem. For each path $\mathcal{P}$ spanning through the entire cross-section along the x-axis, we compute the maximum shear force it can support according to the local density. Assuming the local slope of the path is always small, this maximum force $F(\mathcal{P})$ is simply proportional to the sum of local friction coefficients, and thus making use of the assumed linear variation of the friction coefficient with the density, $F(\mathcal{P})$ is proportional to the sum of local densities,

$$S(\mathcal{P}) = \sum_{(x,y)\in\mathcal{P}} \varrho(x, y) \ , \tag{2.1}$$

where the sum runs over the sites of the path. Among all the possible paths, the weakest $\mathcal{P}^*$ will fail first, and thus it fixes the value of the shear force $F = F(\mathcal{P}^*)$. In agreement with the previously mentioned observation, at the basic time step, the shear strain is localized along a single shear band. Away from this shear band, the strain rate is zero, and thus the density is kept constant in time. However, inside the shear band, there is a relative motion of grains, and thus the density is susceptible to evolve.

Even though it is observed that large strains are necessary in order for a system to reach its critical state, we argue that at the microscopic level, the evolution of the medium *cannot* depend on the total imposed strain. Thus the evolution rules for the density within the shear band should be designed in such a way that they are independent of the entire history. As the density should contain the basic variability of the local characteristics, we propose that within the shear band, the local density $\varrho(x, y)$ is randomly modified. More precisely, in one elementary time step, corresponding to the "life-time"[1] of the shear band, we assume that the density along the shear band in loose granular media, acquire random uncorrelated values picked from a statistical distribution $p(\varrho)$.

This is a key assumption of our model which may appear as precluding the occurrence of a slow evolution toward a critical state. In fact, we will show below that, on

[1]We will not discuss the value of the "life-time" of a shear band. We consider it as being a constant defining our microscopic time unit.

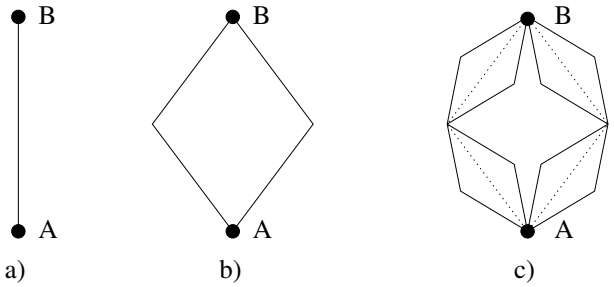

Figure 2.2: The 0th a), 1st b) and 2nd c) generations of the hierarchical lattice.

the contrary, a collective and purely statistical effect will produce a slow increase of the macroscopic friction coefficient over large strains. This will be one of the major conclusions of the model we propose here.

Thus after this elementary strain event, we have a new density map $\varrho(x, y)$. We now simply reiterate this procedure as long as desired: Namely we identify the path which minimizes $S(\mathcal{P})$, and we update the value of the densities along this path randomly. As the purpose of the present article is to illustrate some statistical aspects of the model, we do not try to mimic any specific granular system, and thus we will choose here simple examples for $p(\varrho)$. We will consider either a uniform distribution between $[0 : 1]$, or a Gaussian distribution. The mean value and amplitude of the distribution p can be chosen arbitrarily, since a translation and rescaling of ϱ does not affect the result.

Our model is further discretized on a lattice. Regular square and hierarchical diamond lattices were used. The latter had the aim to solve analytically our model on it in the asymptotic limit. In the following section we present the numerical data of the hierarchical lattice together with the regular sample to visualize their similarity and justify thus the relevance of the analytical solution on the hierarchical lattice.

The hierarchical diamond lattice is constructed as follows: Let us take a line that connects two points A and B. To get the first level hierarchical lattice we replace the line with a diamond [Fig. 2.2 b)]. In the next step [Fig. 2.2 c)] we replace the lines of the diamond by a diamond itself. Repeating the above procedure N times will create the next generation of the hierarchical lattice that we note by N.

We used also two kinds of regular square lattices leading to the same results. In the first one the value of the density ϱ is carried by the bonds. The interface is lying preferentially along the x axis. The orientation of the lattice is chosen so that the principal directions lies at $\pi/4$ with respect to the (x, y) axis as shown on Fig. 2.3 a). In the other version the value of the density were assigned to the sites of a square lattice. In this case the minimal path can be connected through the next nearest neighbours too as shown on Fig. 2.3 b).

Appendix A describes the algorithm used to determine numerically the position

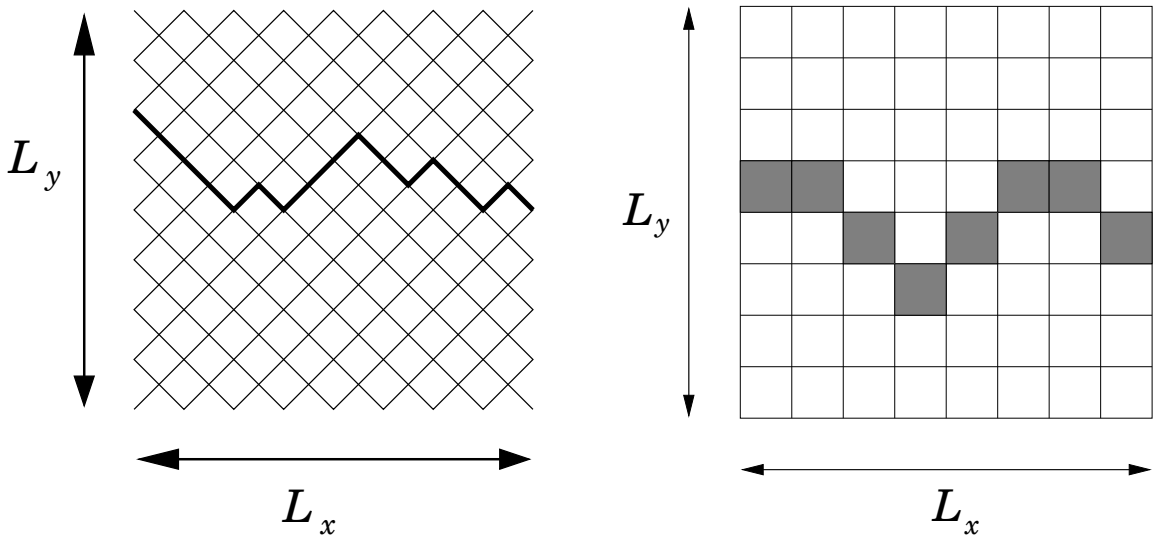

Figure 2.3: a) Visualization of the tilted lattice. The shear band is marked with a thick line.
b) A sample configuration of the minimal path on the normal square lattice with densities assigned to sites.

of the shear band.

2.1.1 Relation to other statistical physics models

Before reporting the result of numerical simulations of our model, we point out a few analogies which can be drawn with classical problems of statistical physics of non-equilibrium phenomena.

The rules of our model at every instant are the same as those of the directed polymers [H-HZ95] when we are interested in its ground state: We search for the minimal directed path in a random potential. However, in our case this potential is not *a priori* frozen and has a self-organized development. From this analogy we can state that our shear band is self-affine with an Hurst exponent $\zeta = 2/3$ at the beginning, i.e. the fluctuations grow with the size (L) of the polymer as L^{ζ}.

Let us also remark that our model in its rules can be regarded as some kind of two-dimensional generalization of the Bak-Sneppen model of evolution [BakSne93]. The Bak-Sneppen model is defined on a one dimensional periodic array of numbers where in every turn the least and its neighbours are updated from a given time independent probability distribution. They found self-organized criticality in that model, i.e. a scaling statistics of the connected events (avalanches).

In spite of the similarities there are essential differences. In our model we change the values only of the sites belonging to the minimal path. Changing the neighbours

leads to trivial behavior in two-dimensions. In one dimension, one can define an avalanche in the following way: an avalanche ends when the minimal site is not among the previously refreshed sites but somewhere else, i.e. not connected to the first refreshing that triggered the avalanche. In the two dimensional version the first avalanche survives forever because the number of the refreshed sites is too large. No interesting feature can be observed as nothing really changes in that variant of the model.

On the other hand, if we modify the one dimensional Bak-Snappen model to be the one dimensional specific case of our model, namely in a one dimensional array we update only the minimal site and none of the neighbours, we get a useful and interesting model which, as we will see contributes a lot to the understanding of our two-dimensional model, though self-organized critical behaviour gets lost.

2.2 Numerical results on the square lattice

2.2.1 Definitions

Let us define here the quantities we measured numerically.

The most important one is the *average density* of the sample that we define as the mean of the density of the inactive sites, i.e. the sites not belonging to the shear band, and we denote it by $\langle \varrho \rangle$. This definition is convenient as this quantity is monotonously increasing by the rules of our model. In experiments one of the most often measured quantity is the volumetric strain which is just the change in the inverse of the average density.

It is also natural to define the *density of the shear band* that we denote by ϱ_{SB}. As already mentioned in the introduction we assume that the maximal static shear force is a single function of the density in this concept. Thus the density of the shear band can be related to the shear stress in experiments.

We also use the *Hamming distance* of the shear bands which is defined as the average number of different sites (or bonds) between successive shear bands and denote by d.

An other experimentally important quantity is the *cumulative shearing* that we note by σ_{cum}. This can be measured if initially one marks a straight line perpendicular to the shear plane. This line is deformed during the shear and its derivate indicates the local velocity.

The numerical procedure we follow to obtain this quantity in our model is the following (see Fig. 2.4): We consider a vertical cut of the system perpendicular to the shear band. At every site along this line, we define a quantity (the cumulative shearing) σ_{cum} which is the sum of the total activity to the left of this line (the number of times the shear band was there). It is more convenient to subtract the mean value

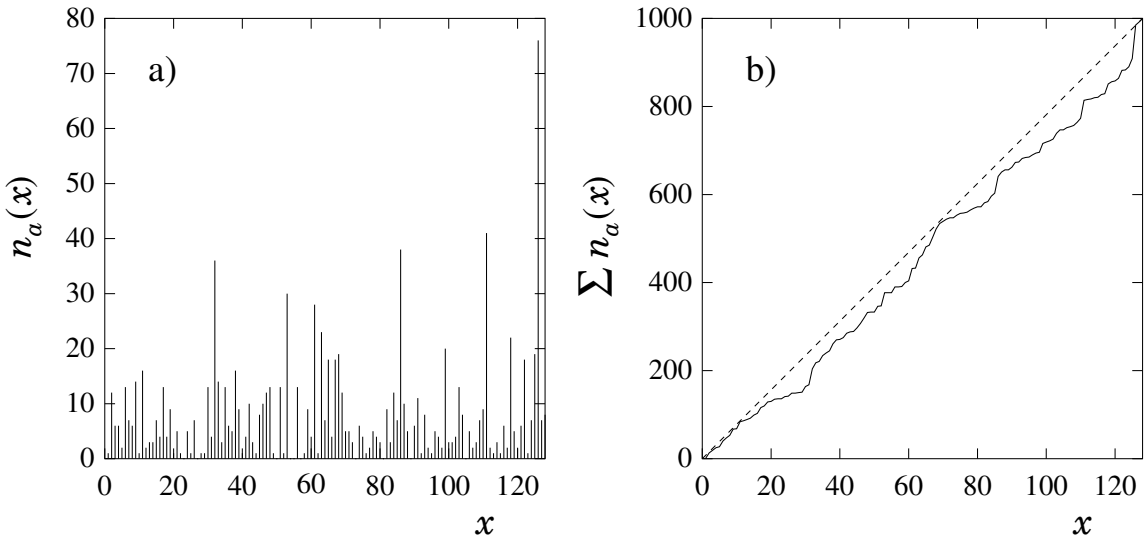

Figure 2.4: Demonstration of the numerical calculation of the cumulative shearing σ_{sum}. Figure a) represents the number of times (n_a) a site was active up to time $t = 1000$ in a cut on a 128 by 128 sample. Figure b) is the cumulative representation of a): $\sum_{j=0}^{i} n_a(i)$. The dashed line indicates the homogeneous case.

from σ_{cum} which is a straight line with a slope determined by the displacement of the moving boundary and the height of the sample. Thus the resulting curves start from 0 and end also there (see later in Fig. 2.9).

In the following we study the time evolution of the above defined quantities.

2.2.2 Early time regime

It is apparent from 2.5, 2.6 and 2.7 that the initial behaviour of the model is very different from the late stages. In all of the above showed figures a very nice t/L scaling can be observed and all of the quantities starting with a plateau on the log−log plots that lasts about $t_{c1} \simeq 2L$ irrespective of the lattice type and of the considered quantity.

The distance d (Fig. 2.7) is equal to the system size indicating that in this regime successive shear bands do not overlap, in other words there is a strong repulsive interaction between them.

The density of the shear band (Fig. 2.6) provides an answer for this behaviour. From the directed polymer [H-HZ95] analogy it is known that the first shear band has a mean density of $\varrho_{SB}(t = 0) \simeq 0.22$. The state of the shear band after refresh is independent of its previous state so the mean density of the first minimal path after refresh will vary around 0.5 with a very narrow distribution (sum of L independent random numbers).

As initially there are multiple local minimal paths with more or less the same

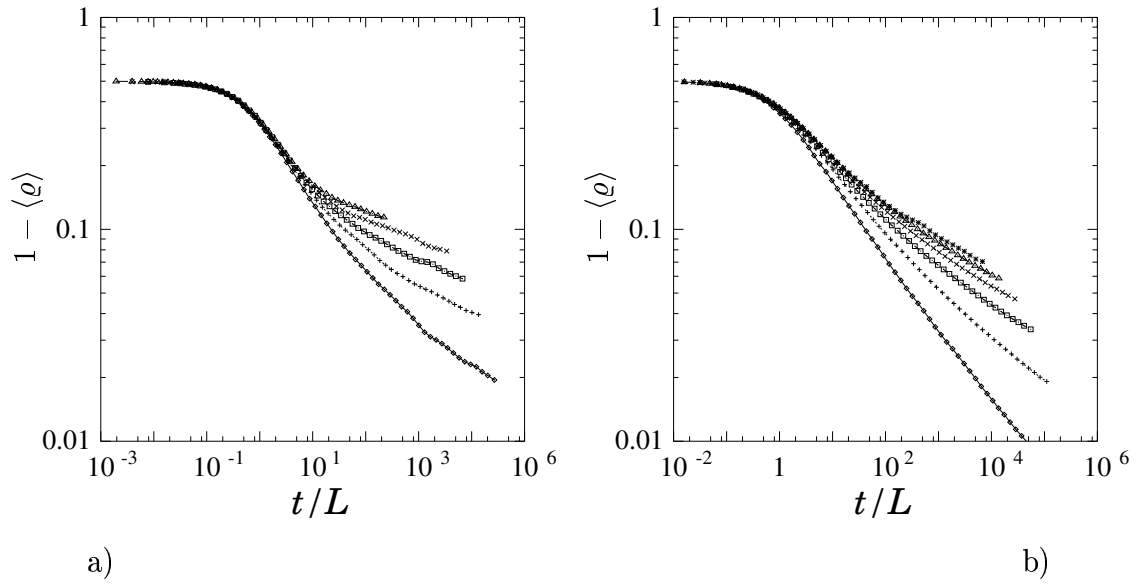

Figure 2.5: On these graph the difference of the average density from its asymptotic value 1 is plotted as the function of time. The system sizes are $L = 32$, 64, 128, 256, 512 for the square lattice (left) and $N = 2$ to $N = 7$ for the hierarchical lattice (right) from bottom to top respectively. The average was done for the inactive sites in a lattice and for an ensemble of 20 to 1000 samples.

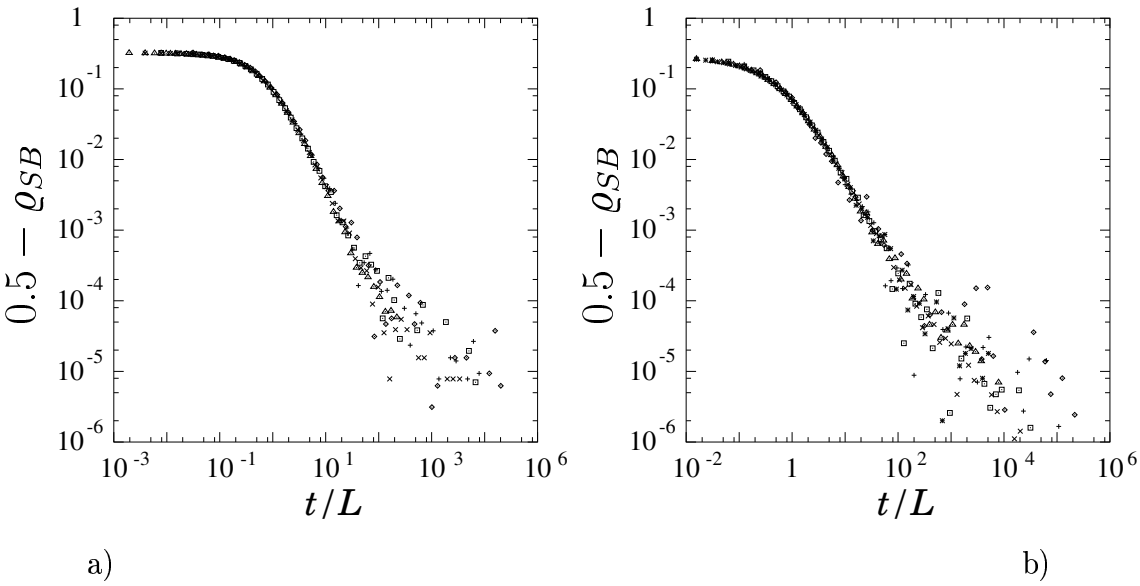

Figure 2.6: The difference of the mean density of the shear band from its asymptotic value 0.5 vs. time for square (left) and hierarchical lattice (right). The same system sizes were scaled together as in Fig. 2.5.

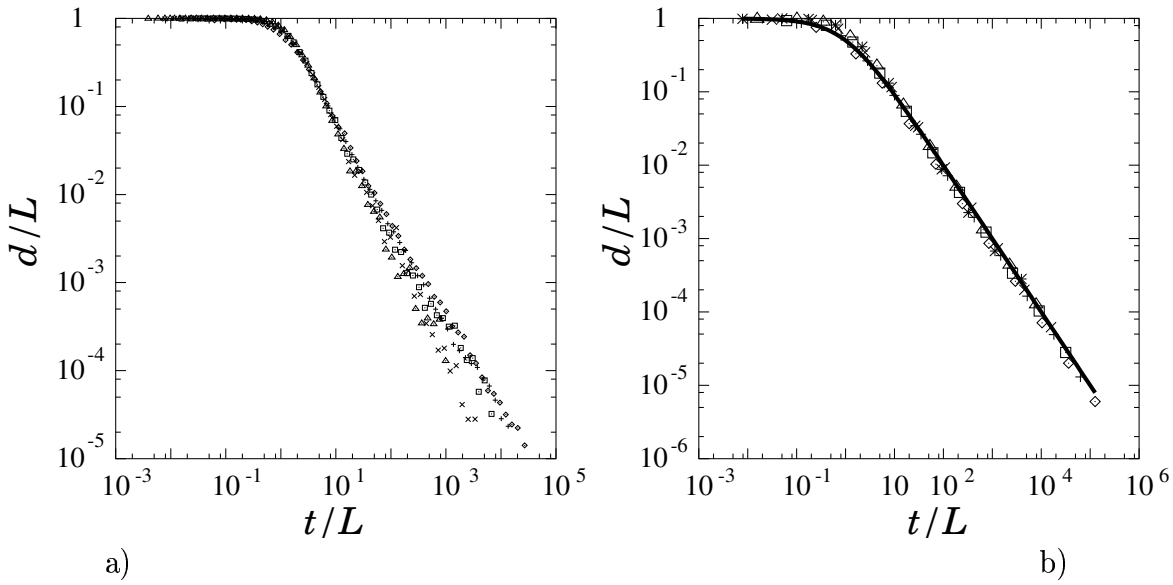

Figure 2.7: The average Hamming distance versus time for square (left) and hierarchical lattice (right). The same system sizes were scaled together as on Fig. 2.5. On the hierarchical figure the analytical $1/(t+1)$ curve is plotted over the data. Let us note that the scaling is excellent for the hierarchical lattice while it breaks down for the square lattice at about $t/L \simeq 20$. In larger systems the decrease is steeper indicating faster localization.

density that is smaller than 0.5 the next shear band will be one of these other local minimal paths with most probably no common point with the previous one. This kind of dynamics lasts until all sites have been visited some times and there are no paths with density smaller than 0.5.

As in this regime the path visits all sites with the same probability the cumulative shearing appears to be homogeneous (Fig. 2.9 first plot). This uniform shear strain can be best interpreted that in loose samples no well defined shear band can be observed that is consistent with the experimental observations.

2.2.3 Localization

The above described behaviour is changed to the opposite as time goes on and it turns to a positive feed backed localization.

The average density $\langle\varrho\rangle$ of the system is a monotonously increasing quantity and as it is bounded ($\langle\varrho\rangle \leq 1$) it must have an asymptotic value (Fig. 2.5). It is easy to see that it is 1 in our model as in a finite sample every site with density less than 1 is visited with a finite probability. In the concept of the critical state [LamWhi68, PLR00] it means that we can study only the low density limit and its convergence to the critical state.

As the average density increases the probability of having a path apart from the

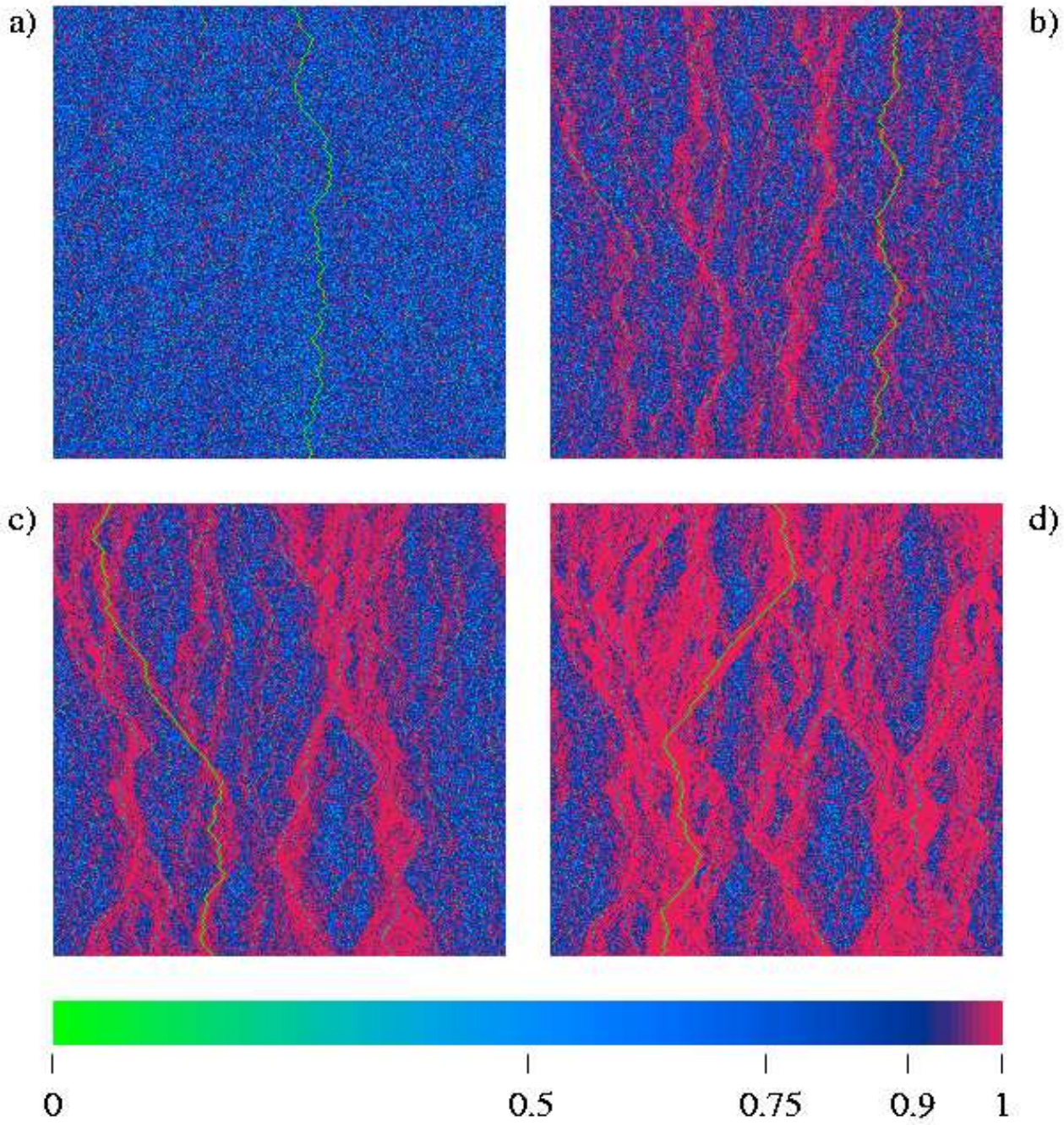

Figure 2.8: Snapshots of densities of a square lattice of size 256 by 256 at time a) $1000 = 4L$, b) $10^4 = 40L$, c) $10^5 = 400L$ and d) $10^6 = 4000L$. The colour coding is presented at the bottom. The actual shear band is drawn in green.

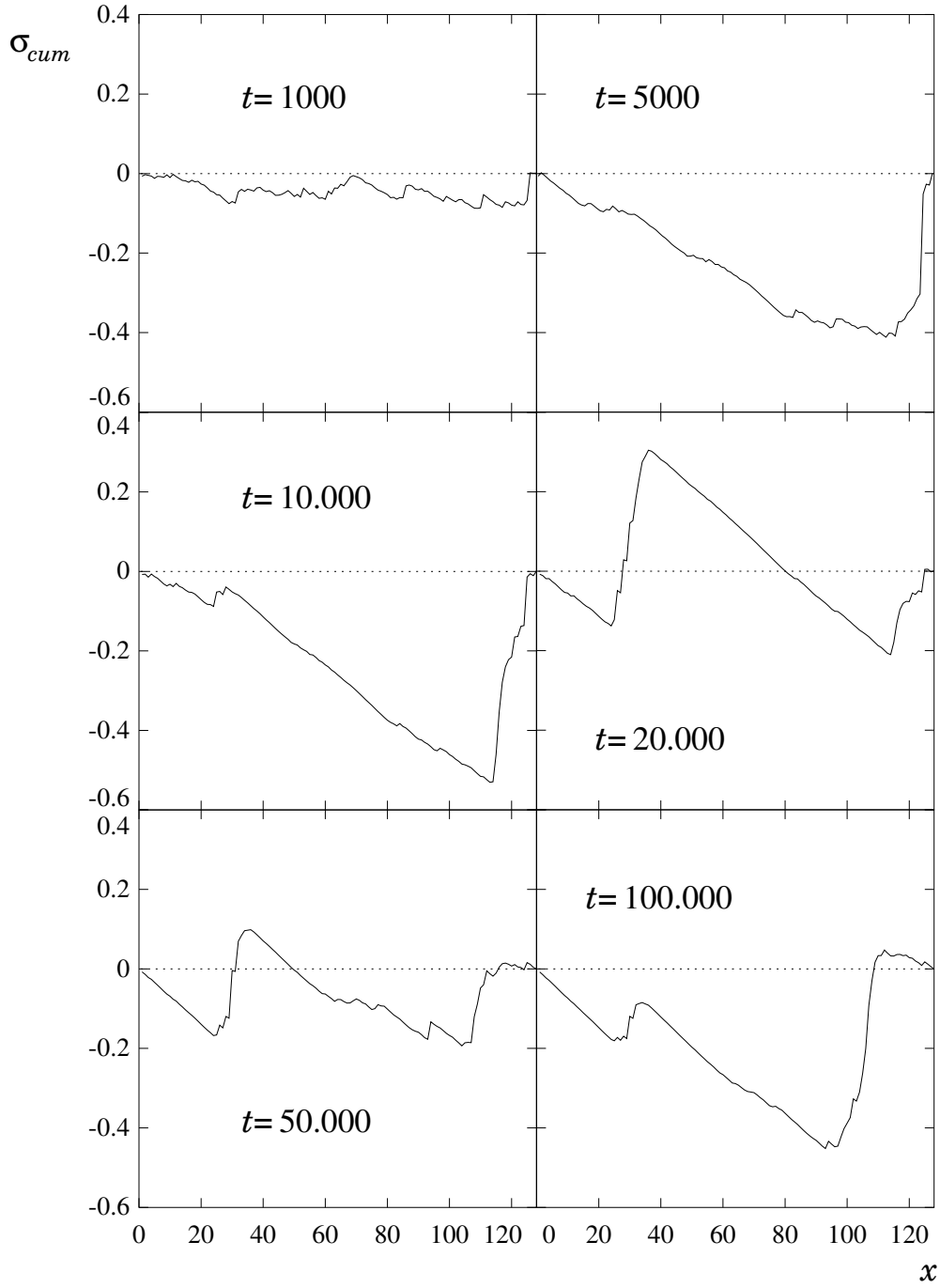

Figure 2.9: The cumulative shear corrected by the average displacement for a system of size 128 by 128. One can observe that first the shear band has been localized at around $x = 100$ then it jumped to $x = 40$ ($10^4 < t < 2\ 10^4$) after spending some time there it jumped back to its previous position ($2\ 10^4 < t < 5\ 10^4$).

shear band with density less than 0.5 vanishes and thus for the new path it becomes more favourable to choose larger and larger parts from the previous shear band. The repulsive interaction is thus inverted to an attractive one as it is shown by the rapid $1/t$ like decrease of the Hamming distance (Fig. 2.7).

There are a number of consequences of the localization. First, as time goes on a more and more apparent shear bands can be observed which finally become localized for macroscopic times. This is in accordance with experiments and with the critical state concept. Secondly, as we choose most of the cases the same path for shear band its density saturates to its asymptotic value 0.5 (Fig. 2.6) as the shear stress saturates in granular shear experiments [Wood90].

On the cumulative shear which is a straight line with small statistical fluctuations in the early time regime, there appear step-like structures, indicators of localization (Fig. 2.9). However, this localization is not ever lasting as the shear band may perform big jumps to other local minima. This can be seen on the series of cumulative shear curves as certain steps disappear and others become more determining. This a result that could be easily tested experimentally.

The apparent shape change of the cumulative shear can be quantified and thus can be used to determine the starting point of the localization process. Let us define the roughness exponent be the following expression:

$$\left\langle \sqrt{|\sigma_{cum}(x) - \sigma_{cum}(x+l)|} \right\rangle_x \sim l^{\alpha} \tag{2.2}$$

The value of α defined in this way is $\alpha = 1$ for a step like structure and it should be smaller for a random surface. On Fig. 2.10 we show the numerical values of α measured for various system sizes which is characterized by a power law like increase at the beginning towards a plateau at $\alpha = 1$. The transition point was found to be at $t/L \simeq 20$.

Let us note here that on the square lattice there is a transition regime between $t/L \simeq 2$ and $t/L \simeq 20$ which is totally absent in the hierarchical lattice realizations. In this regime the histogram of the Hamming distance (Fig. 2.11) stretches through the whole available range. In the early time regime it is concentrated around the maximal value while in the localized regime around the minimal value. This cannot be the case for the hierarchical lattice due to the unusual connectivity of the sites that is responsible of this difference.

First we survey the square lattice dynamics. As the path gets more and more localized due to the average density increase the activity that is related to the position of the shear band is also restricted to the same small domain. Thus the density of this domain will be further increased accelerating thus the localization and finally the path finds itself in a canyon like structure surrounded by extremely high density region (blue lines in red surrounding on Fig. 2.8 b)-d); an alternative representation can be found in Appendix B). At his stage there are two options. The path may

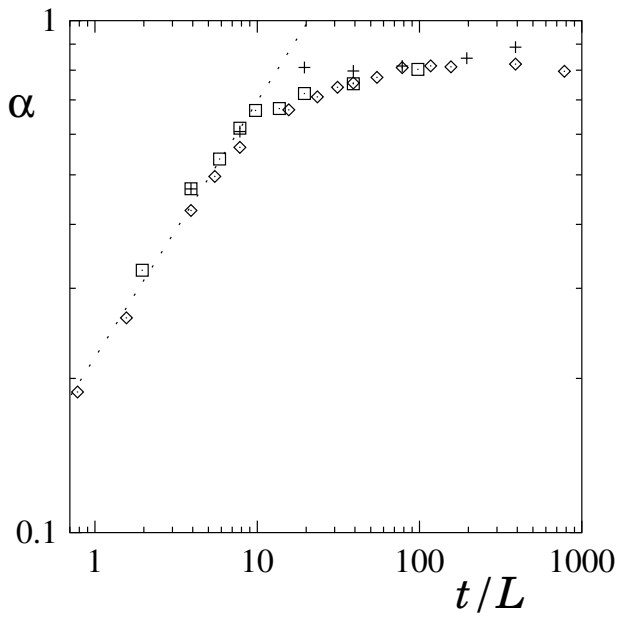

Figure 2.10: The roughness of the corrected cumulative shear. The dotted line has the slope of 0.5. The crossing point is at $t/L \simeq 20$. The diamond ($\diamond$) is for $L = 128$, the plus sign ($+$) is for $L = 256$, the square ($\square$) is for $L = 512$.

perform a big jump to an other local minima (as can be seen on the cumulative shear curves on Fig. 2.9), however the probability of such a jump soon becomes extremely small as the distribution of the mean of L independent uniform random numbers is very narrow around 0.5. The other possibility is that small — generally one site — changes are performed on the path which may have much higher probability than a big jump, as in this case only one generated random number has to be larger than a given value in the bulk.

It is easy to see that from practical point of view the large jumps do not play important role in the very late stage dynamics as their occurrence is very rare. An important question that arises is whether the small fluctuating motion can win over the ever increasing strong localization. The answer was given in a different context [TKKR00d] that even the one site change dynamics is enough for the path to explore the whole system. However, extremely (astronomically) large times are needed [$\mathcal{O}(10^{10000})$].

Let us also note that in our case, as in many other examples of granular materials, the high density and thus more resistant regions protect the looser and thus less resistant ones (see Section 1.2.3).

While identifying the two possibilities for the dynamics in the localized regime we should point out that both of them are extremely slow and have a non-trivial system size dependence which is manifested in the unusual behaviour of the average density

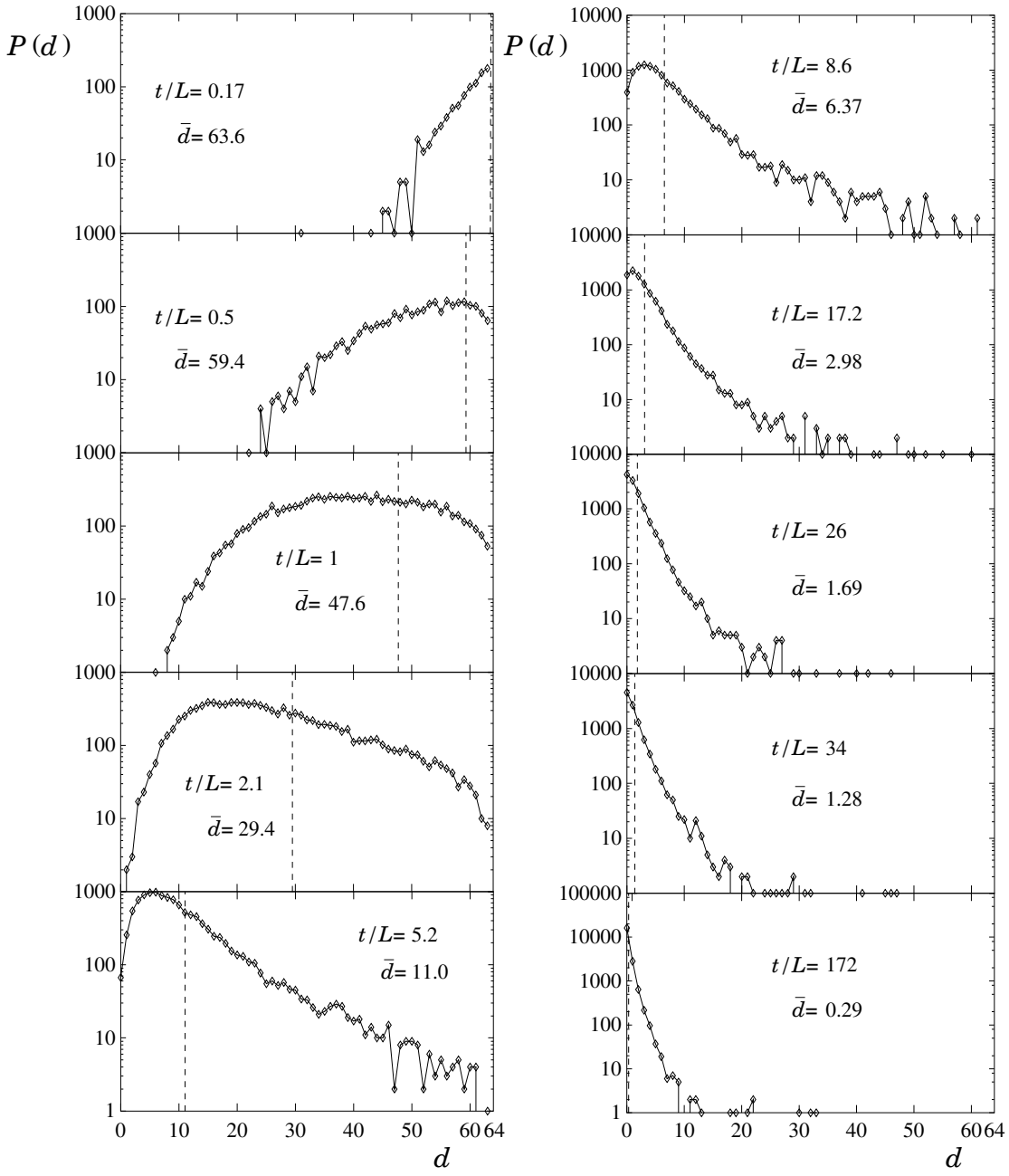

Figure 2.11: The distribution of the distance on a 64 by 64 system for different times. The dashed lines indicate the mean ($\bar{d}$).

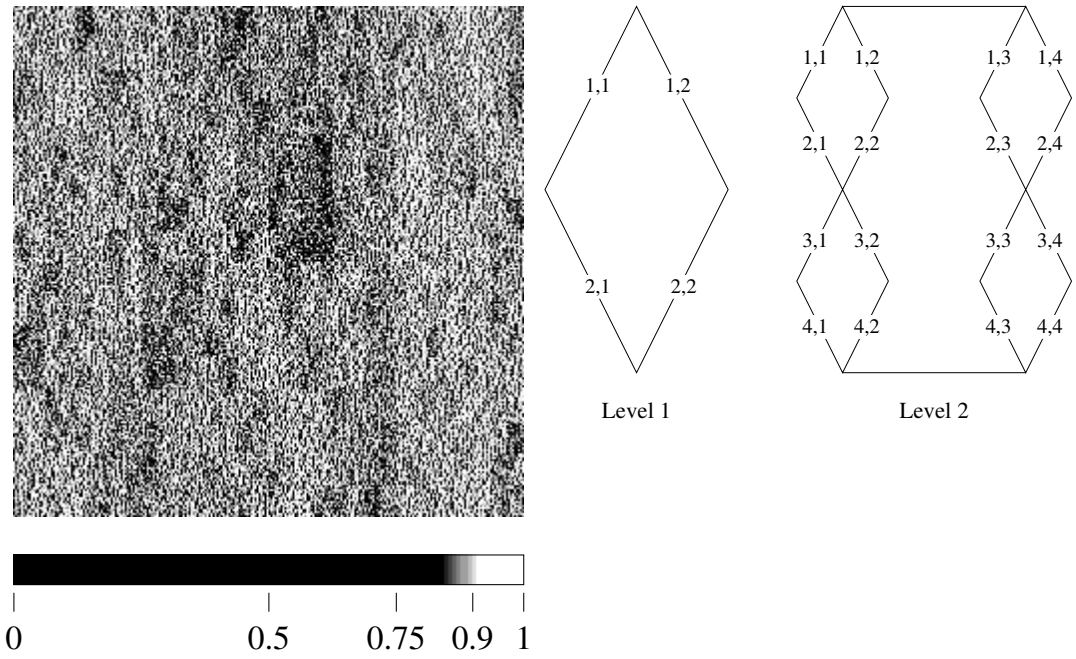

Figure 2.12: Snapshot of density of a hierarchical lattice of level 8. Let us note that, although the structure of the hierarchical lattice allows for a square lattice representation (right), however the connectivity among the sites is very strange.

(Fig. 2.5). The approach to the asymptotics is slower than a power law but faster than logarithmic at least for the numerically achievable system sizes. The hierarchical solution in Chapter 3 indicates that it could be a power law with sum of decreasing powers and coefficients.

Now we turn to the hierarchical lattice. The connectivity difference between hierarchical and normal square lattice plays an important role in the second type of dynamics. The hierarchical lattice cannot be explored by only one site changes of the path. For example to get from the left side to the right side we need a N site change of the path. So the Hamming distance distribution will never get so concentrated around 0 and values of 2^i must have non-neglectable probability compared to the one site change even at very large times. The dynamics is thus a competition of these 2^i site changes that becomes clear in the analytical solution presented in Chapter 3.

The above difference is also clear from the density maps (Fig. 2.8 d) and 2.12). On the square lattice sample the locally densified structures can be easily identified. Low density regions are relatively large domains protected by the high density parts. In the hierarchical lattice sample low density sites are scattered through the whole sample. The shear band is not able to access them because it would need possibly a large 2^i site jump that has relatively low probability at late times. It is very striking that in spite of such a difference in the spatial arrangement the density distributions

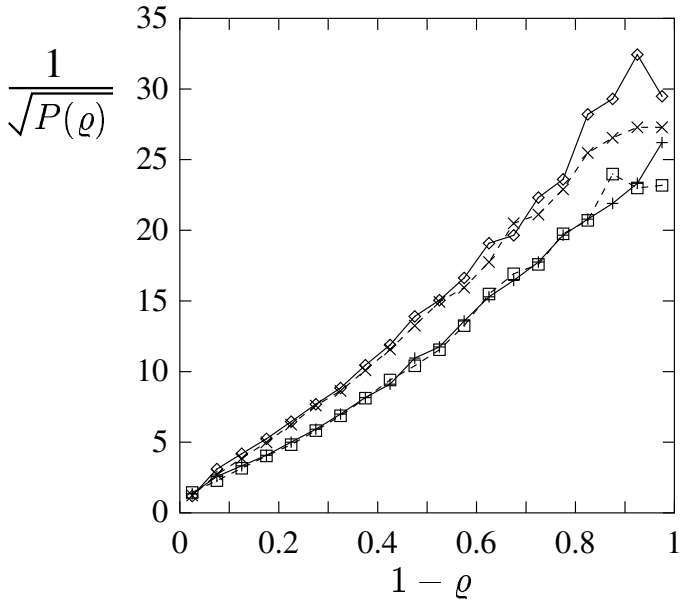

Figure 2.13: Histogram of the density on square lattice (solid lines) of size 256 by 256 and on hierarchical lattice (dashed lines) level 8. Both of then have 256^2 number of sites/bonds. Time was $t = 10^5$ for bottom curves and $t = 10^6$ for the upper curves.

in both case are very similar as shown on Fig. 2.13.

2.2.4 Systems with high initial densities

It was mentioned in the introduction that that the shear band is the lowest density state of the granular material [OnoLin90]. In this concept it means that up to now we studied samples with lowest possible density. It is also of interest to study samples with higher initial density. As one may suspect if the initial density is very close to the critical density 1 in our case the shear band is from the very beginning in a very localized state. In this section we study the interesting crossover to that state from the previously described dynamics.

We chose initial densities from the interval $[\varrho_{init} : 1]$ with a uniform distribution and varying ϱ_{init}. On Fig. 2.14 the time evolution of the difference of the average density form its asymptotic value is plotted using different initial conditions. Since all previous arguments hold we assume that in finite systems the asymptotic value of the average density is 1 irrespect to the initial density.

The striking result of these simulations that if $\varrho_{init} < 0.5$ all curves fall on each other after reaching the decreasing part. However, if $\varrho_{init} > 0.5$ a different time evolution is observed for large times. Thus we can assume that in the early time regime when the shear band is swapping uncorrelatedly it visits all sites that have a

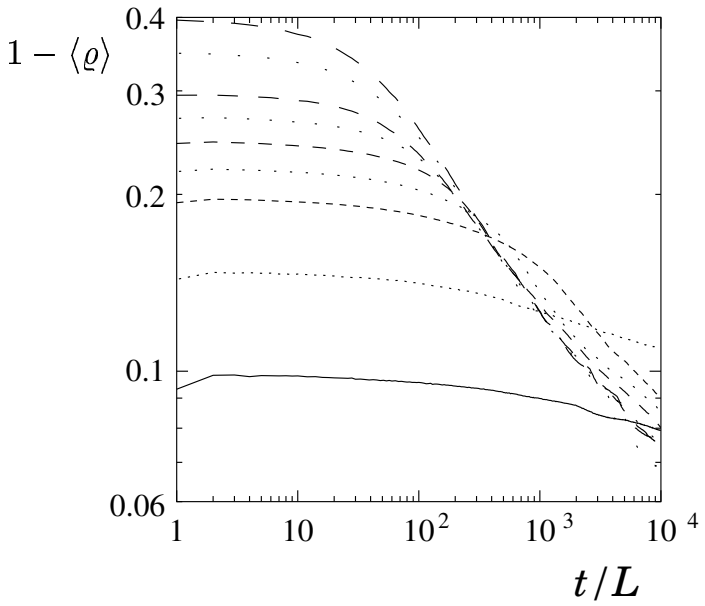

Figure 2.14: Time dependence of the difference of the average density from its asymptotic value for starting densities with initial density ranges $[\varrho_{init} : 1]$ from top to bottom respectively: $\varrho_{init} = 0.2$, 0.3, 0.4, 0.45, 0.5, 0.55, 0.6, 0.7, 0.8. The system size is 64.

value less than the expectation value of the refreshing density distribution thus 0.5. After the first regime as all small values are eliminated the systems effaces the initial condition and its previous history.

On the other hand, starting from initial conditions with $\varrho_{init} > 0.5$ we basically eliminate the possibility of the large jumps. The whole sample must be invaded by the shear band with small fluctuating few site change motion, which is rather slow. The above behaviour can be identified to the case when the position of the shear band is more or less fixed.

2.2.5 Systems with different aspect ratios

Further insight can be obtained by examining systems with different aspect ratios. Let us note that we use the terms *long* and *narrow* for samples with $L_y < L_x$ and *wide* in the case of $L_y > L_x$. So we look at the system from the point of view of the shear band.

With very narrow and wide systems we are able to separate the two kinds of dynamics described in Section 2.2.3. If one considers a narrow sample (L_y is small) one may expect that the large jumps will disappear and the average density will solely scale by the L_y (Fig. 2.15). While in the case of a wide sample a number of independently evolving subsystems should be observed.

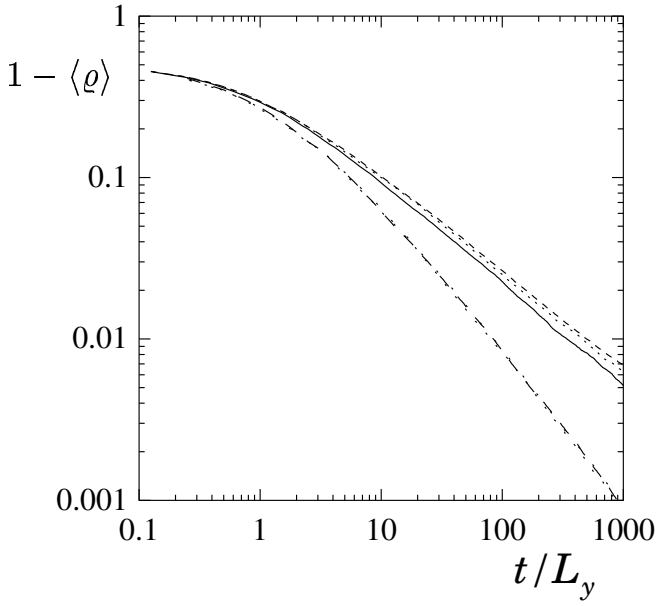

Figure 2.15: Long samples with width $L_y = 4$ (lower curves) and $L_y = 8$ (upper curves). Three different height was used in both cases $L_x = 10$, 20, 40.

Narrow systems

On Fig. 2.15 we plotted the time dependence of the density in long samples with $L_y = 4$ (lower curves) and $L_y = 8$ (upper curves). The t/L_y scaling is excellent in the first case while small deviation appear as the width of the sample is increased to $L_y = 8$. This suggests that large jumps become important even at that width. This can be studied more precisely and quantitatively with the help of the wide samples.

Wide systems

Wide samples can be considered as subsystems placed next to each other and coupled in parallel. The high density regions and the localization of the shear band prevents smooth movement from one subsystem to the other, large jumps are needed to do this. In the following we will determine the mean size of such subsystems.

In the case of the wide systems the same plot as before (Fig. 2.16) shows no t/L_y scaling for small system sizes but the curves fall on top of each other if the sample is wide enough.

Let us propose the following explanation: From the previous analysis we know that in the initial regime that should be the same also in this different aspect ratio case, i.e. the shear band visits all sites which have densities less than 0.5. Afterwards the localization process takes place. The probability of a large jump soon gets very small and thus such events become very rare.

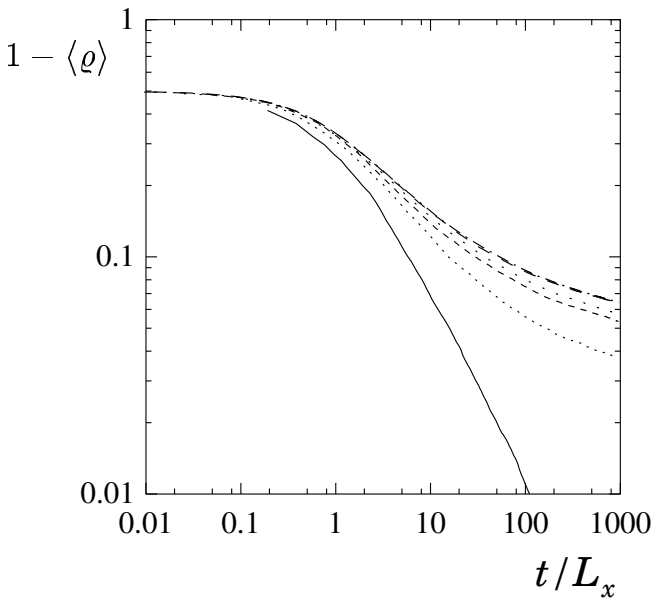

Figure 2.16: Time dependence of the density difference from its asymptotic value for wide samples. The length of the system along the shear band is $L_x = 5$ the widths are from $L_y = 5$ to $L_y = 160$ from bottom to top respectively with a factor of 2 among system sizes.

Here we suppose that up to the measured time ($t/L_y = 1000$) the probability of having such a jump is indeed very small. In other words we postulate that up to time $t/L_y = 1000$ the shear band has spent all the time in one subsystem. In this case the average density can be written in the following form:

$$1 - \langle\varrho\rangle = \left[\left(\frac{L_y}{l} - 1\right)(1 - \varrho_0) + \frac{a}{t^\alpha}\right]\frac{l}{L_y}, \tag{2.3}$$

where l is the average size and ϱ_0 is the average density of a subsystem at the end of the early time regime. Here we supposed that the density of the active subsystem evolves as power law with time. This can be justified e.g. by Fig. 2.16 on the system 5 by 5 where the decay of the difference between the asymptotic and the current densities can well be approximated by a power law over several decades. We rewrite the above equation (Eq. 2.3) in a more convenient form:

$$1 - \langle\varrho\rangle - \underbrace{(1 - l/L_y)(1 - \varrho_0)}_{\varrho^*} = \frac{l}{L_y}\frac{a}{t^\alpha} \tag{2.4}$$

Thus as we see by choosing an effective asymptotic density $(1 - \varrho^*)$ the deviation of the average density from this effective density should be a power law. This power law should describe the time evolution of one subsystem thus it should be independent

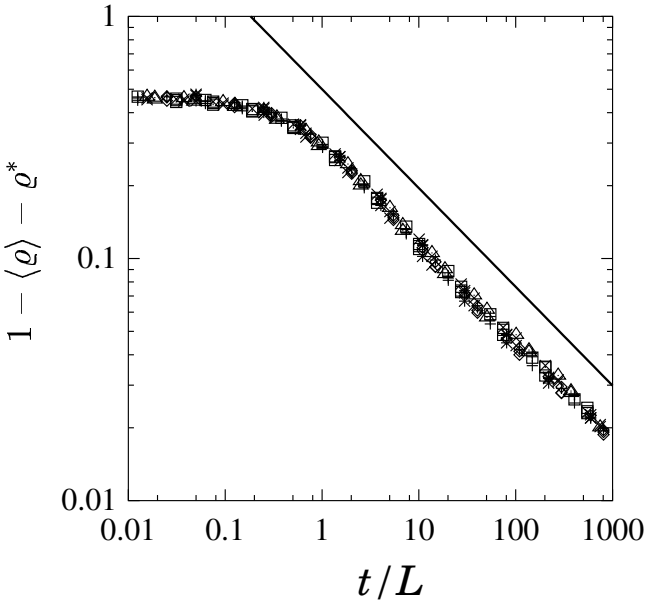

Figure 2.17: Time dependence of the density difference from the biased density value for wide samples. On the figure data of 21 different systems were scaled together with $L_x = 5$, 10, 20, 40 and L_y varying from 20 to 640. The slope of the solid line is $\alpha = -0.408$.

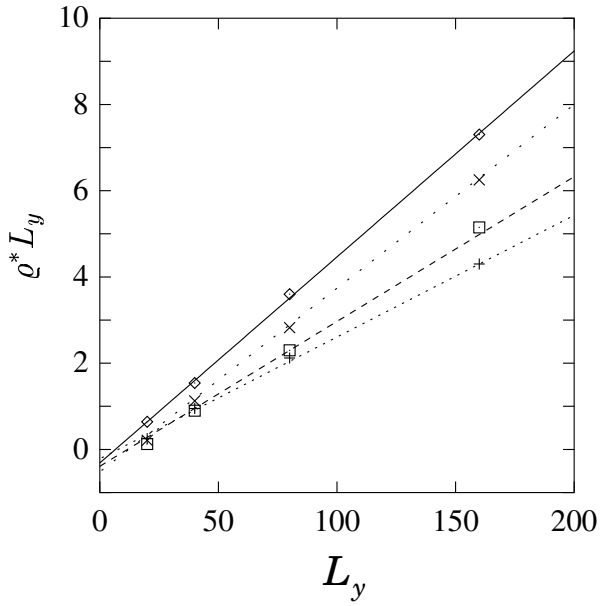

Figure 2.18: $\varrho^* L_y$ versus L_y for four different L_x. The numerical values are plotted with symbols ($L_x = 5$: $\diamond$, 10: $+$, 20: $\square$, 40: $\times$), the solid lines are linear fits with:
$L_x = 5$: $y = 0.048x - 0.313$ $L_x = 10$: $y = 0.028x - 0.217$
$L_x = 20$: $y = 0.034x - 0.391$ $L_x = 40$: $y = 0.043x - 0.519$

of the system size. This can be observed on Fig. 2.17 where 21 different system size were scaled together with the only fit parameter of ϱ^*. The system size in the x direction was varied by a factor of 8 and in the y by a factor of 32. We found the exponent

$$\alpha = 0.408 \pm 0.005. \tag{2.5}$$

From ϱ^* one can determine the value of l for a given L_x by tracing $\varrho^* L_y$ versus L_y. The slope of the linear fit divided by the y axes cut (Fig. 2.18) should give the average length l of a subsystem. We found the following values:

L_x	l		
5	6.55	$\pm$	0.5
10	7.75	$\pm$	0.6
20	11.67	$\pm$	0.8
40	12.2	$\pm$	1

From the above we suspect that the size of a given subsystem does not grow to infinity with the x size of the sample but remains finite. This supposition is underlined by the faster decay of the Hamming distance for large systems (Fig. 2.7). The localization is done within one subsystem where the density of the sites is nearly increased to the maximum and the path is trapped in a canyon like structure. If the width of these structures does not grow with increasing system size the path gets localized earlier and earlier on the t/L_x scale.

Hamming distance

We also measured the Hamming distance of the above used samples (Fig. 2.19). Because all these systems are very small at least in one coordinate they fall on each other and furthermore on the theoretical estimate of the hierarchical lattice (Section 3.5) of

$$d(t)/L_x = \frac{1}{t/L_y + 1}. \tag{2.6}$$

On the one hand this indicates the relevance of the hierarchical study of the system on the other hand it shows that the complexity of the system is due to the complicated interplay of the long jumping and smooth moving dynamics which induces the unusual system size dependence.

2.2.6 Roughness exponent of the shear band

From the directed polymer analogy we know that the shape of the shear band is self-affine with an exponent of $\zeta = 2/3$ for infinitely large systems. It is an interesting question whether this property of self-affinity is conserved in the time evolution of our

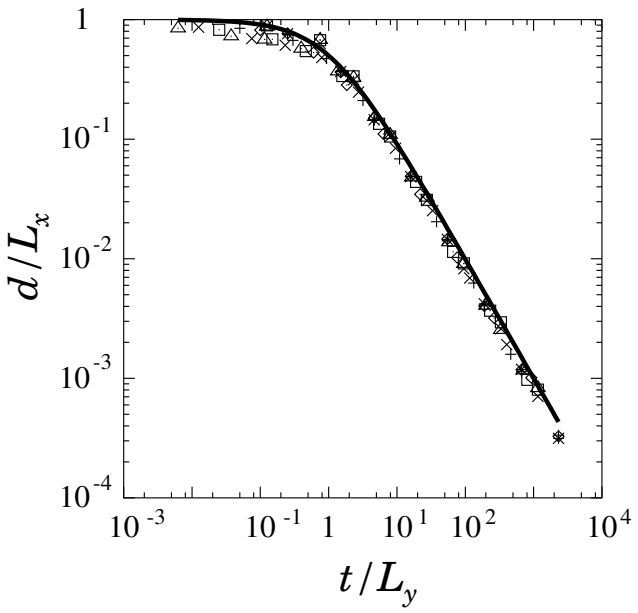

Figure 2.19: The Hamming distance of 11 different systems with aspect ratio from 3 by 10 to 8 by 40. The thick line is $1/(1+x)$.

system. We analyzed the geometry of the shear band and found excellent self-affine scaling for all times, however with time dependent Hurst exponent (Fig. 2.10).

The numerical procedure was to calculate the with of the shear band (w) in a detrended way for different window length (l). The following scaling relation defines the roughness exponent:

$$w \propto l^{\zeta}. \tag{2.7}$$

One can also see on Fig. 2.20 that the exponent is changing extremely slowly. The middle part seems to have a logarithmic increase. The increasing self-affine exponent shows an increasing width of the shear band. We emphasize that the one-site activities that can take place only at points where the path makes a turn. The increasing width indicates a decreasing number of turning points. Such an event can emerge from a situation for example when one part of the shear band tries to escape upwards from the high density regions while the other part goes downwards. It is very probable that those parts will be interconnected with a more or less fully stretched line. See e.g. Fig. 2.8 d). This is also a feature that slows down the dynamics.

We also tried to extrapolate the value of ζ in the infinite systems. To do this we measured the width of the density landscape for different system sizes and used the formula

$$\ln\left(\frac{w_{L_1}(t)}{w_{L_2}(t)}\right) = \zeta(t)\ln 2, \quad \text{if} \quad L_2 = 2L_1 \tag{2.8}$$

where $w_L(t)$ is the width of a sample of size L by L. The results obtained for the tilted

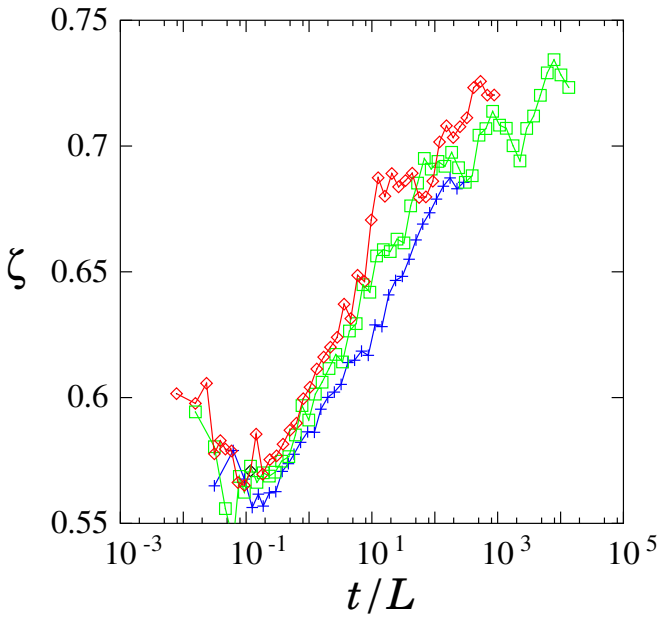

Figure 2.20: The roughness exponent of the shear band vs. time on normal square lattice. The system size is $L = 32$ solid, $L = 64$ dotted and $L = 256$ dashed. The long time curves are averaged over $100 - 1000$.

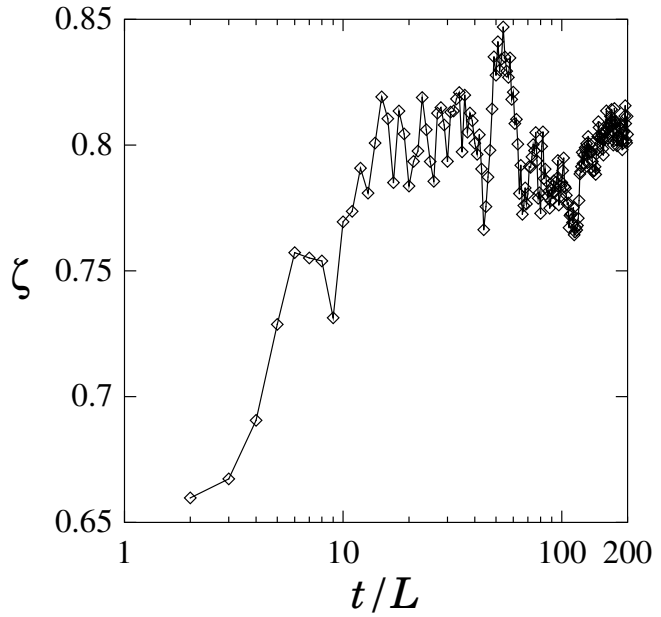

Figure 2.21: Estimated self-affine exponent for the infinitely large system obtained by a careful ensemble average of Eq. 2.8.

square lattice can be seen on Fig. 2.21. It starts from $\zeta(t = 0) = 2/3$ as expected from the directed polymer result and has an asymptotic value of $\zeta \simeq 0.8$.

2.3 Conclusion

Though very simple, our model seems to capture the essential features of granular shear and provides at the same time several predictions. The model demonstrates the self-organized mechanism of the localization of the shear band in loose granular materials. As the sample ages, very high fluctuations in density appear where we can observe some kind of arching effect: high density, more resistant regions protect the looser ones. This model also gives an insight into a dynamics that gives rise to very non-trivial system size effects.

We have introduced a simple stochastic model to describe the large-strain behaviour of a granular medium. The rules of the model do not include any dependence on the total amount of shear imposed to the medium, nevertheless, a slow hardening (increase of the friction angle) and densification is observed — a property referred to as "ageing" — which reproduces the experimental results qualitatively. By construction, the strain takes place through local shear bands which initially travel through the medium homogeneously (and hence produce a uniform shear), and which progressively becomes more permanent giving rise to more steady shear bands, a feature also observed experimentally.

Thus our model reproduces a number of features seen in experiments and numerical simulations, including the high frequency fluctuations of the local shear strain. In addition, we predict a complex self-organization of these shear bands, which has a signature in the local density which incorporate most of this ageing. This feature can be studied experimentally, in particular through the use of a scanner to access the local density of a sheared medium.

Chapter 3

Analytical results on the hierarchical diamond lattice

In the following sections we show how some of the above listed properties of our model can be understood analytically on the hierarchical lattice. The techniques we use are essentially those of extreme order statistics. First we we define the model on the hierarchical lattice in the second section we summarize the whole procedure of the solution and then we will proceed along the calculation.

3.1 Definition of the model on the hierarchical lattice

The model on the hierarchical lattice (Fig. 3.1) is the same as on the square one. At the beginning we impose densities on every bond generated randomly from a distribution $p(x)$, say the uniform distribution between 0 and 1. We find the path connecting A and B which has the minimal sum of densities among all possible paths that connect A and B. Along this path we change the densities randomly from the same distribution $p(x)$. We repeat the above procedure and study the development of the system in time.

Like for the square lattice, we are interested in the time evolution of the average density of the inactive bonds, i.e. the bonds that are not a part of the last minimal path.

3.2 Summary of the hierarchical solution

In the following we will try to sketch the main line of the analytic solution. We will use the hierarchical nature of the diamond lattice to calculate the average density for level N knowing the results on level $N-1$.

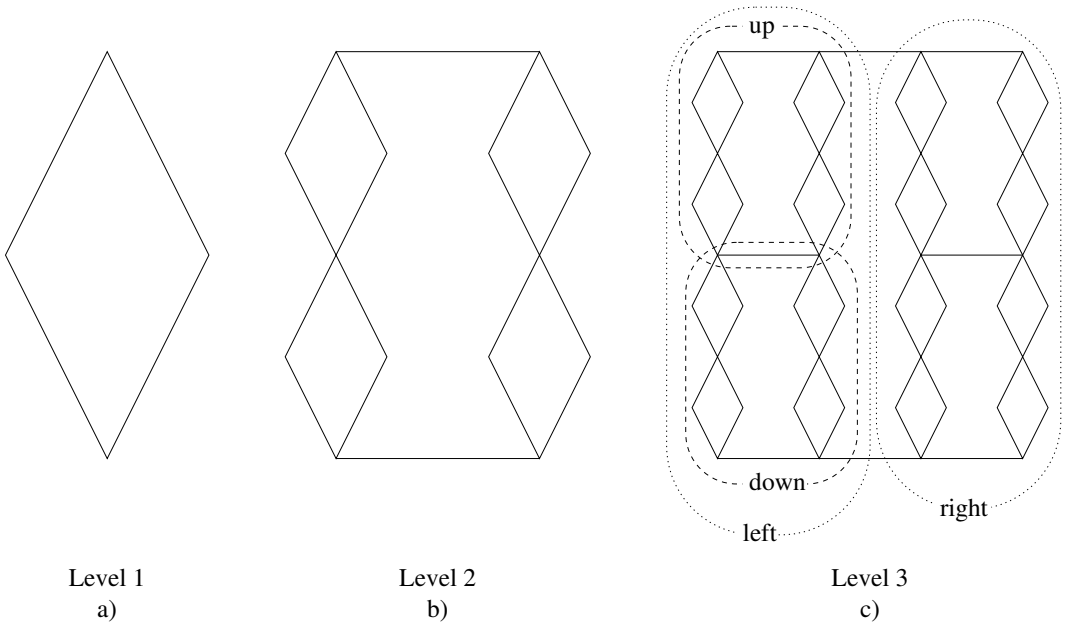

Figure 3.1: The 1st a), 2nd b) and 3rd c) generations of the hierarchical lattice.

A hierarchical lattice at level N is composed out of 4 level $N-1$ hierarchical lattices, two-two of which are coupled in series and these couplets are coupled in parallel, See Fig. 2.2 and Fig. 3.1. Let us introduce the following notations: The average density of the inactive sites in a (sub)lattice level N is $\varrho^{(N)}(t)$, the density of the active sites is $x^{(N)}(t)$. In (sub)lattices we define the active site to be the minimal path of this (sub)lattice regardless that it is the part of the real active minimal path or not.

The series coupling of the sublattices is very simple, both the density of the minimal path and of the bulk is simply averaged:

$$\varrho^{(S(N-1))}(t) = \frac{1}{2}\left(\varrho_u^{(N-1)}(t) + \varrho_d^{(N-1)}(t)\right) = \varrho^{(N-1)}(t) \tag{3.1}$$

$$x^{(S(N-1))}(t) = \frac{1}{2}\left(x_u^{(N-1)}(t) + x_d^{(N-1)}(t)\right) = x^{(N-1)}(t) \tag{3.2}$$

where the index u and d denotes *up* and *down*, and the superscript S refers to a system couples in series.

The next step is the coupling in parallel of two series couplet. The density of the shear band is simply the minimum of that of the two subsystems. However, the average density of the bulk is more complicated since the time evolution of the density of a subsystem depends on the local time, i.e. the number of time steps the shear band has spent in it. In section 3.3.1 we will prove that the time the shear band spends in either subsystems is *uniformly* distributed. Thus we can get the parallelly

coupled density via a uniformly weighted sum of the two subsystems and we should not forget about the larger minimal path of the subsystems hence it belongs to the bulk.

$$\begin{aligned}\varrho^{(N)}(t) &= \frac{2\left(4^{N-1}-2^{N-1}\right)}{4^N-2^N}\int_0^1 \left\{\varrho_l^{S(N-1)}(xt)+\varrho_r^{S(N-1)}((1-x)t)\right\}dx + \\ &+\frac{2^N}{4^N-2^N}\max\left(x_l^{S(N-1)},x_r^{S(N-1)}\right) = \\ &= \frac{\left(4^N-2^{N+1}\right)}{4^N-2^N}\underbrace{\frac{1}{t}\int_0^t \varrho^{(N-1)}(t')dt'}_{I_1} \quad +\frac{2^N}{4^N-2^N}\max\left(x_l^{S(N-1)},x_r^{S(N-1)}\right)\end{aligned} \tag{3.3}$$

$$x^{(N)} = \min\left(x_l^{S(N-1)},x_r^{S(N-1)}\right) \tag{3.4}$$

where subindexes l and r denote *left* and *right*, 4^N is the total number of bonds 2^N is the number of the bonds in a path on a lattice of level N, the multiplicative factors in Eq. 3.3 are the portion of bonds belonging to that class.

In Eq. 3.3 the second term is a very interesting part. There are two subsystems competing for the minimal path. Due to the geometry of the system a change from one side to the other is only possible via a large jump. Thus we need to generate 2^N random numbers the mean of which is larger than that of the concurrent one. Then we swap to the other half. Thus we may convert this problem to a simpler one that we call the *two site model*.

The two site model is defined as follows: There are two sites, each with a single value that is called *density* generated by a random number drawn from a given distribution $p(x)$. We choose the site with the smaller density and refresh it with a random number generated with the same $p(x)$ distribution. The dynamics consist of repeating the refreshing procedure.

The problem of the two competing minimal paths can be described by this model if time is not too small i.e. there are not too large changes in the position inside a subsystem of the minimal path before and after the jump i.e. densities are much higher than 0.5. In our case $p(x)$ is the distribution of the sum of $n = 2^N$ independent uniformly distributed random numbers which is normalized to 1.

Let us note that the first level hierarchical lattice Fig. 3.1 a) also belongs to the two site model. In Sections 3.3.2 and 3.3.3 we calculate the time dependence of the average density of the inactive site $B^{(n)}(t)$ of the two site model and in the large time limit we find analytically:

$$B^{(n)}(t) = 1-\Gamma(1/n)(n!)^{1/n}n^{-2}\left(t+\frac{3n+1}{2n}\right)^{-1/n}+\mathcal{O}\left(\frac{1}{t^{1/n+1}}\right) \tag{3.5}$$

where $n = 2^N$ the number of summed independent random numbers on a site.

The next problem that arises if one wants to give a closed formula for the average density for arbitrary N is the evaluation of the integral I_1. The integration I_1 of functions like Eq. 3.5 gives rise to terms that separately diverge on further integration:

$$I_1 = \frac{1}{t}\int_0^t \frac{a}{(t'+c)^b}dt' = \frac{a}{1-b}\left(\frac{(t+c)^{1-b}}{t} - \frac{c^{1-b}}{t}\right) \tag{3.6}$$

In Section 3.3.4 we show that the result of the above integral can be rewritten in the same form of Eq. 3.5 with different a and c parameters (the exponent b remains the same!). This can be done in a way that the whole calculation remains exact asymptotically to the order $1/t$:

$$I_1 = \frac{1}{t}\int_0^t \frac{a}{(t'+c)^b}dt' \simeq \frac{a}{(1-b)}\frac{1}{(t+c)^b} + \mathcal{O}\left(\frac{1}{t^{b+1}}\right) \tag{3.7}$$

We can put the above results together to formulate the final result for the average density:

$$\varrho^{(N)}(t) = 1 - \sum_{i=1}^{N}\left(\frac{2^{N-i}}{2^N-1}\right)\frac{a(i)}{(t+c(N))^{b(i)}} \tag{3.8}$$

where (using $n = 2^i$):

$$\begin{aligned} a(i) &= \Gamma(1/n)(n!)^{1/n}n^{-2}\left(\frac{2^i}{2^i-1}\right)^{N-i} \\ b(i) &= 1/n \\ c(N) &= \frac{3n+1}{2n} \end{aligned} \tag{3.9}$$

Figure 3.2 visualizes this result compared to the numerical data. Let us note that the above formula is exact in the $1/t$ limit and one can observe small deviations for early times in large systems. Let us also mention that the above formula is a sum of power laws with rapidly decreasing exponents. In very large systems this can be regarded as a slow logarithmic decay.

3.2.1 Discussion of the iterative equation

Before going to the details of the analytical solution let us have a closer look of Eq. 3.3. If iterative equations are concerned the most natural question is the fixed point or in other words the asymptotics. If we consider N large enough we have to solve the following equation for the fixed point:

$$\varrho^{(N)}(t) = \frac{1}{t}\int_0^t \varrho^{(N-1)}(t')dt' \tag{3.10}$$

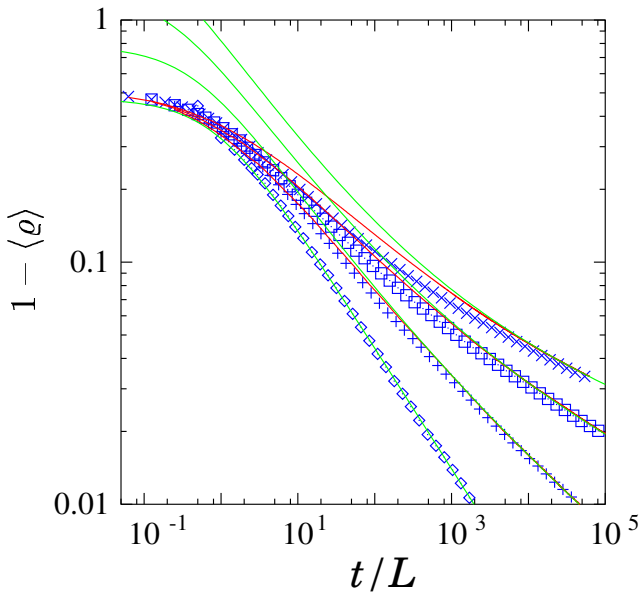

Figure 3.2: The test of the analytic results on the hierarchical lattice (green lines) against numerical simulations (symbols). Red curves are numerical integrates of Eq. 3.3. The hierarchical level is 1, 2, 3 and 4, from bottom to top.

The only solution of such an equation is a

$$\lim_{N\to\infty} \varrho^{(N)}(t) = const. \tag{3.11}$$

This surprising result shows that if we consider first the $N \to \infty$ limit the average density does not change. However, if one starts from Eq. 3.8 and takes the $N \to \infty$ limit, finds a logarithmic solution (as the result of the sum of vanishing powers). This strange contradiction indicates that the order of the limits in our model is very important. For a given system size we can tell what happens in the $t \to \infty$ limit but in the $N \to \infty$ limit we cannot give a conclusive answer.

3.2.2 Numerical integration of the iterative equations

A good check of the analytic solution is if we integrate and iterate numerically Eq. 3.3. The aim of this study is that from our analytical solution we cannot extrapolate how good is the equal time distribution assumption that is a crucial point of our solution. We may thus check if it is worth to push one order forward our calculations or not.

For the numerical integration we took numerical data even for the two site model. As Figure 3.2 shows the analytical solution falls on the top of the numerical integration before together they meet the numerical data points. Indicating that the chosen first

order analysis is enough for our purpose and with the given assumptions we cannot make better.

A possibility to improve the situation would be to describe the time distribution inside the sample for early times where numerically we found deviations from the uniform case. This analysis is not done in the scope of this thesis.

3.3 Detailed presentation of the hierarchical solution

3.3.1 Time partitioning in the two-site problem

We now prove that after the elapse of a time t, the probability that a given site has been visited T times is uniformly distributed between 0 and t. The following proof is valid for *any* distribution $p(x)$. In order to see this, note that for any distribution $p(x)$ we can consider the cumulative distribution:

$$P(\varrho) = \int_0^{\varrho} p(x)dx. \tag{3.12}$$

Let us now compute $q(T,t)$, the probability that *the active site* has been refreshed T times up to time t. Let the value of the recently refreshed site be denoted by x and the inactive site at t be b_t. At time t two things may happen:

i) either $x < b_{t-1}$, and thus $T_t = T_{t-1} + 1$. This happens with probability $(t+1)/(t+2)$

ii) or $x > b_{t-1}$, and thus $T_t = t - T_{t-1}$ with probability $1/(t+2)$.

Note that the activity change can only be due to the fact that the largest generated random number up to time t is at instant t. This happens with probability $1/(t+2)$ because in independent time series of random numbers the largest number is equally likely to be anywhere. At time $t = 0$ we have to initialize the system and so generate two random numbers for the two sites. This is the reason for the plus two.

Now we can write down a simple evolution equation for $q(T,t)$

$$q(T,t) = q(T-1,t-1)\frac{t+1}{t+2} + q(t-T-1,t-1)\frac{1}{t+2} \tag{3.13}$$

We take the following *Ansatz* for the form of the solution:

$$q(T,t) = A\frac{(T+1)}{(t+1)(t+2)} + B \tag{3.14}$$

It is simple to compute $q(t,t)$ from the above recurrence, and get

$$q(t,t) = \frac{2}{(t+2)} \tag{3.15}$$

and thus $B = 0$ and $A = 2$. Thus finally

$$q(T,t) = \frac{2(T+1)}{(t+1)(t+2)} \tag{3.16}$$

Now, the number of updates of the other site is simply $q(t-T,t)$, thus we can formulate the probability distribution that a site has been updated T times:

$$r(T,t) = \frac{1}{2}(q(T,t) + q(t-T,t)) = \frac{(T+1)+(t-T+1)}{(t+1)(t+2)} = \frac{1}{(t+1)} \tag{3.17}$$

indeed independent of T thus $r(T,t)$ is uniform.

3.3.2 Average density of the inactive site for the two site model with $n = 2$

In this section we will calculate the average density of the inactive site in the two site problem when the random numbers are taken from the arithmetic mean of two uniformly distributed random numbers ($n = 2$). We go through this simple case to help us with the general case. All these calculations are carried out such that the $1/t \to 0$ limit is kept exact.

The probability distribution in this case is the following:

$$p_2(x) = \begin{cases} 4x, & 0 \le x \le 1/2 \\ 4(1-x), & 1 \ge x > 1/2 \end{cases} \tag{3.18}$$

The cumulative distribution is just the integral of the above:

$$P_2(x) = \begin{cases} 2x^2, & 0 \le x \le 1/2 \\ 1 - 2(1-x)^2, & 1 \ge x > 1/2 \end{cases} \tag{3.19}$$

The average value of the largest generated random number up to time t in the general case can be formulated as follows:

$$B(t) = (t+1)\int_0^1 x p_2(x) P_2^t(x) dx, \tag{3.20}$$

where $P^t(x)$ accounts for the probability that the t other numbers were less than x. $p(x)$ is the probability of having a number with value x, the position of the largest number can be anywhere among the $t+1$ generated random number thus a $(t+1)$ factor is needed to take this into account. In our case we expand the above integral in a more useful form:

$$B^{(n)}(t) = \underbrace{4(t+1)\int_0^{1/2} x^2 \left(2x^2\right)^t dx}_{I_2} + \underbrace{4(t+1)\int_{1/2}^1 x(1-x)\left(1-2(1-x)^2\right)^t dx}_{I_3} \tag{3.21}$$

The first integral is straightforward and gives an exponentially decreasing term:

$$I_2 = 2^{t+2}(t+1)\int_0^{1/2} x^{2t+2}dt = 2^{t+1}(t+1)\left[\frac{x^{2t+3}}{2t+3}\right]_0^{1/2} = \frac{t+1}{2t+3}\frac{1}{2^{t+2}} \tag{3.22}$$

We introduce a variable change ($y = 1-x$) in I_3 and we split it into two terms:

$$\begin{aligned} I_3 &= 4(t+1)\int_0^{1/2}(1-y)y\left(1-2y^2\right)^t dy = \\ &= \underbrace{4(t+1)\int_0^{1/2} y\left(1-2y^2\right)^t dy}_{I_{31}} - \underbrace{4(t+1)\int_0^{1/2} y^2\left(1-2y^2\right)^t dy}_{I_{32}} \end{aligned} \tag{3.23}$$

From this expression the first integral is very easy to calculate and gives the asymptotic constant 1 and an exponentially decreasing term:

$$I_{31} = -\left[\left(1-2y^2\right)^{t+1}\right]_0^{1/2} = 1 - \frac{1}{2^{t+1}} \tag{3.24}$$

The second part (I_{32}) can be integrated by parts using:

$$I_{32} = \int_0^{1/2} \underbrace{y}_{g}\underbrace{4(t+1)y\left(1-2y^2\right)^t}_{f'} dy \tag{3.25}$$

So $f = -(1-2y^2)^{t+1}$. The result is an exponentially decreasing term and an integral that will give as the leading order term for large values of t:

$$I_{32} = \left[-y\left(1-2y^2\right)^{t+1}\right]_0^{1/2} + \int_0^{1/2}\left(1-2y^2\right)^{t+1} dy = \frac{-1}{2^{t+1}} + \underbrace{\int_0^{1/2}\left(1-2y^2\right)^{t+1} dy}_{I_4} \tag{3.26}$$

Let us remark that if t is large enough we get contributions only for very small values of y when $(1-2y^2)$ is close to 1. So we write the the integrand in the form of an exponential and we develop it in Taylor series around $y = 0$.

$$\begin{aligned} I_4 &= \int_0^{1/2} \exp\left((t+1)\ln\left(1-2y^2\right)\right) dy \simeq \int_0^{\infty} e^{-2\left(y^2+y^4\right)(t+1)} dy \\ &\simeq \int_0^{\infty} e^{-2(t+1)y^4} e^{-2(t+1)y^2} dy \end{aligned} \tag{3.27}$$

We will use further the above mentioned fact the y is small compared to 1 using the approximation: $\exp(y^4) \simeq 1 - y^4$.

$$I_4 \simeq \int_0^{\infty} e^{-2(t+1)y^2} dy - 2(t+1)\int_0^{\infty} y^4 e^{-2(t+1)y^2} dy \tag{3.28}$$

The first term of I_4 is a Gaussian integral:

$$I_4 = \sqrt{\frac{\pi}{8}}\frac{1}{\sqrt{t+1}} - \underbrace{2(t+1)\int_0^\infty y^4 e^{-2(t+1)y^2}dy}_{I_5} \tag{3.29}$$

The second term can be integrated using two integrations by parts:

$$\begin{array}{llll} 1.) & g = y^3 & f = \frac{1}{2}e^{-2(t+1)y^2} & f' = 2(t+1)ye^{-2(t+1)y^2} \\ 2.) & g = y & f = \frac{-1}{4(t+1)}e^{-2(t+1)y^2} & f' = ye^{-2(t+1)y^2} \end{array} \tag{3.30}$$

The fully integrated parts are zero because the above functions have zero value both at $y = 0$ and at $y \to \infty$. The result is a Gaussian integral:

$$I_5 = \frac{3}{8}\frac{1}{(t+1)}\int_0^\infty e^{-2(t+1)y^2}dy = \sqrt{\frac{\pi}{8}}\frac{1}{(t+1)^{3/2}} \tag{3.31}$$

The complete result for I_4 reads in the following form:

$$I_4 \simeq \sqrt{\frac{\pi}{8}}\left(\frac{1}{\sqrt{t+1}} + \frac{3}{8}\frac{1}{(t+1)^{3/2}}\right) + \mathcal{O}\left(t^{-5/2}\right) \tag{3.32}$$

Considering now the final result we may omit the exponentially decaying terms as they do not play any role in the $t \to \infty$ limit while we have power law decaying terms.

$$B^{(2)}(t) = 1 - \sqrt{\frac{\pi}{8}}\left(\frac{1}{\sqrt{t+1}} - \frac{3}{8}\frac{1}{(t+1)^{3/2}}\right) + \mathcal{O}\left(t^{-5/2}\right) \tag{3.33}$$

We would like to approximate the above expression in a simpler form where only the leading order term is retained but with a different time shift that can be determined from a Taylor expansion at the $t \to \infty$ limit:

$$B^{(2)}(t) \simeq 1 - \sqrt{\frac{\pi}{8}}\frac{1}{\sqrt{t+a}}, \tag{3.34}$$

The equation for a:

$$\begin{aligned} B^{(2)}(t) &= 1 - \sqrt{\frac{\pi}{8}}\left(\frac{1}{\sqrt{t+1}} - \frac{3}{8}\frac{1}{(t+1)^{3/2}}\right) = 1 - \sqrt{\frac{\pi}{8}}\frac{1}{\sqrt{t}}\left(1 - \frac{1}{2t} - \frac{3}{8}\frac{1}{t} + \mathcal{O}\left(\frac{1}{t^2}\right)\right) \\ &= 1 - \sqrt{\frac{\pi}{8}}\frac{1}{\sqrt{t}}\left(1 - \frac{a}{2t} + \mathcal{O}\left(\frac{1}{t^2}\right)\right) \end{aligned} \tag{3.35}$$

We find $a = 7/4$ thus the final result for the time dependence of the value of the inactive site in the two site model for $n = 2$ reads in the following form:

$$B^{(2)}(t) = 1 - \sqrt{\frac{\pi}{8}}\frac{1}{\sqrt{t+7/4}} \tag{3.36}$$

In the next chapter we will try to reformulate the above procedure for the general case.

3.3.3 Average density of the inactive site in the two site model for general n

Our task in this section is to generalize the calculation of the previous section. Let us note that we only need to solve this problem for $n = 2^N$ as the length of the hierarchical lattice can only be of this form. Unfortunately we cannot formulate the whole probability distribution of the sum of n independent uniform random numbers in a general way. The calculation is only possible at the limits i.e. at $x < 1/n$ or $x > 1 - 1/n$ (cases when only one number out of n may reach its extreme value 1 in the $x < 1/n$ case and 0 in the $x > 1-1/n$ case) but as we will see that this is enough for us.

Let us recall the formula in Eq. 3.20 in the general case for the average value of the largest generated number up to time t:

$$B^{(n)}(t) = (t+1)\int_0^1 x p_n(x) P_n^t(x) dx \tag{3.37}$$

Any cumulative distribution $P(\varrho)$ is a monotonously increasing function with $P(0) \equiv 0$ and $P(1) \equiv 1$. If t is very large the $P_n^t(x)$ term gets neglectable if $P_n^t(x)$ is far from 1. So in the integration the most important contribution comes from the part that is close to 1. This permits us to restrict the integral to the part that we can calculate without loss of consistency:

$$B^{(n)}(t) \simeq \int_{1-1/n}^1 (t+1) x p_n(x) P_n^t(x) dx \qquad (t \gg 1) \tag{3.38}$$

In the following we scratch the calculation of probability distribution $p_n(x)$ for $x < 1/n$. As at most one number may reach 1 we can write this formula in one integral:

$$\begin{aligned}
p(x)|_{x<1/n} &= n\int_0^{nx} dy_1 \int_0^{nx-y_1} dy_2 \cdots \int_0^{nx-\sum_{i=0}^{n-2} y_i} dy_{n-1} = \\
&= n\int_0^{nx} dy_1 \int_0^{nx-y_1} dy_2 \cdots \int_0^{nx-\sum_{i=0}^{n-3} y_i} dy_{n-2} \left\{\left(nx - \sum_{i=0}^{n-3} y_i\right) - y_{n-2}\right\} = \\
&= n\int_0^{nx} dy_1 \int_0^{nx-y_1} dy_2 \cdots \int_0^{nx-\sum_{i=0}^{n-4} y_i} dy_{n-3} \frac{1}{2}\left\{\left(nx - \sum_{i=0}^{n-4} y_i\right) - y_{n-3}\right\}^2 = \\
&\vdots \\
&= \frac{n^n}{(n-1)!} x^{n-1}
\end{aligned} \tag{3.39}$$

For symmetry reasons:

$$p_n(x)|_{x>1-1/n} = \frac{n^n}{(n-1)!}(1-x)^{n-1} \tag{3.40}$$

The cumulative distribution is the integral of the above:

$$P_n(x)|_{x>1-1/n} = 1 - \frac{n^{n-1}}{(n-1)!}(1-x)^n \tag{3.41}$$

Let us now turn back to Eq. 3.38 using an $x = 1 - y$ variable replacement:

$$\begin{aligned} B^{(n)}(t) &= (t+1)\frac{n^n}{(n-1)!}\int_0^{1/n}(1-y)y^{n-1}\left(1-\frac{n^{n-1}}{(n-1)!}y^n\right)^t dy = \\ &= \underbrace{(t+1)\frac{n^n}{(n-1)!}\int_0^{1/n} y^{n-1}\left(1-\frac{n^{n-1}}{(n-1)!}y^n\right)^t dy}_{I_a} - \\ &\quad \underbrace{-(t+1)\frac{n^n}{(n-1)!}\int_0^{1/n} y^n\left(1-\frac{n^{n-1}}{(n-1)!}y^n\right)^t dy}_{I_b} \end{aligned} \tag{3.42}$$

It is easy to evaluate the first integral:

$$I_a = -\left[\left(1-\frac{n^{n-1}}{(n-1)!}y^n\right)^{t+1}\right]_0^{1/4} = 1-\left(1-\frac{n^{n-1}}{(n-1)!}2^{-n}\right)^{t+1} = 1+\mathcal{O}\left(\frac{1}{t}\right) \tag{3.43}$$

The calculation of the second term follows the same path as in the $n = 2$ case. After an integration by parts with

$$g = y \quad \text{and} \quad f' = (t+1)\frac{n^n}{(n-1)!}y^{n-1}\left(1-\frac{n^{n-1}}{(n-1)!}y^n\right)^t \tag{3.44}$$

the fully integrated part decays exponentially with t so we keep only the other term:

$$I_b = \left[-y\left(1-\frac{n^{n-1}}{(n-1)!}y^n\right)^{t+1}\right]_0^{1/n} + \int_0^{1/n}\left(1-\frac{n^{n-1}}{(n-1)!}y^n\right)^{t+1} dy \tag{3.45}$$

The first term can be neglected as it decays exponentially. The second term can be evaluated as the $n = 2$ case using Taylor expansion and partial integration leading to the following result:

$$\begin{aligned} I_b &= \int_0^{1/n}\exp\left\{(t+1)\ln\left(1-\frac{n^{n-1}}{(n-1)!}y^n\right)\right\}dy \\ &\simeq \int_0^{\infty}\exp\left\{-(t+1)\frac{n^{n-1}}{(n-1)!}y^n - \frac{1}{2}(t+1)\frac{n^{2(n-1)}}{(n-1)!^2}y^{2n}\right\}dy \\ &\simeq \int_0^{\infty}\left\{1-\frac{1}{2}(t+1)\frac{n^{2(n-1)}}{(n-1)!^2}y^{2n}\right\}\exp\left\{-(t+1)\frac{n^{n-1}}{(n-1)!}y^n\right\}dy \\ &= \frac{\Gamma(1/n)(n!)^{1/n}}{(t+1)^{1/n}n^2}\left(1-\frac{n+1}{2n^2(t+1)}\right)+\mathcal{O}\left(\frac{1}{t^2}\right) \end{aligned} \tag{3.46}$$

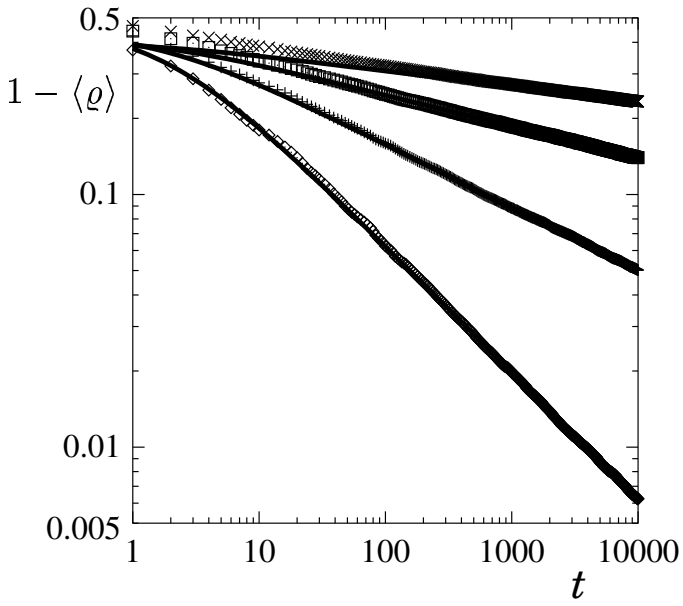

Figure 3.3: The test of the results in Eq. 3.47 against numerical simulations on the same model. The solid lines are the analytical the points are numerical simulation results. The system sizes are $n = 2(\diamond),\ 4(+),\ 8(\square),\ 16(\times)$

We approximate the above result with only one power law function using a different time shift as in the case of $n = 2$ and thus we get the final result:

$$B^{(n)}(t) = 1 - \Gamma(1/n)(n!)^{1/n} n^{-2} \left(t + \frac{3n+1}{2n}\right)^{-1/n} \tag{3.47}$$

On Fig. 3.3 we can see that the above approximation is excellent for small n and large t.

3.3.4 Evaluation of integrals of type I_1

We know that $\varrho^{(1)} = B^{(2)}(t)$ thus in Eq. 3.3 at $N = 2$ in the integration I_1 the integrand is $B^{(2)}(t)$. Furthermore at every level through the competition of the two minimal paths we add the density of the inactive minimal path that can be described by a two site model. Thus during the integration in Eq. 3.3 we have to face the evaluation of integrals of type I_1 with the integrand $B^{(n)}(t)$ with $n = 2^N$. Additionally, we have to be able to repeat this integration to get higher level results. We will thus study the integration of type I_1 in detail.

The problem consists of evaluation integrals of the following form:

$$I_1 = \frac{1}{t}\int_0^t f(t')dt' \tag{3.48}$$

First we use integrands of type $B^{(n)}(t)$:

$$B^{(n)}(t) = \frac{a}{(t+c)^b}, \tag{3.49}$$

with $0 < b < 1$ and $c > 0$. Thus the integration I_1 in Eq. 3.48 reads in the following form:

$$I_1 = \frac{1}{t}\int_0^t \frac{a}{(t'+c)^b}dt' = \frac{a}{1-b}\left(\frac{(t+c)^{1-b}}{t} - \frac{c^{1-b}}{t}\right) \tag{3.50}$$

The further integration of I_1 gives rise to difficulties since both terms of the result diverge at $t = 0$. Thus we use again the same technique as in the case of the two site model that we reformulate this expression in a simpler form that is consistent in the $t \to \infty$ limit.

We find (see Appendix C) that the best choice is to use again the same type of expressions that we used as an input for the integration 3.49:

$$I_1 = \frac{a}{(1-b)}\frac{1}{(t+c')^b} \tag{3.51}$$

This choice is consistent, gives an acceptable approximation that is exact in the asymptotic $1/t$ limit and we could not find any other consistent formula that allows for a complete analytical treatment.

So let us see the Taylor expansion of these two terms at $t \to \infty$:

$$\frac{I_1(1-b)}{a} = \frac{1}{t^b} - \frac{c^{1-b}}{t} + \frac{(1-b)c}{t^{1+b}} + \mathcal{O}\left(\frac{1}{t^2}\right) = \frac{1}{t^b} - \frac{c'b}{t^{b+1}} + \mathcal{O}\left(\frac{1}{t^2}\right) \tag{3.52}$$

As one can see, the leading order terms are the same in both expressions. The next order terms can be identified to each-other if we assume b to be small which is the case if the hierarchical level is large enough (b decays as 2^{-N} with the hierarchical level). In the following we determine c' using this approximation:

$$c' \simeq \frac{c^{1-b} - (1-b)c}{b} \simeq c \tag{3.53}$$

Now we can formulate the approximation for I_1:

$$I_1 = \frac{1}{t}\int_0^t \frac{a}{(t'+c)^b}dt' \simeq \frac{a}{(1-b)}\frac{1}{(t+\frac{2-b}{b}c)^b} \tag{3.54}$$

As in Eq. 3.3 all terms can be reformulated in the form of Eq. 3.49 we closed the system of iterative equations. Thus we can write the time dependence of the density evolution in a N level hierarchical lattice as in Eq. 3.8.

3.4 The Gaussian case

As mentioned in the introduction apart from uniform distributions we also tried Gaussian random number distributions. The idea behind this is that these distribution functions are stable with respect to addition. In the uniform case we could determine the probability distribution only for very large values of densities if the system was large. We also know that the evolution of the average density slows down considerably if the system size increases. Thus we reach later and later the point where our approximation becomes exact (see Fig. 3.2).

However, new difficulties arise in calculating cumulative distributions. An important difference between the uniform and Gaussian cases is that in the latter, there is no upper bound in the density therefore the average density $\langle\varrho\rangle$ of the system, keeps increasing with time.

If the distribution of a single bond is:

$$p(x) = \frac{1}{\sqrt{2\pi}} \exp(-x^2/2) \tag{3.55}$$

then the distribution for a sum of $2n$ bonds is simply

$$p_n(x) = \sqrt{\frac{n}{\pi}} \exp\left(-nx^2\right) \tag{3.56}$$

Now for a Gaussian the cumulative distribution is:

$$P_n(\varrho) = \int_{-\infty}^{\varrho} p_n(x)dx. \tag{3.57}$$

We calculate the average value of the maximal random number out of $t+1$ independent tries using the same formula as for the uniform case that we transform in a simpler form using the previous equation 3.57:

$$B^{(n)}(t) = \int_{-\infty}^{\infty} (t+1)xp_n(x)P_n^t(x)dx = \int_{-\infty}^{\infty} \left.\frac{\partial P_n^{t+1}(y)}{\partial y}\right|_{y=x} x\ dx \tag{3.58}$$

As we mentioned before $P_n(x \to -\infty) = 0$ and $P_n(x \to \infty) = 1$ and monotonously increasing in between which in our case is a relatively sharp, Gaussian change. If we put it on some power the transition from 0 to 1 gets sharper and sharper (Fig. 3.4). Thus for large enough t we can consider this change as a step function.

Before going further with the integration let us identify the position of the step in the $P_n^{t+1}(x)$ functions. The simplest way is to use the value of x_0 at the maximum of the derivate of $P_n^{t+1}(x)$. The cumulative probability distribution in the Gaussian case is an error function:

$$P_n(\varrho) = \sqrt{\frac{n}{\pi}} \int_{-\infty}^{\varrho} \exp\left(-nx^2\right) dx = 1 - \frac{1}{2}\mathrm{ercf}\left(\varrho\sqrt{n}\right) \simeq 1 - \frac{1}{2\sqrt{n\pi}} \frac{\exp(-n\varrho^2)}{\varrho + \sqrt{\varrho^2 + a/n}} \tag{3.59}$$

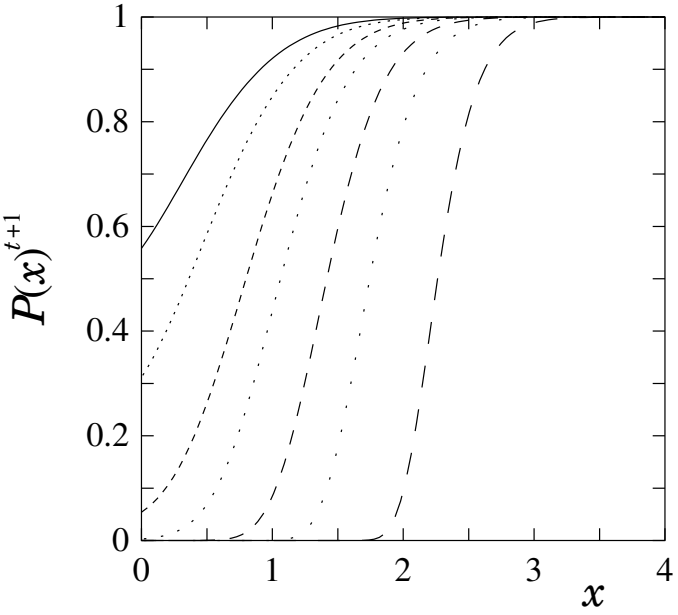

Figure 3.4: The changing region of the $P_n^{t+1}(x)$ curves for $t = 1$, 2, 5, 10, 30, 100, 1000, respectively from left to right.

where a is a constant and $4/\pi < a < 2$. We solve the following equation:

$$\left.\frac{\partial^2 P_n^{t+1}(x)}{\partial x^2}\right|_{x=x_0} = \frac{\partial^2}{\partial x^2}\left[\left(1 - \frac{1}{2\sqrt{n\pi}}\,\frac{\exp(-nx^2)}{x+\sqrt{x^2+a/n}}\right)^{t+1}\right]\Bigg|_{x=x_0} = 0 \tag{3.60}$$

If we consider t to be large enough we get the following result (see Appendix D):

$$x_0(t) = \frac{1}{\sqrt{n}}\sqrt{\ln\frac{t}{4\sqrt{\pi n}}} \tag{3.61}$$

With this step point we rewrite Eq. 3.58 using step functions (θ):

$$B^{(n)}(t) = \int_{-\infty}^{\infty} x\theta'(x-x_0(t))dx = \int_{-\infty}^{\infty} x\delta(x-x_0(t))dx = x_0 = \frac{1}{\sqrt{n}}\sqrt{\ln\frac{t}{4\sqrt{\pi n}}}, \tag{3.62}$$

where $\delta(x)$ is the Dirac delta function. As one can see for all n we get the same functional form, the very slowly increasing function of $\sqrt{\ln t}$. The above result is compared with the numerical data on the same system. The functional form qualitatively correct, however a slight deviation can be observed.

Now we apply this result to the hierarchical lattice. The integration in the parallel coupling Eq. 3.3 reads in the following form:

$$I_1 = \frac{1}{t}\int_1^t B^{(n)}(t')dt' = \frac{1}{\sqrt{n}t}\int_1^t \sqrt{\ln\frac{t'}{4\sqrt{\pi n}}}dt' = \tag{3.63}$$

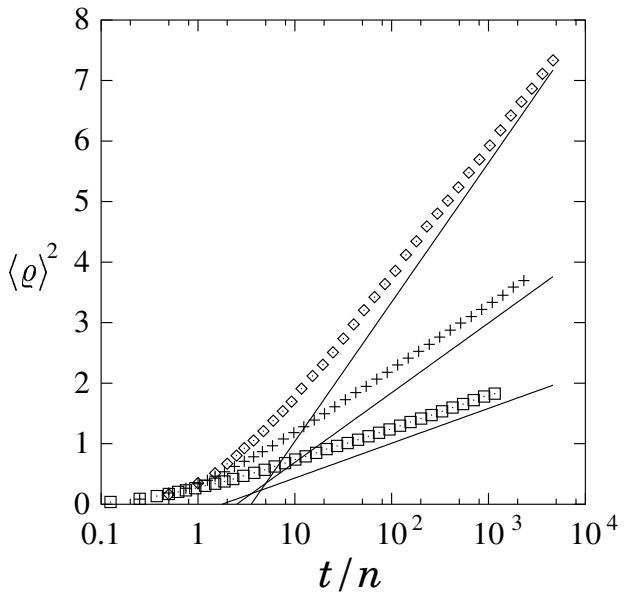

Figure 3.5: The square of the average density of the inactive site in the two site model for the Gaussian case. The analytic results (continuous lines) of Eq. 3.62 are compared to the numerical data (points). The number of used independent random numbers are 2, 4 and 8 respectively from top to bottom.

$$= \frac{1}{\sqrt{n}}\sqrt{\ln\frac{t}{4\sqrt{\pi n}}} - \frac{1}{2t\sqrt{n}} \int_1^t \frac{dt'}{\sqrt{\ln t' - \ln(4\sqrt{\pi n})}}$$

If we are interested in the asymptotics we may use:

$$\lim_{t\to\infty} \frac{1}{2t\sqrt{n}} \int_1^t \frac{dt'}{\sqrt{\ln t' - \ln(4\sqrt{\pi n})}} = 0 \tag{3.64}$$

However the above integral decreases much slower than $1/\sqrt{\ln t}$ and thus for practical point of view it can be very well extrapolated by an effective constant (c_{eff}) that one can set to zero to study the asymptotics. Thus we use:

$$\frac{1}{2t\sqrt{n}} \int_1^t \frac{dt'}{\sqrt{\ln t' - \ln(4\sqrt{\pi n})}} \simeq c_{eff}(n) \tag{3.65}$$

Thus we can conclude that the parallel coupling formula read as:

$$I_1 = \frac{1}{\sqrt{n}}\sqrt{\ln\frac{t}{4\sqrt{\pi n}}} + c_{eff}(n) \tag{3.66}$$

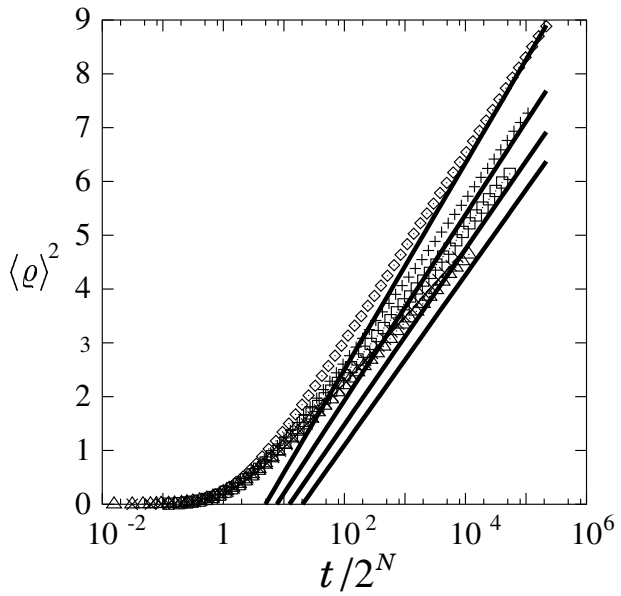

Figure 3.6: Square of the average density versus scaled time for hierarchical lattice of level 2 to 6 from top to bottom respectively. The solid lines are the analytical results from Eq. 3.67 with c_{eff} obtained from numerical integration of Eq. 3.64.

Thus using the results of the uniform case we get the time dependence of the average density of the hierarchical lattice in the form of:

$$\varrho^{(L)}(t) = \sum_{i=1}^{L} \left(\frac{2^{L-i}}{2^L - 1} \right) \left(\frac{1}{\sqrt{2^i}} \sqrt{\ln \frac{t}{4\sqrt{\pi 2^i}}} - (L-i) c_{eff}(2^i) \right) \tag{3.67}$$

As one can observe on Fig. 3.6 the correspondence of this result with the numerical data is very good especially for large times. The most important result in this case is that the functional form of the time dependence of the density does not change with increasing system size and is $\sqrt{\ln t}$. This time dependence can be also observed on the square lattice with Gaussian random number distribution, see Fig. 3.7.

3.5 Hamming distance

As we have seen our numerical and analytical estimates of the process match quite well with the simulations as far as the slow density increase of the system is concerned. Consider now a different quantity like the overlap function shown in Fig. 2.7. For the hierarchical lattice, the overlap has a simple interpretation. If two successive paths differ by $2n$ bonds then this could have been caused by any one of several possibilities — there could have been n one-bond flips, *i.e.* n events at the lowest level, or $n-2$

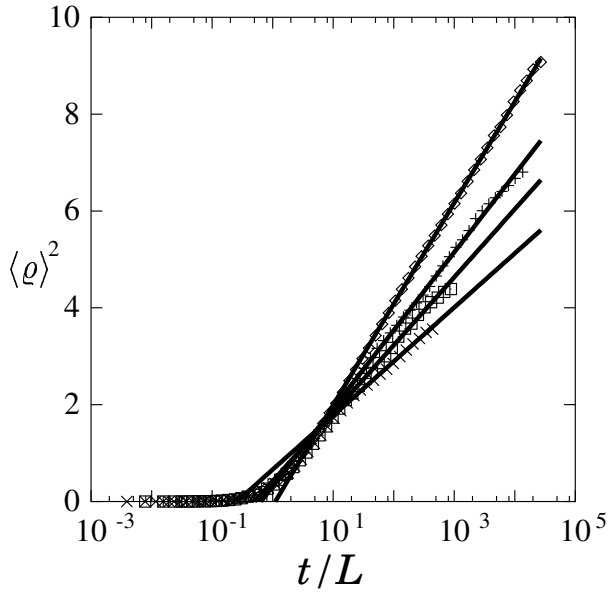

Figure 3.7: The square of the average density of the square lattice vs. time. The system size changes from 32 to 512 from bottom to top. The dashed lines are the numerical data while the solid lines are linear fits.

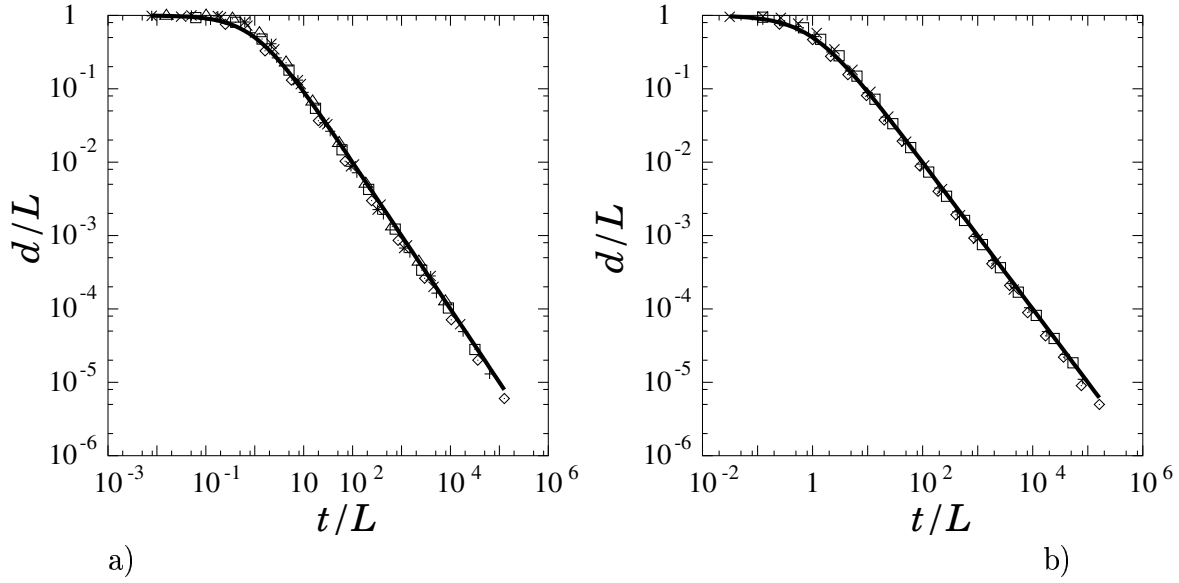

Figure 3.8: The Hamming distance versus time on the hierarchical lattice using uniform a) and Gaussian b) density distributions. Results for systems of level $2-7$ [a)] and $2-5$ [b)] were scaled together. The solid line on both figures is $1/(t+1)$.

events at the lowest level and one event at the second level *etc.* An event takes place every time the activity changes from the currently active subsystem to the inactive one. As we have seen however, this does not depend on the distribution $p_n(x)$ and happens with a probability $\sim 1/(t+1)$. If the time dependence is the same at every level, then the average overlap will also behave this way. In fact as can be seen from the Figure 3.8, the power law seems an excellent fit.

3.6 Conclusion and discussion

In the present Chapter we solved analytically our model exactly in the $\mathcal{O}(1/t)$ limit. The solution describes very well the long time behaviour of finite samples. This allowed us to model accurately the slow dynamics of the densification of the medium that was found to behave as the sum of power functions with exponentially decreasing powers for uniform and the square root of a logarithm for the Gaussian density distribution. Such slow dynamics has been observed in granular media under vibration [KFL+95, NKB+98, CLHN97] and shear [LMP00, NicPou00]. Among the modeling proposed to account for such a slow dynamics, a remarkable success has been obtained with a spin-glass model incorporating geometrical frustration [NCH97]. The model we proposed here considers a different situation, which also suffers from such a slow dynamics, but without any explicit recourse to a glass description.

An other important result which is also a limitation of the present calculation is that the order of the limits is important as usual in slow glassy like dynamics. In the framework of the present study we cannot give a conclusive answer to the $N \to \infty$ limit, however, the logarithmic dependence from the $t \to \infty$ limit of the finite samples seems a reasonable estimate.

Chapter 4

Self-Quenching Walk

In the previous chapter we discussed the late time behaviour of the shear band in a continuously sheared granular material. It was a fluctuating motion that slowed down extremely with passing time. This dynamics inspired us for a model of a random walk describing the dynamics of the shear band. Meanwhile it turned out that this model alone is interesting and complex enough to have a detailed study that we present here.

In this chapter we study a simple model of an active walker which exhibits *logarithmically* slow dynamics entirely due to the local interaction of the walker with a self-created random environment – a kind of self-organized trapping or self-burying effect. This could be observed in the model that we studied in the previous chapter where the wandering of shear bands and the related restructuring of the material was shown to lead to extremely slow relaxation processes and inhomogeneous aging [TKKR00a].

4.1 Definition of the SQW model

Our model is defined as follows. A walker can move on a hyper-cubic lattice in a d dimensional space with linear size L and $N = L^d$ number of sites. Periodic boundary conditions are imposed. A variable s_i chosen from a uniform random distribution $[0, 1]$ is initially assigned to every site i on the lattice. We call the site with the walker the *active* site.

The only permitted elementary moves for the walker are to the nearest neighbours. At every time step a new random number $s_i(t)$ (uniformly sampled between 0 and 1) is assigned to the active site i. If this random number is larger than the value of the s variable of *all* the nearest neighbours, then the same site remains active. Otherwise, the activity moves to the neighbouring site with the largest value of s and the same procedure is repeated. We have chosen here a uniform distribution for s, however, this specific form can be shown to play no role in the time evolution of the active site.

In the following we will refer to this model as Self-Quenching Walk (SQW).

As time goes on, the average value of s decreases and as a result, the probability that the activity moves to one of the neighbours decreases. The definition of the model is thus quite inconvenient in terms of numerical simulation since intervals when nothing happens grow longer and longer with time. However, it is easy to circumvent this difficulty. Let σ be s_j, the largest s value amongst the neighboring sites of the active one, i. For the activity to move to j, the s_i value has to be smaller than σ which is an event with probability σ. Thus the waiting time before a move is a Poisson process with a characteristic time $\tau = 1/\sigma$. Once $s_i < \sigma$, the evolution of the activity is deterministic. Moreover, the distribution of s_i when the activity moves to j is uniform between 0 and σ. Therefore, we can directly reproduce the evolution of the model in terms of the number of moves n rather than in time t. It turns out that the variable n is also more convenient for the analytical treatment.

Similarly, since the s values quickly evolve toward 0, as t increases, it is more convenient to use an equivalent parameterization introducing $r \equiv -\log(s)$. The uniform distribution of s between 0 and σ implies that r is distributed with a density $e^{\varrho - r}$ for $r > \varrho = -\log(\sigma)$. Alternatively, we note that $r - \varrho$ is a random variable exponentially distributed from 0 to ∞. This reformulation allows simulations to be carried out over practically unlimited times without loosing any accuracy. Moreover, as we will see below, r is the appropriate scale for providing an accurate description of the long time regime.

Let us thus consider the motion of the activity (the walker) as a function of the number of moves n, in a potential $V(i,n)$ [where the value of the potential $V(i,n) = r_i(n)$]. The walker moves to the neighbouring site with the *smaller* value of r [since $r \equiv -\log(s)$] after having changed the value of V on the site it was on. The above statement can be made more quantitative in the following two coupled equations of evolution for the walker and the r-landscape:

$$\frac{d\mathbf{X}}{dn} = -\nabla V(\mathbf{X}(n), n) + \eta(n) \tag{4.1}$$

$$\frac{\partial V(\mathbf{x}, n)}{\partial n} = \lambda \delta^d(\mathbf{x} - \mathbf{X}(n)) \tag{4.2}$$

where $\langle \eta(n) \rangle = 0$ and $\langle \eta(n)\eta(n') \rangle = C\delta(n - n')$. Here $\mathbf{X}(n)$ is the position of the walker at 'time' n.

Eq. 4.1 quantifies the rules of the SQW in any dimension. When the walker is on a slope, it moves down towards the valley. When it is in a flat region, it moves to any of the nearest neighbours with equal probability (this is the reason for the uncorrelated noise term). Eq. 4.2 accounts for the increase of the r-landscape at the position of the walker. In this simplified continuum description, we have neglected the randomness in the distribution of the local increments in r, and only retained the average value λ. However, as we shall see below, all the essential features of the

problem are contained in the equations.

4.2 Correspondence with the TSAW model

It turns out that the Langevin equations (Eqs. 4.1 and 4.2) of the SQW in terms of n and r are the same as that of the TSAW as a function of time and position [APP83]. As already mentioned in the Introduction the sum over i of p_i is equal to 1, meaning that the traveler never stays at the points as the SQW in n 'time' units.

In the SQW the values of s decrease exponentially in average as, at each time the walker passes the site we multiply the s value by an random number taken from a uniform distribution between 0 and 1. The values of $r = -\log(s)$ thus increase linearly with the number of times the traveler has passed this site.

In the SQW, whenever the walker can move, it goes deterministically to the neighbouring site with the higher value which is realized by the $g \to \infty$ limit of the TSAW model.

The above mapping thus ensures that in the continuum limit the two models have to be governed by the same Langevin equations which is indeed the case. The TSAW model was studied exhaustively by means of numerical simulations [RAB84, BerPie84], Flory theory [FamDao84], scaling analysis [Pietronero83] and later by exact calculations [Toth94, Toth95].

The critical dimension of the TSAW problem is $d_c = 2$ above which the mean field solution applies and the traveler's asymptotic behavior is not influenced by the interaction with its former path and performs basically a Brownian motion. Bellow two dimensions the trace of the walker is a *fractional* Brownian motion thus the root mean square distance from the origin increases as

$$\langle |\mathbf{X}(n) - \mathbf{X}(n')|^2 \rangle^{1/2} \propto |n - n'|^{\nu} \tag{4.3}$$

with

$$\nu = \begin{cases} 2/(d+2) & \text{for } d \leq 2 \\ 1/2 & \text{for } d > 2 \end{cases} \tag{4.4}$$

Thus in one dimension the walker is super-diffusive with a Hurst exponent of $\nu_{d=1} = 2/3$ which is due to the repulsive interaction with its former path. This asymptotic behavior is numerically verified for the SQW in Fig. 4.1.

We can define other important exponents through the scaling relations: $X \to bX$, $n \to b^z n$ and $V \to b^{\chi} V$, where χ is the so called *roughness exponent* of the r landscape. The exponents have the following values:

$$\begin{array}{llll} \chi = 1/2 & z = 3/2 & \text{in} & d = 1 \\ \chi = 0 & z = d & \text{for} & d \geq 2. \end{array} \tag{4.5}$$

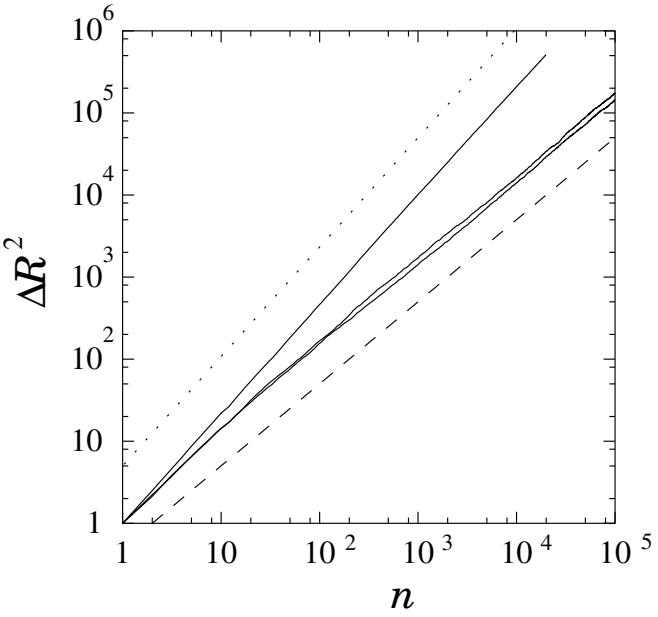

Figure 4.1: The mean square distance from the origin covered by the walker in the steady state, as a function of the number of moves n. The dotted line shows power law with exponent 4/3 (upper) and the dashed with an exponent 1 (lower). The curves are for dimensions 1, 2 and 3 from top to bottom respectively.

We have confirmed the value of χ and z by measuring the width of the r landscape in our model. The width of a self-affine interface is defined as the root mean square fluctuation of the interface.

4.3 Roughness of the potential

In a number of growth models, this width obeys the Family-Vicsek scaling [FamVic91] with a dynamic exponent z such that the overall roughness follows the law:

$$w(n) \propto L^{\chi} \varphi \left(\frac{n}{L^z} \right) \tag{4.6}$$

Fig. 4.2 shows our numerical determination of the width of the r landscape for five different system sizes in one and three dimensions. The collapse with the above mentioned value of the exponents indicates that the r landscape is self-affine in one dimension. However, the growth exponent β describing the roughening of the landscape fluctuations for early times ($n < n^* \sim L^z$) as $w \sim n^{\beta}$ does not obey the Family-Vicsek scaling $\beta = \chi/z$. It is instead given by the formula

$$\beta = (\chi + 1/2)/(1 + \chi), \tag{4.7}$$

which is typical for growth models with extremal dynamics [KTR00, PMB95, TGR98, TKAR99]. Thus our model, though it does not contain a global extremum criterion, belongs to the class of extremal growth models.

The reason why the interface growth (or the r landscape evolution) is similar to extremal dynamics is the following. The activity is a 'random' walk trapped by the maxima of the r-landscape. Before the activity can escape, the landscape has to be filled. In order to escape from a region of extent $\tilde{l}$, the number of moves to be made is of the order of the size of the valley, $\tilde{l}^d$, times its typical depth $\tilde{l}^\chi$. The growth is pinned everywhere except in the immediate vicinity of the walker. The walker itself is, however, in a hierarchically ordered valley structure with maxima of increasing heights. Thus the interface progresses jerkily just as in other extremal growth models. The correspondence with extremal dynamics does not hold above $d_c = 2$. This is because above two dimensions, the walker is no longer trapped by surrounding maxima. It can also find its way around them instead of over them. As a result the interface is no longer rough and $\chi = 0$. However, though the width saturates to a system size-independent value, the exponent β is non-zero for the following trivial reason. In the random initial state, in n steps, a number n sites grow by, say, a uniform amount h. Therefore the width w scales trivially as $w \sim hn^{1/2}L^{-1/2}$. The exponent β is hence equal to $1/2$ for all $d \geq 2$.

4.4 Real time behaviour

We now turn to the behaviour of the walker in real time. In order to understand this, we first note that the mean value of r in the steady state increases linearly with the number of moves. Hence the mean increase of r per site in the steady state is $1/N$, where $N = L^d$ is the number of sites in the system.

We now compute $\langle r^*(n)\rangle$ (the r value of the active site as a function of n) and observe two regimes that we describe by the scaling assumption:

$$\langle r^*(n)\rangle \propto n^\alpha \psi\left(\frac{n}{L^z}\right) \tag{4.8}$$

with $\psi(a) \propto a^0$ for $a \ll 1$ and $\psi(a) \propto a^{1-\alpha}$ for $a \gg 1$. Therefore, for long times $\langle r^*(n)\rangle \propto nL^{-z(1-\alpha)}$. However, in the long time regime, r^* has to increase at the same rate as the mean velocity of the front $\langle r\rangle$, and hence, for $n \gg L^z$, $\langle r^*(n)\rangle = n/N = nL^{-d}$. This imposes

$$z(1-\alpha) = d \quad \text{or} \quad \alpha = 1 - \frac{d}{z} = \frac{\chi}{d+\chi} \tag{4.9}$$

i.e. $\alpha = 1/3$ for $d = 1$ and 0 for $d \geq 2$ consistently with our numerics as shown in Fig. 4.3.

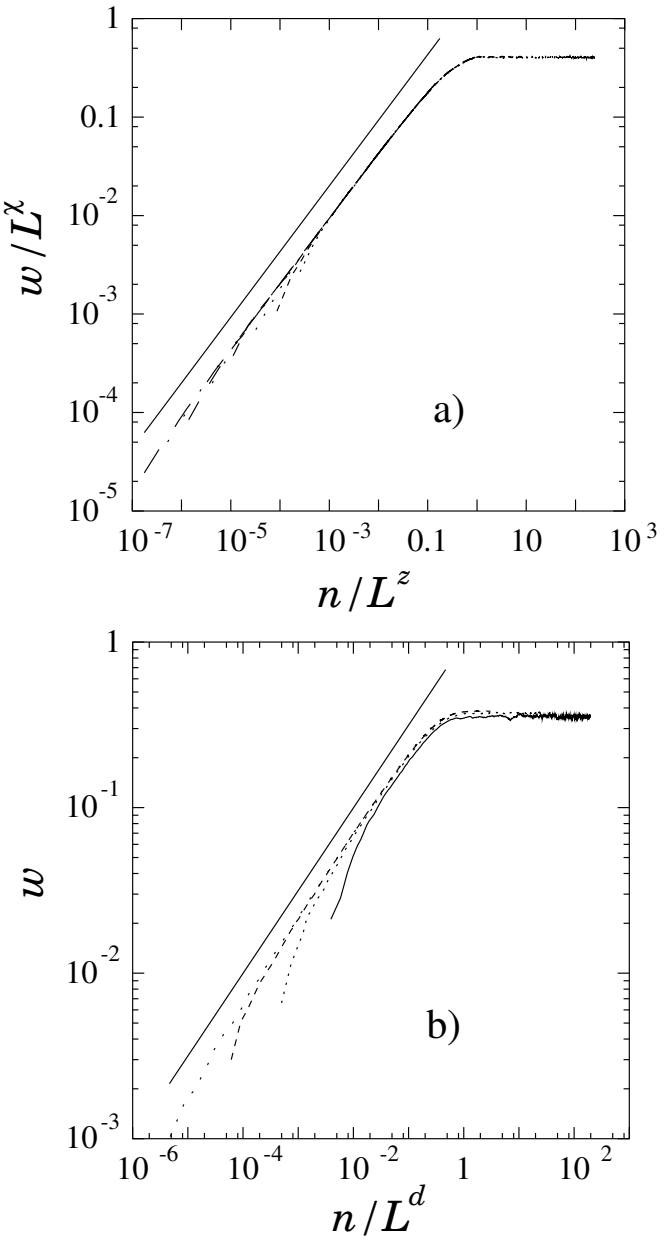

Figure 4.2: a) (Above) Average of squared roughness w in one dimension scaled by L^{χ} as a function of the number of moves n scaled by the dynamic exponent L^{z}. The different curves refer to system sizes 256*1,2,4,8,16; each averaged over 1000 realizations. The slope of the solid line is $\beta = 2/3$.
b) (Bellow) In 3 dimensions the steady state value of the width does not depend on the system size. System sizes 8, 16, 32, 60 were used each averaged over 1000 realizations. The slope of the solid line is $\beta = 1/2$.

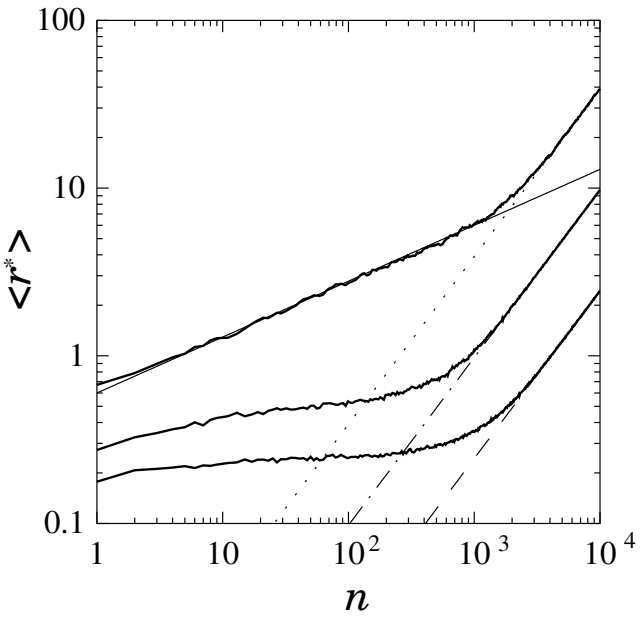

Figure 4.3: Average of r^* as a function of the number of moves n, for a system of size $L = 256$, $L = 32$ and $L = 16$ in 1, 2 and 3 dimensions respectively from top to bottom averaged over 1000 samples. The solid line shows the a power-law of exponent 1/3, whereas the dashed lines are the asymptotic exact increase $r^* = n/N$.

Since, in the late stage regime, r^* increases as n/N, s^* decreases as $e^{-n/N}$. Therefore the expectation value of the real time lapse between two consecutive moves $t(n) - t(n-1)$ is $1/s^*$ or

$$t(n) - t(n-1) \approx e^{n/N} \tag{4.10}$$

$$t(n) = \frac{e^{(n+1)/N} - 1}{e^{1/N} - 1} \sim N e^{n/N} \tag{4.11}$$

This law refers in fact only to the mean value of t. However, the distribution of each increment being exponentially distributed (a Poisson process), the central-limit theorem applies, and the relative standard deviation of t with respect to its mean value vanishes. Figure 4.4 shows the numerically determined time as a function of the number of moves n.

The average value of s as a function of time is thus

$$\langle s \rangle \propto \exp(-n/N) \propto \exp(-\log(t/N)) \propto N/t \tag{4.12}$$

for long times.

Therefore in real time the walker is logarithmically slow with $R(t) \sim \log(t)^{2/3}$ in one dimension and $R(t) \sim \log(t)^{1/2}$ in higher dimensions. The logarithmic dependence of the RMS distance of the walker is just the consequence of Eq. 4.12 as a result of which, the probability of making a jump to a neighbouring site decreases as $1/t$. It is

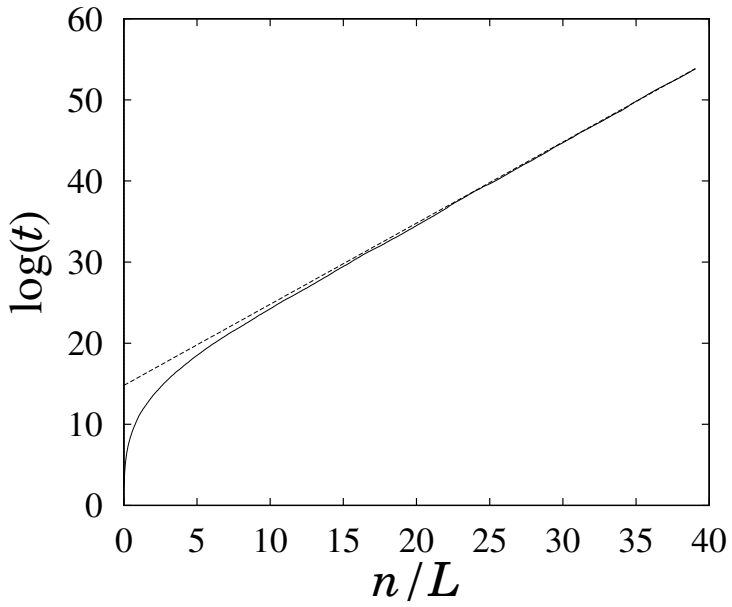

Figure 4.4: Average of the logarithm of the time as a function of the number of moves in $d = 1$, scaled by the system size n/L. The system size is $L = 256$ and the average is performed over 1000 samples. The dotted line is a line of slope 1, as theoretically expected.

thus valid in any dimension. The value of the exponent of the log in one dimension, is however a non-trivial consequence of the coupling between the walker and the medium which induces long-range memory effects.

4.5 Conclusion

In summary, we have introduced and studied a simple model of a walker interacting with its environment. By choosing the correct measures of the time and the potential we could map the SQW problem to the TSAW model thus use the known exact results to describe the SQW walker. In addition, we have studied the emerging landscape too. Though the SQW is local, a relationship with the so called extremal models could be established. The critical dimension is $d_c = 2$ below which the potential landscape gets self-affine and the walker super-diffusive in terms of moves. In real time the walker is logarithmically slow in any dimension.

Appendix A

Transfer matrix method

In this appendix we present the algorithm used to determine the shear band or, in other words, the ground state of a directed polymer in a random potential [DVP78, KarZha87, H-HZ95]. In the following we refer to it as the minimal path. We present this algorithm in the case of the normal square lattice with next nearest neighbours but the tilted square lattice case can be handled in the same way.

Let us consider a square lattice of size L_x by L_y where every site has a density $\varrho(x, y) \in [0 : 1]$. The problem we pose is thus the following: We have to identify the path $\mathcal{P}$ for which

$$S(\mathcal{P}) = \sum_{(x,y)\in\mathcal{P}} \varrho(x, y) = \sum_{x=1}^{L_x} \varrho(x, \mathcal{P}(x)) \tag{A.1}$$

is minimal among all possible paths.

In the following we give an iterative algorithm. First, we note that the above problem is trivial for $L_x = 1$, hence it is enough to choose the smallest value of $\varrho(1, y)$.

Let us now consider a general site (x, y). To every point the path may arrive from three sites [$(x-1, y-1)$, $(x-1, y)$ and $(x-1, y+1)$ see Fig. A.1 a)] thus the minimal path to the site (x, y) has to go through one of these three sites. If we know the minimal path to these points we now the sum of the density along it. The minimum is chosen among them and the site (x, y) is added to this path to get the minimal path to site (x, y). In the previous paragraph we gave the solution for the first column, here from column $x-1$ to x thus we can now determine the path for arbitrary large system.

Thus the determination of the minimal path spanning the sample in the x direction needs the selection of the minimum among three numbers for $(L_x - 1)L_y$ times and once selecting the minimum out of L_y numbers for the last column.

The elementary step in our model (Chapter 2) consists of altering the values of the density along the minimal path and finding anew the minimal path. If we keep the whole result of the previous search in the memory, only a triangle part of the

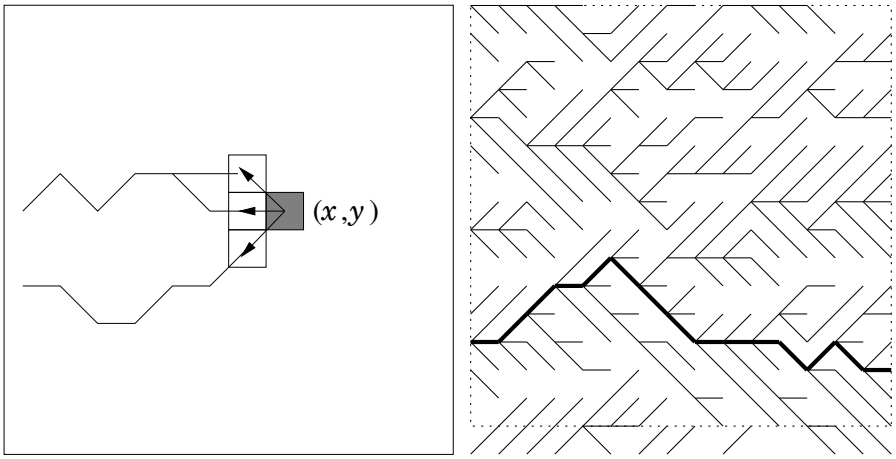

Figure A.1: a) For the site (x, y) we use the paths $(x-1, y-1)$, $(x-1, y)$ and $(x-1, y+1)$. The minimal among these three is chosen and the site (x, y) is added to it.
b) The resulting network from the algorithm. Once the minimum is chosen on the right side the path can be traced back as shown with thick lines. The lines out of the square on the bottom result from the periodic boundary conditions.

sample has to be recalculated that can be further confined if we consider the tree structure [see Fig. A.1 b)] emerging from the initial algorithm and we modify only the necessary branches.

Appendix B

An alternative representation of the localization

The transfer matrix method presented in the previous Appendix can also be used as a nice representation of the system as can be seen on Fig. B.1. However, it is somewhat difficult to read such a figure. First of all one can also start the algorithm on the other side of the sample resulting in an opposite orientation of the lines. Moreover, the current value of the shear band plays an important role in the appearance of the picture since one value change in the shear band (thick lines) can alter regions very far from it.

In spite of these remarks the localization is very apparent through the nice organization of the lines indicating the remarkable depth difference of the valley of the shear band compared to the rest of the system. Beside the overall dominating tree of the shear band one can also trace an alternative route even on the latest figure that is a possible candidate for a large jump if occasionally the mean density of the shear band gets high enough.

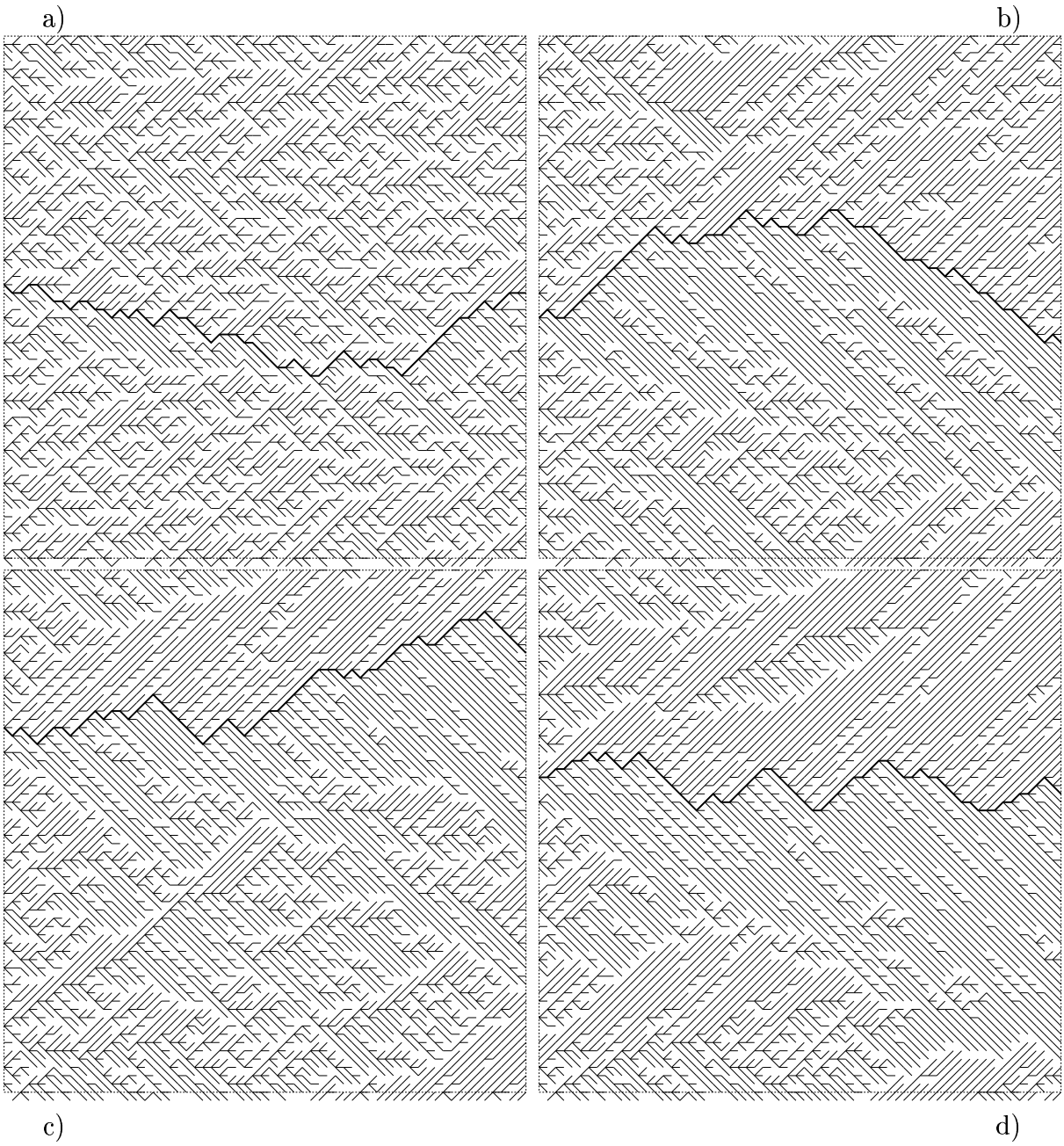

Figure B.1: The tree structure of the transfer matrix method on a 64 by 64 system on a regular square lattice at times: a) $t = 100$, b) $t = 1000$, c) $t = 10^5$ and d) $t = 10^6$. The thick line indicates the current minimal path.

Appendix C

A more general evaluation of the integral I_1

We recall the result of Eq. 3.50 that we want to approximate with an appropriate function:

$$I_1/a = \frac{1}{t}\int_0^t \frac{1}{(t'+c)^b}dt' = \frac{1}{1-b}\left(\frac{(t+c)^{1-b}}{t} - \frac{c^{1-b}}{t}\right) \tag{C.1}$$

An obvious choice of sufficiently general approximation is the following:

$$I_1 \simeq \underbrace{\frac{1}{(t+c't^\alpha)^b}}_{B}, \tag{C.2}$$

where $0 \leq \alpha < 1$.

Now let us check what values of α which makes this form stable respect to further integrations. It is very difficult to determine the primitive function of B so we transform it to a more convenient form using a variable change $y = t^{\alpha-1}$:

$$\begin{aligned} I_{1'} &= \frac{1}{t}\int_0^t \frac{dt'}{(t'+ct'^\alpha)^b} = \frac{1}{t}\int_0^t \frac{dt'}{t'^b(1+ct'^{\alpha-1})^b} = \\ &= \frac{1}{t(1-\alpha)}\int_{t^{\alpha-1}}^\infty y^{\frac{2-\alpha}{\alpha-1}} y^{\frac{-b}{\alpha-1}} \frac{1}{(1+cy)^b}dy = \frac{1}{t(1-\alpha)}\int_{t^{\alpha-1}}^\infty y^A \frac{1}{(1+cy)^b}dy, \end{aligned} \tag{C.3}$$

where $A = (\alpha+b-2)/(1-\alpha) < 0$. Using Mathematica one can evaluate the integral:

$$I_{1'} = \frac{c^{-b}}{(1-\alpha)(b-A-1)} t^{(1-\alpha)(b-A-1)-1}\ {}_2F_1(b, b-A-1; b-A; -t^{1-\alpha}/c), \tag{C.4}$$

where ${}_2F_1(a,b;c;z)$ is a hyperbolic function:

$${}_2F_1(a,b;c;z) = \sum_{k=0}^\infty (a)_k(b)_k/(c)_k \frac{z^k}{k!} \quad \text{and} \quad (a)_k = a(a+1)\cdots(a+k) \tag{C.5}$$

We know also the Taylor expansion of the above hyperbolic function at $t \to \infty$:

$$ {}_2F_1(b, b-A-1; b-A; -x) \simeq \Gamma(b-A)\left\{x^{1+A-b}\left(\frac{\Gamma(1+\alpha)}{\Gamma(b)} + \mathcal{O}\left(\frac{1}{x^2}\right)\right) + \right. $$
$$ \left. + \frac{\Gamma(-1-A)}{\Gamma(-A)\Gamma(b-\alpha-1)}x^{-b} + \frac{-(1+A)b\Gamma(-1-A)}{(2+A)\Gamma(-A)\Gamma(b-1-A)}x^{-1-b} + \mathcal{O}\left(\frac{1}{x^2}\right)\right\} \tag{C.6} $$

Let us put these results together simplifying the powers:

$$ \begin{aligned} (1-\alpha)(b-A-1) - 1 - (1-\alpha)(1+A-b) &= -1 \\ (1-\alpha)(b-A-1) - 1 - (1-\alpha)b &= -b \\ (1-\alpha)(b-A-1) - 1 - (1+b)(1-\alpha) &= \alpha - b - 1 \end{aligned} \tag{C.7} $$

We get:

$$ I_{1'} \simeq \frac{\Gamma(b-A)}{(1-\alpha)(b-A-1)}\left\{\frac{\Gamma(-1-A)}{\Gamma(-A)\Gamma(b-\alpha-1)}t^{-b} + \right. \tag{C.8} $$
$$ \left. + \frac{\Gamma(1+A)c}{\Gamma(b)}t^{-1} + \frac{-(1+A)b\Gamma(-1-A)c^2}{(2+A)\Gamma(-A)\Gamma(b-1-A)}t^{\alpha-b-1} + \mathcal{O}(t^{-2})\right\} $$

This formula is valid only if all Gamma functions are well defined namely none of them has a non-positive integer argument. We have two type of possible singularities:

$$ A = -k, \quad k \in \mathbb{N} \quad \text{and} \quad A = b-1 \tag{C.9} $$

The second one gives $\alpha b = 1$ but as both $0 \leq \alpha,\ b < 1$ this relation cannot occur. The first one gives the restriction for $A \leq -2$: Now one can try to reevaluate the above expansion in series using explicitly $A = -k$:

$$ I_{1'}|_{A=-2} = \frac{\Gamma(2+b)}{(1-\alpha)\Gamma(1+b)^2}\left\{t^{-b} + \frac{b\left[\gamma - 1 + \psi(1+b)\right]}{c}t^{-1-b}\right\} + \mathcal{O}(t^{-2}) $$
$$ I_{1'}|_{A=-3} = \frac{\Gamma(3+b)}{(1-\alpha)\Gamma(2+b)^2}\left\{t^{-b} + \frac{b\left[3/2 - \gamma + \psi(2+b)\right]}{c}t^{-1-b}\right\} + \mathcal{O}(t^{-2}) $$
$$ I_{1'}|_{A\leq -4, A\in\mathbb{N}} = \frac{\Gamma(1-A)}{(1-\alpha)\Gamma(2-A)\Gamma(1+b-A)}\left\{t^{-b} + \frac{b(1-A)}{cA}t^{-1-b}\right\} + \mathcal{O}(t^{-2}), $$

where $\gamma = 0.577\ldots$ is the Euler gamma and $\psi(x) = -\sum_{k=0}^{\infty}(x+k)^{-1}$ is the *digamma* function.

We want to write these integration results back in the original form. So let us write the series expansion of B:

$$ B = \frac{1}{(t+ct^{\alpha})^b} = \frac{1}{t^b} - cbt^{\alpha-b-1} + \frac{1}{2}b(1+b)c^2t^{2a-b-2} + \mathcal{O}(t^{-2}) \tag{C.10} $$

As one can see there is only one possibility to match the order of the leading terms if $\alpha = 0$. In this case the possible powers up to $\mathcal{O}(1/t^2)$ are t^{-b}, t^{-1-b}. This is exactly the approximation we used in section 3.3.4.

Appendix D

Calculation of the inflection point

Let us recall Eq. 3.60 that we want to solve in the $t \to \infty$ limit:

$$\left.\frac{\partial^2 P_n^{t+1}(x)}{\partial t^2}\right|_{x=x_0} = \frac{\partial^2}{\partial t^2}\left[\left(1 - \frac{1}{2\sqrt{n\pi}}\,\frac{\exp(-nx^2)}{x+\sqrt{x^2+a/n}}\right)^{t+1}\right]\Bigg|_{x=x_0} = 0 \tag{D.1}$$

Before turning to the evaluation of the derivate let us note that x_0 grows with increasing time however much slower as t. If we wait long enough x^2 can be much larger than a/n. Thus we rewrite the denominator in the following form:

$$x + \sqrt{x^2 + a/n} \simeq 2x \tag{D.2}$$

With this simplification we get the following:

$$\left.\frac{\partial^2 P_n^{t+1}(x)}{\partial x^2}\right|_{x=x_0} = t(t+1)\left(1 - \frac{\exp(-nx_0^2)}{4\sqrt{n\pi}x_0}\right)^{t-1}\frac{(2nx_0^2+1)^2\exp(-2nx_0^2)}{(4\sqrt{n\pi}x_0^2)^2} - \tag{D.3}$$

$$-(t+1)\left(1 - \frac{\exp(-nx_0^2)}{4\sqrt{n\pi}x_0}\right)^{t}\frac{(4n^2x_0^4+2nx_0^2+2)\exp(-nx_0^2)}{4\sqrt{n\pi}x_0^3} = 0$$

$$\frac{t(2nx_0^2+1)^2\exp(-nx_0^2)}{4\sqrt{n\pi}x_0} = \underbrace{\left(1 - \frac{\exp(-nx_0^2)}{4\sqrt{n\pi}x_0}\right)}_{\simeq 1}\left((2nx_0^2+1)^2 + 2nx_0 + 1\right) \tag{D.4}$$

$$t = \frac{4\sqrt{n\pi}}{\exp(-nx_0^2)}\left(x_0 + \frac{2nx_0+1}{(2nx_0^2+1)^2}\right) \tag{D.5}$$

If we use again the already assumed relation that $x_0 \gg 1$ one gets:

$$t = 4\sqrt{n\pi}x_0\exp(nx_0^2) \tag{D.6}$$

This transcendental equation cannot be solved exactly but only by iterations. The zeroth order solution is the following:

$$x_0^{(1)} = \frac{1}{\sqrt{n}}\sqrt{\ln\frac{t}{4\sqrt{n\pi}}} \tag{D.7}$$

The second order solution:

$$x_0^{(2)} = \frac{1}{\sqrt{n}} \sqrt{\ln \frac{t}{4\sqrt{n\pi}\sqrt{\ln \frac{t}{4\sqrt{n\pi}}}}} \tag{D.8}$$

In the calculations we use only the first order solution that gives already sufficient precision.

Bibliography

[AhaSpa99] E. Aharonov and D. Sparks, *Rigidity phase transition in granular packings*, Phys. Rev. E **60**, 6890 (1999).

[AldWai57] B. J. Alder and T. E. Wainwright, *Phase Transition for a Hard Sphere System*, J. Chem. Phys. **27**, 1208 (1957).

[ABSO81] S. Alexander, J. Bernasconi, W. R. Schneider and R. Orback, *Excitation dynamics in reandom one-dimensional systems*, Rev. Mod. Phys. **53**, 175 (1981).

[APP83] D. J. Amit, G. Parisi and L. Peliti, *Asymptotic behavior of the "true" self-avoiding walk*, Phys. Rev. E **27** 1635, (1983).

[AHT00] J. A. Åström, H. J. Herrmann and J. Timonen, *Granular Packings and Fault Zones*, Phys. Rev. Lett. **84**, 638 (2000).

[BakSne93] P. Bak and K. Sneppen, *Punctuated equilibrium and criticality in a simple model of evolution*, Phys. Rev. Lett. **71**, 4083 (1993).

[BTK87] P. Bak, C. Tang and K. Weisenfeld, *Self-organized criticality: An explanation of the 1/f noise*, Phys. Rev. Lett. **59**, 381 (1987).

[BST+94] E. Ben-Jacob, O. Shochet, A. Tenenbaum, I. Cohen, A. Czirók and T. Vicsek, *Communication, regulation and control during complex patterning of bacterial colonies*, Fractals **2**, 15 (1994).

[BKN98] E. Ben-Naim, J. B. Knight and E. R. Nowak, *Slow relaxation in granular compaction*, Physica D **123**, 380 (1998).

[Bernal65] J. D. Bernal, Proc. R Soc. London Ser. **280**, 299 (1965), and P. M. Chaikin, *Thermodynamics and hydrodynamics of hard spheres: the role of gravity*, page 315 edited by M. E. Cates and M. R. Evans *Soft and Fragile Matter*, (J. W. Arrowsmith Ltd, Bristol 2000).

[BBSA79] J. Bernasconi, H. Beyeler, S. Strässler and S. Alexander, *Anomalous Frequency-Dependent Conductivity in Disordered One-Dimensional Systems*, Phys. Rev. Lett. **42**, 819 (1979).

[BerPie84] J. Bernasconi and L. Pietronero, *True self-avoiding walk in one dimension*, Phys. Rev. B **29** 5196, (1984).

[Berryman83] J. G. Berryman, *Random close packing of hard spheres and disks*, Phys. Rev. A **27**, 1053 (1983).

[BCPE94] J.-P. Bouchaud, M. Cates, J. R. Prakash and S. F. Edwards, *A Model for the Dynamics of Sandpile Surfaces*, J. Phys. I France **4**, 1383 (1994).

[BCPE95] J.-P. Bouchaud, M. Cates, J. R. Prakash and S. F. Edwards, *Hysteresis and metastability in a continuum sandpile model*, Phys. Rev. Lett. **74**, 1982 (1995).

[BCGD90] J.-P. Bouchaud, A. Comtet, A. Georges and P. Le Doussal, *Classical diffusion of a particle in a one-dimensional random force-field* Ann. Phys. **201**, 285 (1990).

[BouGeo90] J.-P. Bouchaud and A. Georges, *Anomalous diffusion in disordered media: Statistical mechanisms, models and physical applications*, Phys. Rep. **195**, 127 (1990).

[BouGen96] T. Boutreaux and P.-G. de Gennes, *Surface Flows of Granular Mixtures: I. General Principles and Minimal Model*, J. Phys. I France **6**, 1295 (1996).

[BPA99] J. J. Brey, A. Prados and B. Sánchez-Rey, *Simple model with facilitated dynamics for granular compaction*, Phys. Rev. E **60**, 5685 (1999).

[BroRic66] R. L. Brown and J. C. Richard, *Principles of Powder Mechanics*, (Pergamon, New York, 1966).

[CLHN97] E. Caglioti, V. Loreto, H. J. Herrmann and M. Nicodemi, *A "Tetris-Like" Model for the Compaction of Dry Granular Media*, Phys. Rev. Lett. **79**, 1575 (1997).

[CWBC98] M. E. Cates, J. P. Wittmer, J.-P. Bouchaud and P. Claudin, *Jamming, Force Chains and Fragile Matter*, Phys. Rev. Lett. **81**, 1841 (1998).

[ClaBou97] P. Claudin and J.-P. Bouchaud, *Static Avalanches and Giant Stress Fluctuations in Silos*, Phys. Rev. Lett. **78**, 231 (1997).

[CBCW98] P. Claudin, J.-P. Bouchaud, M. E. Cates and J. P. Wittmer, *Models of stress fluctuations in granular media*, Phys. Rev. E **57**, 4441 (1998).

[ConHerr96] A. Coniglio and H. J. Herrmann, *Phase transitions in granular packings*, Physica A **255**, 1 (1996).

[CSB76] M. H. Cooke, J. Stephens and J. Bridgwater, *Powder Mixing — A Literature Survey*, Powder Technology **15**, 1 (1976).

[CLM+96] S. N. Coppersmith, C.-H. Liu, S. Majumdar, O. Narayan and T. A. Witten, *Model for force fluctuations in bead packs*, Phys. Rev. E **53**, 4673 (1996).

[CumCra87] D. J. Cumberland and R. J. Crawford, *The packing of Particles*, Handbook of Powder Thecnology Vol. 6 (Elsevier, New York, 1987).

[DVP78] B. Derrida, J. Vannimenus and Y. Pomeau, *Simple frustrated systems: Chains, strips and squares*, J. Phys. C **11**, 4749 (1978).

[Dhar90] D. Dhar, *Self-organized critical state of sandpile automaton models*, Phys. Rev. Lett. **64**, 1613 (1990).

[DAD99] S. Douady, B. Andreotti and A. Daerr, *On granular surface flow equations*, Eur. Phys. J. B **11**, 131 (1999).

[DouDae98] S. Douady and A. Daerr, *Formation of Sandpiles, Avalanches on an Inclined Plane*, page 339, in *Physics of Dry Granular Media* edited by H. J. Herrmann *et al.* (The Netherlands: Kluwer Academic Publisher, 1998).

[DMF99] P. Le Doussal, C. Monthus and D. S. Fisher, *Random walkers in one-dimensional random environments: Exact renormalization group analysis*, Phys. Rev. E **59**, 4795 (1999).

[DurMaz99] J. Duran and T. Mazozi, *Granular boycott effect: How to mix granulates*, Phys. Rev. E **60**, 6199 (1999).

[DKV98] J. Duran, E. Kolb and L. Vanel *Static friction and arch formation in granular materials*, Phys. Rev. E **58**, 805 (1998).

[DML96] J. Duran, T. Mazozi, S. Luding, E. Clément and J. Rajchenbach, *Discontinuous decompaction of a falling sandpile*, Phys. Rev. E **53**, 1923 (1996).

[FamDao84] F. Family and M. Daoud, *Experimental realization of true self-avoiding walks*, Phys. Rev. B **29** 1506, (1984).

[FamVic91] F. Family and T. Vicsek, *Dynamics of fractal surfaces*, (World Scientific, Singapore, 1991).

[FTVV99] Z. Farkas, P. Tegzes. A. Vukics and T. Vicsek, *Transitions in the horizontal transport of vertically vibrated granular layers*, Phys. Rev. E **60**, 7022 (1999).

[FMB97] R. S. Farr, J. R. Melrose and R. C. Ball, *Kinetic theory of jamming in hard-sphere startup flows*, Phys. Rev. E **55**, 7203 (1997).

[GarTho85] E. J. Garboczi and M. F. Thorpe, *Effective-medium theory of percolation on central-force elastic networks. II. Further results*, Phys. Rev. B **31**, 7276 (1985).

[deGennes79] P.-G. de Gennes, *Scaling Concepts in Polymer Physics*, (Cornell University Press, 1979).

[deGennes98] P.-G. de Gennes, *Reflections on the mechanics of granular matter*, Phys. A **261**, 267 (1998).

[GolZan93] I. Goldhirsch and G. Zanetti, *Clustering instability in dissipative gases*, Phys. Rev. Lett. **70**, 1619 (1993).

[H-HZ95] T. Halpin-Healy and Y.-C. Zhang, *Kinetic roughening phenomena, stochastical growth, directed polymers and all that. Aspects of multidisciplinary statistical mechanics*, Phys. Rep. **254**, 215 (1995).

[HalLev98] T. C. Halsey and A. J. Levine, *How Sandcastles Fall*, Phys. Rev. Lett. **80**, 3141 (1998).

[HHR91] A. Hansen, E. L. Hinrichsen ans S. Roux, *Roughness of crack interfaces*, Phys. Rev. Lett. **66**, 2476 (1991).

[HavAvr87] S. Havlin, D. Ben-Avraham, Adv. Phys. **36**, 695 (1987).

[HSK+97] D. Helbing, F. Schweitzer, J. Keltsch, P. Molnár, *Active walker model for the formation of human and animal trail systems*, Phys. Rev. E **56**, 2527 (1997) and references therein.

[HHR97] J. Hemmingsson, H. J. Herrmann and S. Roux, *Vectorial Cellular Automaton for the Stress in Granular Media*, J. Phys. I France **7**, 291 (1997).

[HHL98] H. J. Herrmann, J.-P. Hovi and S. Luding, *Physics of Dry Granular Media*, (The Netherlands: Kluwer Academic Publisher, 1998).

[Hertz82] H. Hertz, Z. reine und angewandte Matematik **92**, 156 (1882).

[Hong93] D. C. Hong, *Stress distributions of a hexagonally packed granular pile*, Phys. Rev. E **47**, 760 (1993).

[HAA+97] D. Hornbaker, R. Albert, I.Albert, A. L. Barabasi, P. Schiffer, *What keeps sand-castles up*, Nature **387**, 6635 (1997).

[HJV96] V. K. Horváth, I. M. Jánosi and P. J. Vella, *Anomalous density dependence of static friction in sand*, Phys. Rev. E **54**, 2005 (1996).

[HBV99] D. Howell, R. P. Behringer and C. T. Veje, *Stress Fluctuations in a 2D Granular Couette Experiment: A Contiuous Transition*, Phys. Rev. Lett. **82**, 5241 (1999).

[Huntley93] J. M. Huntley, *Vacancy effects on the force distributions in a two-dimensional granular pile*, Phys. Rev. E **48**, 4099 (1993).

[HusHen85] D. A. Huse and C. L. Henley, *Pinning and roughening of domain walls in Ising systems due to random impurities*, Phys. Rev. Lett. **54**, 2708 (1985).

[JaeNag92] H. M. Jaeger and S. R. Nagel, *Physics of the Granular State*, Science **255**, 1523 (1992).

[JNB96] H. M. Jaeger, S. R. Nagel and R. P. Behringer, *Granular solids, liquids, and gases*, Rev. Mod. Phys. **68**, 1259 (1996).

[JodTor85] W. S. Jodrey and E. M. Tory, *Computer simulation of close random packing of equal spheres*, Phys. Rev. A **32**, 2347 (1985).

[Johnson85] K. L. Johnson, *Contact mechanics*, (Cambridge University Press, Cambridge, 1985).

[Kardar85] M. Kardar, *Roughening by impurities at finite temperatures*, Phys. Rev. Lett. **55**, 2913 (1985).

[KarZha87] M. Kardar and Y.-C. Zhang, *Scaling of directed polymers in random media*, Phys. Rev. Lett. **58**, 2087 (1987).

[Kertesz92] J. Kertész, *Fractal fracture*, Phys. A **191**, 208 (1992).

[KHW92] J. Kertész, V. K. Horváth and F. Weber, *Self-affinne rupture lines in paper sheets*, Fractals **1**, 67 (1992).

[KFL+95] J. B. Knight, C. G. Fandrich, C. N. Lau, H. M. Jaeger and S. R. Nagel, *Density relaxation in a vibrated granular material*, Phys. Rev. E **51**, 3957 (1995).

[KJN93] J. B. Knight, H. M. Jaeger and S. R. Nagel, *Vibration-Induced Size Separation in Granular Media: The Convection Connection*, Phys. Rev. Lett. **70**, 3728 (1993).

[KNT99] A. J. Kolan. E. R. Nowak and A. V. Tkachenko, *Glassy behavior of the parking lot model*, Phys. Rev. E **59**, 3094 (1999).

[KTR00] S. Krishnamurthy, A. Tanguy and S. Roux, *Dynamic exponent in extremal models of pinning*, Eur. Phys. J. B **15**, 149 (2000).

[LalDou98] L. Laloux and P. Le Doussal, *Aging and diffusion in low dimensional environments*, Phys. Rev. E **57**, 6296 (1998).

[LamWhi68] T. W. Lambe and R. V. Whitman, *Soil-Mechanics* (Wiley, New York, 1968).

[LinCha82] H. M. Linsaya nd P. M. Chaikin, *Elastic Properties of Colloidal Crystals and Glasses*, J. Chem. Phys. **76**, 3774 (1982).

[Liu94] C.-H. Liu, *Spatial patterns of sound propagation in sand*, Phys. Rev. B **50**, 782 (1994).

[LiuNag93] C.-H. Liu and S. R. Nagel, *Sound in a granular material: Disorder and nonlinearity*, Phys. Rev. B **48**, 15646 (1993).

[LNS+95] C.-H. Liu, S. R. Nagel, D. A. Schecter, S. N. Coppersmith, S. Mujumdar, O. Narayan and T. A. Witten, *Force Fluctuations in Bead Packs*, Science **269**, 513 (1995).

[LGNG00] W. Losert, J.-C. Géminard, S. Nasuno and J. P. Gollub, *Mechanism for slow strengthening in granular materials*, Phys. Rev. E **61**, 4060 (2000).

[Louge96] A. Louge, *Étude théorique et éxpreimentale du comportement et de la ségrégation de milieux pâteux lors de l'extrusion*, Ph.D thesis, Université de la Méditerranée, Aix-Marseille, 1996.

[LMF99] G. Løvoll, K. J. Måløy and E. G. Flekkøy, *Force measurement on static granular materials*, Phys. Rev. E **60**, 5872 (1999).

[LMOT99] V. A. Luchnikov, N. N. Medvedev, L. Oger and J.-P. Troadec, *Voronoï-Delaunay analysis of voids in systems of nonspherical particles*, Phys. Rev. E **59**, 7105 (1999).

[Luding97] S. Luding, *Stress distribution in static two-dimensional granular model media in the absence of friction*, Phys. Rev. E **55**, 4720 (1997).

[LMP00] S. Luding, M. Nicolas and O. Pouliquen, *A minimal model for slow dynamics: Compaction of granular media under vibration or shear*, page 241 in *Compaction of Soils, Granulates and Powders*, D. Kolymbas and W. Fellin eds., (A. A. Balkema, Rotterdam 2000), also at cond-mat/0003172.

[Makse97] H. A. Makse, *Stratification instability in granular flows*, Phys. Rev. E **56**, 7008 (1997).

[MJS00] H. A. Makse, D. L. Johnson and L. M. Schwartz, *Packing of Compressible Granular Materials*, Phys. Rev. Lett. **84**, 4160 (2000).

[MBCW98] H. A. Makse, R. C. Ball, H. E. Stanley and S. Warr, *Dynamics of granular stratification*, Phys. Rev. E **58**, 3357 (1998).

[MHHR92] K. J. Måløy, A. Hansen, E. L. Hinrichsen and S. Roux, *Experimental Measurements of the Roughness of Brittle Cracks*, Phys. Rev. Lett. **68**, 213 (1992).

[MLEH99] T. G. Mason, A. J. Levine, D. Ertaş and T. C. Halsey, *Critical angle of wet sandpiles*, Phys. Rev. E **60**, R5044 (1999).

[MelBal95] L. R. Melrose and R. C. Ball, *The Pathological Behaviour of Sheared Hard Spheres with Hydrodynamic Interactions*, Europhys. Lett. **32**, 535 (1995).

[MHB96] B. Miller, C. O'Hern and R. P. Behringer, *Stress Fluctuations for Continuously Sheared Granular Materials*, Phys. Rev. Lett. **77**, 3110 (1996).

[MonBou96] C. Monthus and J.-P. Bouchaud, *Models of traps and glass phenomenology*, J. Phys. A: Math. & Gen. **29**, 3847, (1996).

[MJN98] D. M. Mueth, H. M. Jaeger and S. R. Nagel, *Force distribution in a granular medium*, Phys. Rev. E **57**, 3164 (1998).

[NCH97] M. Nicodemi, A. Coniglio and H. J. Herrmann, *Frustration and slow dynamics of granular packings*, Phys. Rev. E **55**, 3962 (1997).

[NicPou00] M. Nicolas, P.Duru and O. Pouliquen, *Compaction of a granular material under cyclic shear*, Eur. Phys. J. E to be published, also at cond-mat/0006252.

[NKB+98] E. R. Nowak, J. B. Knight, E. Ben-Naim, H. M. Jaeger and S. R. Nagel, *Density fluctuations in vibrated granular materials*, Phys. Rev. E **57**, 1971 (1998).

[OnoLin90] G. Y. Onoda and E. G. Liniger, *Random Loose Packings of Uniform Spheres and Dilatancy Onset*, Phys. Rev. Lett. **64**, 2727 (1990).

[OroHer98] G. Oron and H. J. Herrmann, *Exact calculation of force networks in granular piles*, Phys. Rev. E **58**, 2079 (1998).

[OroHer00] G. Oron and H. J. Herrmann, *Generalisation of space-filling bearings to arbitrairy loop size*, J. Phys. A **33**, 1417 (2000).

[Ouaguenouni97] S. Ouaguenouni, Ph.D thesis, Université Pierre et Marie Curie, Paris, 1997.

[OuaRou97] S. Ouaguenouni and J.-N. Roux, *Force distribution in frictionless granular packings at rigidity threshold*, Eurphys. Lett. **39**, 117 (1997).

[PMB95] M. Paczuski, S. Maslov and P. Bak, *Avalanche dynamics in evolution, growth, and depinning models*, Phys. Rev. E **53**, 414 (1995).

[PDB95] H. K. Pak, E. Van Doorn and R. P. Behringer, *Effects of Ambient Gases on Granular Materials under Vertical Vibration*, Phys. Rev. E **23**, 4643 (1995).

[PLR00] M. Piccioni, V. Loreto and S. Roux, *Criticality of the "critical state" of granular media: Dilatancy angle in the Tetris model*, Phys. Rev. E **61**, 2813 (2000).

[Pietronero83] L. Pietronero, *Critical dimensionality and exponent of the true self-avoiding walk*, Phys. Rev. B **27** 5887, (1983).

[PABT92] C. Poirier, M. Ammi, D. Bideau and J.-P. Troadec, *Experimental Study of the Geometrical Effects in the Localization of Deformation*, Phys. Rev. Lett. **68**, 216 (1992).

[PMW97] O. Pouliquen, M. Nicolas and P. D. Weidman, *Crystallization of non-Brownian Spheres under Horizontal Shaking*, Phys. Rev. Lett. **79**, 3640 (1997).

[PDDK96] V. B. Priezzhev, D. Dhar, A. Dhar and S. Krishnamurthy, *Eulerian Walkers as a Model of Self-Organized Criticality*, Phys. Rev. Lett. **77**, 5079 (1996).

[RBR96] F. Radjai, L. Brendel and S. Roux, *Nonsmoothness, indeterminacy, and friction on two-dimensional arrays of rigid particles*, Phys. Rev. E **54**, 861 (1996).

[RJMR96] F. Radjai, M. Jean, J.-J. Moreau, S. Roux, *Force Distributions in Dense Two-Dimensional Granular Systems*, Phys. Rev. Lett. **77**, 274 (1996).

[RadRou95] F. Radjai and S. Roux, *Friction-induced self-organization of a one-dimensional array of particles*, Phys. Rev. E **51**, 6177 (1995).

[RajMor98] S. Rajasekar and K. P. N. Murthy, *Dynamical evolution of escape probability in the presence of Sinai disorder*, Phys. Rev. E **57**, 1315 (1998).

[RAB84] R. Rammal, J-C. Angles d'Auriac and A. Benott, *Statistics of the true self-avoiding walk in one dimension*, J. Phys. A: Math. & Gen. **17** L9, (1984).

[Reynolds85] O. Reynolds, *On the dilatancy of media composed of rigid particles in contact*, Philos. Mag. **20**, 469 (1885).

[ROTG99] P. Richard, L. Oger, J.-P. Troadec and A. Gervois, *Geometrical characterization of hard-sphere systems*, Phys. Rev. E **60**, 4551 (1999).

[ROF64] E. G. Rippie, J. L. Olsen and M. D. Faiman, *Segregation Kinetics of Particulate Solids Systems II.*, Journal of Pharmaceutical Sciences **53**, 1361 (1964).

[RSPS87] A. Rosato, K. J. Strandburg, F. Prinz and R. H. Swendsen, *Why th Brazil Nuts Are on Top: Size Segregation of Particulate Matter by Shaking*, Phys. Rev. Lett. **58**, 1038 (1987).

[Roux00] J.-N. Roux, *On the geometric origin of mechanical properties of granular materials*, Phys. Rev. E to appear, also at cond-mat/0001246.

[RouRad98] S. Roux and F. Radjai, *Texture-Dependent Rigid-Plastic Behavior*, page 229 in *Physics of Dry Granular Media* edited by H. J. Herrmann *et al.* (The Netherlands: Kluwer Academic Publisher, 1998).

[SSH96] S. B. Santra, S. Schwartzer and H. J. Herrmann, *Fluid-induced particles-size segregation in sheared granular assemblies*, Phys. Rev. E **54**, 5066 (1996).

[SKW00] M. Sasvári, J. Kertész and D. E. Wolf, *Instability of the symmetric Couette-flow in a granular gas: hydrodynamic field profiles and transport*, Phys. Rev. E (to be published).

[Savage84] S. B. Savage, *The mechanics of rapid granular flows*, Adv. Appl. Mech. **24**, 289 (1984).

[SavLun88] S. B. Savage and C. K. K. Lun, *Particle size segregation in inclined chute flow of dry cohesionless granular solids*, Journal of Fluid Mechanics **189**, 311 (1988).

[SchSok98] H. Schiessel, I. Sokolov and A. Blumen, *Dynamics of a polyampholyte hooked around an obstacle*, Phys. Rev. E **57**, 2390 (1997).

[SchZia99] B. Schmittmann and R. K. P. Zia, *"Weather" Records: Musings on Cold Days after a Long Hot Indian Summer*, cond-mat/9905103.

[Schollmann99] S. Schöllmann, *Simulation of a two-dimensional shear cell*, Phys. Rev. E **59**, 889 (1999).

[Scott60] G. D. Scott, *Packing of spheres*, Nature **188**, 908 (1960).

[SMB97] L. E. Silbert, J. R. Melrose and R. C. Ball, *Colloidal microdynamics: Pair-drag simulations of model-concentrated aggregated systems*, Phys. Rev. E **56**, 7067 (1997).

[Sinai82] Ya G. Sinai, Theory Probab. Appl. **27**, 247 (1982).

[SzyLab99] K. Szymanski and Y. Labaye, *Energy dissipation of a bouncing ball*, Phys. Rev. E **59**, 2863 (1999).

[TGR98] A. Tanguy, M. Gounelle and S. Roux, *From individual to collective pinning: Effect of long-range elastic interactions*, Phys. Rev. E **58**, 1577 (1998).

[TKAR99] A. Tanguy, S. Krishnamurthy, P. Abry and S. Roux, *A Stichastic Description for Extremal Dynamics*, cond-mat/9908212.

[TAP+99] P. Tegzes, R. Albert, M. Paskvan, A.-L. Barabási, T. Vicsek and P. Schiffer, *Liquid-induced transitions in granular media*, Phys. Rev. E **60**, 5823 (1999).

[ThomGre91] P. A. Thompson and G. S. Grest, *Granular Flow: Friction and the Dilatancy Transition*, Phys. Rev. Lett. **67**, 1751 (1991).

[Toth94] B. Tóth, *True self-avoiding walks with generalized bond repulsion on zeta*, J. Stat. Phys. **77** 17, (1994).

[Toth95] B. Tóth, *The "true" self-avoiding walk with bond repulsion on ζ: Limit theorems*, Ann. Probab. **23** 1523, (1995).

[TKKR00a] J. Török, S. Krishnamurthy, J. Kertész and S. Roux, *Self-organization, Localization of Shear Bands and Aging in Loose Granular Materials*, Phys. Rev. Lett. **84**, 3851 (2000).

[TKKR00b] J. Török, S. Krishnamurthy, J. Kertész and S. Roux, *Formation of Shearbands and Aging in Granular Media*, To be published.

[TKKR00c] J. Török, S. Krishnamurthy, J. Kertész and S. Roux, *Self-Quenched Dynamics*, To be published, also at cond-mat/0004118.

[TKKR00d] J. Török, S. Krishnamurthy, J. Kertész and S. Roux, unpublished.

[TorRou00] J. Török and S. Roux, *Heterogeneous Mohr-Coulomb plastic material*, Granular Matter **2**, 71 (2000).

[TBG+86] T. Travers, D. E. Bideau, A. Gravois, J.P. Troadec, J. C. Message, *Uniaxial compression effects on 2D mixtures of 'hard' and 'soft' cylinders*, J. Phys. A: Math. Gen. **19**, L1033 (1986).

[TVC98a] O. Tsoungui, D. Vallet and J.-C. Charmet, *Experimental Study of the Force Distributions Inside a 2D Granular System*, page 237 in *Physics of Dry Granular Media* edited by H. J. Herrmann *et al.* (The Netherlands: Kluwer Academic Publisher, 1998).

[TVC98b] O. Tsoungui, D. Vallet and J.-C. Charmet, *Use of contact area trace to study the force distributions inside 2D granular systems*, Granular Matter **1**, 65 (1998).

[TVCR98] O. Tsoungui, D. Vallet, J.-C. Charmet and S. Roux, *"Partial pressures" supported by granulometric classes in polydisperse granular media*, Phys. Rev. E **57**, 4458 (1998).

[VCB+00] L. Vanel, P. Claudin, J.-P. Bouchaud, M. E. Cates, E. Clément and J. P. Wittmer *Stresses in Silos: Comparison Between Theoretical Models and New Experiments*, Phys. Rev. Lett. **84**, 1439 (2000).

[VanCle99] L. Vanel and E. Clément, *Pressure screening and uctuations at the bottom of a granular column*, Eur. Phys. J. B **11**, 525 (1999).

[VHC+99] L. Vanel, D. Howell, D. Clark, R. P. Behringer and E. Clément, *Memories in sand: Experimental tests of construction history on stress distributions under sandpiles*, Phys. Rev. E **60**, R5040 (1999).

[VHB99] C. T. Veje, D. W. Howell and R. P. Behringer *Kinematics of a two-dimensional granular Couette experiment at the transition to shearing*, Phys. Rev. E **59**, 739 (1999).

[VHB+98] C. T. Veje, D. W. Howell, R. P. Behringer, S. Schöllmann, S. Luding and H. J. Herrmann, *Fluctuations and Flow for Granular Shearing*, page 237 in *Physics of Dry Granular Media* edited by H. J. Herrmann *et al.* (The Netherlands: Kluwer Academic Publisher, 1998).

[Williams76] J. C. Williams, *The Segregation of Particulate Materials. AReview*, Powder Technology **15**, 245 (1976).

[WCC97] J. P. Wittmer, M. E. Cates and P. Claudin, *Stress Propagation and Arching in Static Sandpiles*, J. Phys. I France **7**, 39 (1997).

[Wood90] D. M. Wood, *Soil Behaviour and Critical State Soil Mechanics*, (Cambridge University Press, New York 1990).

[WooBud80] D. M. Wood and M. Budhu, *Proc. Int. Symp. on Soils under Cyclic and Transient Loading* (Balkema Press, Swansea, 1980).

[WooJac57] W. W. Wood and J. D. Jacobson, *Preliminary Results From a Recalculation of the Monte Carlo Equation of State of Hard Spheres*, J. Chem. Phys. **27**, 1207 (1957).

[ZolChe92] J. A. Zollweg and G. V. Chester, *Melting in two dimension*, Phys. Rev. B **46**, R11186 (1992).

Summary

The purpose of the present thesis was to study the slow dynamics related to the shearing process in loose granular media. We defined a mesoscopic model in very simple terms which shows extremely complex behaviour and mimics in many ways the phenomena observed in granular matter. This model was investigated by numerical simulations and the results are presented in Chapter 2. The model could be treated analytically on the diamond hierarchical lattice and the asymptotically exact solution is for several quantities in good agreement with the numerical data for the Euclidean dimensional model (Chapter 3). The slow dynamics is introduced in our model by a wandering object which influences the landscape where it can move in. This mechanism lead us to the idea of defining the Self-Quenching Walk model which captures the two basic features of the slow dynamics: localization and aging. The study of this model is the topic of Chapter 4.

Our shear band model is based on very crude assumptions: We treat the medium on a mesoscopic level and characterize its properties by a single scalar variable, the density. This is supposed to be in one to one relationship with the stability and it is distributed at the beginning of the shear procedure randomly, with a relatively low mean. We identify the position of the shear band – where the relative motion of the grains take place – by the line of minimal strength, i.e., by the path on which the sum of the densities is minimal. The restructuring of the material along the shear band is taken into account by redistributing random densities on it.

Though very simple, our model shows many interesting features. It reflects the compactification of the material during shear, the slow asymptotic dynamics and the existence of the critical density in the shear band – all phenomena which have been found in experiments. Moreover we have been able to make predictions about the emerging structure in a sheared granular material and made suggestions for its experimental observation.

The model has got a very interesting temporal evolution. The first regime, up to $t \sim 2L$ (where L is the linear dimension of the sample) is characterized by a uniform strain field like in fluid dynamics. After a transition regime, this behaviour is replaced by strong localization (beyond $t \sim 20L$). This crossover is reflected in the time dependence of many quantities.

The average density of the system has a very slow convergence to the asymptotic with a functional dependence between power law and a logarithm. The aging mechanism is reflected in the unusual size dependence of the average density.

The simplified structure of the hierarchical lattice enabled the analytical treatment of the model, at least in the long time limit. Using extremal statistics we arrived at closed formula on the asymptotic behaviour of the density and the Hamming distance. The solution elucidate further the localization mechanism responsible for the slow dynamics.

We studied both the uniform and the Gaussian distribution cases and for the first one the average density was found to be the sum of power law functions with exponentially decreasing powers that can be extrapolated by a logarithm function. The Gaussian case gives the $\sqrt{\ln t}$ dependence for the average density irrespect to the system size and the lattice type.

The Self-Quenching Walk model is in a sense a caricature of the shear band model. It is an active walker model which leads to slow dynamics due to localization caused by the potential influenced by the walker. We have shown that choosing appropriate time and potential measures the problem could be mapped onto the "True" Self-Avoiding Walk model where the walker was found to be super-diffusive in one dimension. This is the case if we measure the time in terms of steps, however, the real time behaviour is logarithmically slow (in any dimension).

We have shown that the appropriately measured landscape formed by the walker is self-affine in one dimension while it is flat above the critical dimension $d_c = 2$ (with logarithmic corrections in $d_c = 2$). The evolution of the landscape follows the rules of the extremal growth models although there are no global extremal criterion and and long range interactions. This correspondence gives a possibility to study the extremal dynamics on a simple model.

Résumé

Le but de la présente thèse est d'étudier la dynamique lente des processus de cisaillement dans les matériaux granulaires en vrac. On a défini d'une manière très simple un modèle qui montre un comportement extrêmement complexe et est en même temps décrit plusieurs détails des phénomènes observés dans les matériaux granulaires. On a étudié le modèle à l'aide des simulations numériques et les résultats sont présenté dans le Chapitre 2. Il était possible d'analyser le modèle analytiquement sur un réseau hiérarchique de rhomboèdre et de trouver une solution exacte asymptotiquement qui est en accord qualitatif avec des donnés numériques sur les réseaux Euclidiens (Chapitre 3.). La dynamique lente dans notre modèle est le résultat d'un objet qui modifie le potentiel dans lequel il bouge. Ce comportement nous a inspiré de définir le modèle Self-Quenching Walk qui prend en compte les phénomènes principaux de la dynamique lente: la localisation et le vieillissement. L'analyse du modèle se trouve dans le Chapitre 4.

Notre modèle de la bande de cisaillement est basé sur de solides hypothèses: On considère le matériau sur une échelle mesoscopique qui est caractérisé par une seule variable scalar, la densité qui est supposée être en relation bijective avec la stabilité et être distribué au début du processus de cisaillement d'une manière aléatoire avec une moyenne modérée. On identifie la position de la bande de cisaillement – où la motion relative des grains est effectuée – du chemin minimal en d'autres termes du chemin sur lequel la somme des densités est minimale. La restructuralisation des grains dans la bande de cisaillement est considérée par la redistribution des densités sur la bande.

Bien que notre modèle soit très simple, il montre beaucoup de phénomènes très intéressants. Il reflète la compactification du matériau dû au cisaillement, dynamique asymptotique très lent et l'existence d'une densité critique – des phénomènes qui sont produits dans les expériences. De plus nous étions capables d'établir des prédictions de la structure dans un matériau granulaire cisaillé et de données des suggestions de son observation expérimentale.

Le modèle a une évolution temporaire très intéressante. Le régime premier qui dure jusqu'à $t \sim 2L$ (où L est la dimension linéaire de l'échantillon) est caractérisée par une déformation uniforme comme dans les mécaniques des fluides. Après un régime transitoire (après $t \sim 20L$) ce comportement est remplacé par une localisation

forte. Ce changement brusque de comportement peut être observé sur des multitudes de quantités.

La densité moyenne du système converge très lentement vers sa valeur asymptotique avec une dépendance temporaire plus lente que loi de puissance mais plus rapide que logarithmique. Le mécanisme de vieillissement est démontré par la dépendance de taille irrégulière et inhabituelle.

La structure simplifiée du réseau hiérarchique permet de traiter analytiquement notre modèle au moins dans la limite des temps assez large. En utilisant des statistiques d'extrêmes on est arrivé à des formules fermées sur le comportement asymptotique de la densité moyenne et de la distance de Hamming. La solution éclaire le processus de la localisation responsable de la dynamique lente.

On a même étudié les cas de distribution de la densité uniforme et Gaussienne. Pour le dernier on a reproduit quantitativement la forme fonctionnelle de la dépendance temporaire de la densité moyenne qui varie comme $1/\sqrt{\ln t}$ indépendamment du type de réseau et de la taille. Cette dépendance logarithmiquement lente est observé aussi dans les expériences.

Le modèle Self-Quenching Walk est dans un sens une caricature de la motion de la bande de cisaillement. C'est un modèle d'une marche aléatoire active, qui donne vie comme la précédente à une dynamique lente due à l'interaction mutuelle de promeneur et de potentiel qui est altérée par le promeneur même. On a montré qu'en choisissant les mesures du temps et du potentiel que le problème pouvait être identifié avec le modèle de "True" Self-Avoiding Walk. Dans ce modèle le promeneur est superdiffusive dans une dimension qui est aussi le cas dans notre modèle si on considère les pas de promeneur mais en temps réel, la marche devient logarithmiquement lente (dans tous les dimensions).

On a montré que le potentiel dans les mesures appropriées est auto-affine dans une dimension, mais elle est plate au-dessus de la dimension criticale $d_c = 2$ (avec des corrections logarithmiques en deux dimensions). L'évolution de potentiel suit des règles des modèles de croissance extrême bien que il n'y ait pas de critère extrême ni d'interactions de longue portée. Cette correspondance donne une possibilité d'étudier la dynamique extrême sur un modèle aussi simple.

Összefoglalás

A jelen doktori disszertációban laza szemcsés anyagok nyírása során fellépő lassú dinamikával foglalkoztunk. Definiáltunk egy egyszerű mezoszkópikus modellt, amely ennek ellenére meglepően bonyolult viselkedést mutat és több, granuláris anyagokon megfigyelt jelenséget is helyesen visszaad. A modellt először számítógépes szimulációval vizsgáltuk, amelynek eredményeit a 2. fejezetben foglaltuk össze. A modellt hierarchikus gyémántrácson analitikusan is lehetett kezelni és az aszimptotikusan egzakt megoldás több mennyiség esetében is jó egyezést mutat az euklidészi rácson definiált modellen kapott numerikus eredményekkel (3. fejezet). Modellünkben amiatt lép fel a lassú dinamika, hogy egy bolyongó objektum (nyírási sáv) módosítja a mozgását meghatározó potenciált. Ez a mechanizmus vezetett bennünket a Self-Quenching Walk modell tanulmányozásához. Ez a modell szemléletesen ragadja meg lassú dinamika a két meghatározó tulajdonságát: a lokalizációt és az öregedést. A modellt a 4. fejezetben tanulmányoztuk.

A nyírási sáv modellünk néhány nagyon alapvető feltételezéseken alapult: a granuláris mintát mezoszkópikus méretskálán írtuk le és tulajdonságait mindössze egyetlen skaláris paraméterrel, a sűrűséggel jellemeztük. A sűrűségről feltételeztük, hogy monoton bijektív viszonyban áll az anyag lokális stabilitásával, továbbá, hogy kezdetben véletlenszerűen oszlik el viszonylag alacsony átlagértékkel. A nyírási sávot a leggyengébb útvonallal azonosítottuk, amelyik mentén a sűrűségek összege minimális. A szemcsék egymáshoz képest történő elmozdulása, csak a nyírási sáv mentén lehetséges. A lokális átrendeződés hatására létrejövő sűrűségváltozást úgy vettük figyelembe, hogy a nyírási sáv mentén véletlenszerűen újraosztottuk a sűrűségeket.

Egyszerűsége ellenére a modellünk sok érdekes jelenséget mutat. Visszaadja a ritka granuláris anyagok nyírása estén megfigyelt sűrűsödést, a lassú aszimptotikus viselkedést és a kritikus sűrűség létezését. Mindezen jenségeket kísérletek során is megfigyelték. Emellett képesek voltunk prediktív becsléseket adni a nyírt anyag belső szerkezetével kapcsolatban.

A modell időfejlődése rendkívül érdekes és három jól elkülönülő részre osztható. Az első rész, amely körülbelül $t \sim 2L$-ig tart (ahol L a lineáris rendszerméret) egyenletes elmozdulásmezővel jellemezhető, mint a folyadékok esetében. Egy átalakulási rész (kb. $t \sim 20L$-ig) után a fenti viselkedést egy erős lokalizáció váltja fel. Az

átalakulás a rendszert jellemző több mennyiségen is megfigyelhető.

A minta átlagsűrűsége nagyon lassan tart az aszimptotikus értékéhez, amelyet numerikusan gyorsabbnak találtunk, mint logaritmikus, de lassabnak, mint egy hatványfüggvény, legalábbis a numerikusan elérhető rendszerméretek esetén.

A hierarchikus rács egyszerű szerkezete lehetővé tette számunkra, hogy analitikusan is kezelni tudjuk modellünket nagy idők határesetben. Az extremális statisztika módszereivel sikerült konzisztens módon meghátároznunk egy zárt formulát, amely leírja a hierarchikus rácson az átlagsűrűség és a Hamming távolság aszimptotikus viselkedését. Az analitikus megoldás nagyban hozzárájult a lassú dinamikáért felelős lokalizációs folyamat megértéséhez.

Egyenletes és Gauss sűrűségeloszlásokat vizsgáltunk. Az előbbi esetében az átlagsűrűséget exponenciálisan csökkenő hatványfüggvények összegeként tudtuk leírnia, amelyet sor rendszerre logaritmus függvénnyel lehet közelíteni. Gauss eloszlás esetén $\sqrt{\ln t}$ függést kapunk rendszermérettől függetlenül, amely kiválóan leírja a négyzetrácson kapott numerikus eredményeket is.

A Self-Quenching Walk modell bizonyos értelemben a nyírási sáv mozgásának egy karikatúra-szerű modellje. Az aktív véletlen bolyongások közé tartozik és szintén lokalizációnak köszönhető lassú dinamika jellemzi amelyet a potenciál és a bolyongó részecske kölcsönös hatása eredményez. Megmutattuk, hogy ha az időnek és a potenciálnak megfelelő mértéket találunk, akkor a modellt le lehet képezni a "True" Self-Avoiding Walkra. Ebben a modellben a bolyongást szuper-diffuzívnak találták egy dimenzióban, amelynél magasabb dimenziókban a normális Brown mozgást kapunk. A mi modellünk esetében is ez a helyzet, amennyiben az időt lépésszámban mérjük és ezáltal kiküszöböljük a lokalizációs hatásokat. Valós időben azonban logaritmikusan lassú a diffúzió.

Megfelellő mértékkel mérve a potenciált önaffinnak találtuk egy dimenzióban, és simának a kritikus dimenzió ($d_c = 2$) felett (kettő dimenzióban logaritmikus figyelhetők meg). A potenciál időfejlődése az extremális modelleknek megfelelően zajlik, holott esetünkben nincs se globális extrémum keresés, se hosszútávú kölcsönhatás. Egyszerűsége miatt modellünk egy jól tanulmányozható példája extremális dinamikai problémáknak.

List of publications

1.) J. Török, J. Kertész and S. S. Manna, *Phase Transition in a Two-dimensional Green Wave Traffic model*, in *Traffic and Granular Flow*, Proceedings of a Conference, Jülich, 1995 (World Scientific, 1996).

2.) J. Török and J. Kertész, *The Green Wave Model of Two Dimensional Traffic: Transitions in the Flow Properties and in the Geometry of the Traffic Jam*, Physica A **231**, 515 (1996).

3.) J. Török and S. Roux, *Heterogeneous Mohr-Coulomb plastic material*, Granular Matter **2**, 71 (2000).

4.) J. Török, S. Krishnamurthy, J. Kertész and S. Roux, *Aging and Self-Organization of Shear Band in Granular Materials*, Physica A, **274**, 374 (1999).

5.) J. Török, S. Krishnamurthy, J. Kertész and S. Roux, *Self-Organization, Localization of Shear Bands and Aging in Loose Granular Materials*, Physical Review Letters, **84**, 3851 (2000) also at cond-mat/0003070.

6.) J. Török, S. Krishnamurthy, J. Kertész and S. Roux, *Self-Quenched Dynamics*, cond-mat/0004218, preprint.

7.) J. Török, S. Krishnamurthy, J. Kertész and S. Roux, *Large strain shear of loose granular materials: Numerical and analytical study*, preprint.